

Considerations in the use of ML interaction potentials for free energy calculations

*Orlando A. Mendible Barreto, Jonathan K. Whitmer, and Yamil J. Colón**

Department of Chemical and Biomolecular Engineering, University of Notre Dame, Notre Dame, IN, 46556. *Corresponding author, email: ycolon@nd.edu

ABSTRACT: Machine learning potentials (MLPs) hold promise to accurately describe the potential and free energy surface (FES) of molecular systems at the ab initio level of theory but with efficiency akin to what is seen in classical simulations. Within MLPs, equivariant graph neural networks have shown great promise in accuracy and performance when exploring equilibrium trajectories and are thus used in this work. An open question regarding MLPs is whether they can reliably reproduce free energies and transition states, which requires an accurate estimation not only of the energy of a configuration but the multiplicity of similar configurations (entropy). In this work, we investigate whether the distribution of collective variables (CVs) within the training data impacts the accuracy of MLPs in predicting the system's FES using Metadynamics simulations. Twenty MLPs were trained for butane and twenty-three for alanine dipeptide (ADP). Half the models were trained with energies and forces derived from classical molecular dynamics, and the other half used the same configurations but energies calculated via ab initio. The MLPs were trained using different distributions that aim to replicate hypothetical scenarios of sampled CVs that could be obtained if the underlying FES of the system was

unknown. The outcomes for butane indicate that the model's accuracy remains unaffected by the distribution of observed CVs during training when configurations from characteristic regions of the system's FES are incorporated. Nonetheless, in scenarios where not all characteristic areas of the FES are adequately represented in the training data, the model proficiently predicts potential energies for excluded configurations but struggles to reconstruct the free energy associated with those configurations. For ADP, models trained with energies from classical MD showed significant inaccuracies across all tests. While MLPs trained with ab initio data showed good prediction accuracy for potential energy, this did not translate to accuracy in free energy predictions. The findings underscore the difficulties in creating a comprehensive training dataset essential for MLPs to predict the underlying system's FES effectively. Moreover, they highlight the importance of prior knowledge about the system's FES during dataset generation, shedding light on potential constraints MLPs face when used to calculate free energies.

1. INTRODUCTION

A system's free energy surface (FES) delineates its free energy as a function of single or multiple collective variables (CVs) or order parameters.¹ CVs are mathematical functions of atomic coordinates that reduce the system's dimensionality and describe its collective evolution. Selection of the appropriate CV(s) enables examination of metastable states and determination of the system FES². Accurate models of the system's FES are essential for understanding thermodynamic driving forces of phase-transitions²⁻⁴, configurational changes^{5,6}, folding-unfolding of proteins^{7,8}, etc. Sampling the complete FES with unbiased simulations can be challenging as high energy barriers can negate the transition from one energy minimum to another. Various enhanced sampling techniques have been developed to improve sampling and describe transitions between free energy basins. These methods include Metadynamics⁹, umbrella sampling¹⁰, adaptive biasing force¹¹

(ABF), and many more¹²⁻¹⁴. These methods generally add an external biasing force to the system, promoting the sampling of configurations away from minimum free energy equilibrium basins, but which nonetheless contribute significantly to the thermodynamics of the system through (e.g.) their roles as morphological transition states. Added biases may then be extracted to recover the underlying FES. These biased simulations are often conducted with classical molecular dynamics (CLMD) forcefields rather than *ab initio* molecular dynamics (AIMD), given the simulation times required to converge the FES calculation and the computational cost of the latter approach. On the one hand, CLMD simulations base the calculation of energy and forces on atomic coordinates and predefined forcefield parameters, enabling simulations of larger systems and timescales¹⁵. On the other hand, AIMD explicitly considers interactions between electronic orbitals. As a result, its accuracy can describe interactions not captured by CLMD, such as bond-breaking and forming¹⁶, but its computational cost scales cubically with the system size¹⁷. Thus, AIMD is limited in the number of atoms and timescales it can simulate¹⁸. Multiple efforts have successfully implemented enhanced sampling techniques and AIMD engines for small systems with relatively simple FESs¹⁹⁻²². There are two limiting considerations when performing these types of simulations. First, as the system size and complexity increases, the complexity of the FES increases. As a result, the computational cost required to converge the FES increases, making AIMD inaccessible for many molecular systems. Second, a CV must be selected to describe relevant degrees of freedom (i.e., the slowest degree of freedom)²³. Many CVs have been extensively studied for simple systems involving small molecules²⁴, peptides²⁵, and simple reactive systems^{26,27}.

Machine learning forcefields (MLFFs), also referred to as machine learning potentials (MLPs), have emerged as a new tool that aims to maintain the accuracy of *ab initio* calculations while reducing the computational cost by orders of magnitude and maintaining a linear scaling with the

number of atoms in the system²⁸⁻³¹. Many MLFF models have been developed and used, with varying for new materials³²⁻³⁵, chemical reactions³⁶⁻³⁸, large-scale simulations³⁹⁻⁴¹, and understanding complex interatomic and intermolecular interactions^{32,42,43}. The main differences between models rely on the descriptors used to describe the local atomic environments within the system, such as the Smooth Overlap of Atomic Positions (SOAP)⁴⁴, the Atomic Cluster Expansion (ACE)⁴⁵, and others⁴⁶, and the type of machine learning methods, mainly neural networks^{47,48} or kernel-based^{49,50} methods. Various combinations of approaches and atomic representation methods have given rise to an overwhelming amount of open-source computational models to train MLFFs, including DeepMD-Kit⁵¹, SchNet⁵², TorchMD⁵³, sGDLS⁵⁴, NEQUIP⁵⁵, and many more⁵⁶. Among these approaches, equivariant graph neural networks (EGNN) have shown optimal accuracy and scalability⁵⁷. Specifically, the Allegro⁵⁸ model, which will be the focus of this study, represents a cutting-edge approach to learning interatomic potentials through deep neural networks. Unlike other methods relying on atom-centered message passing, Allegro employs strictly local equivariant representations, enabling it to capture many-body interactions with greater accuracy and scalability. This distinction is evidenced by its exceptional accuracy and performance in simulating systems with up to 100 million atoms⁵⁹ and achieving high accuracy on potential energy and atomic force prediction across a range of materials^{58,60,61}. These results demonstrate that the model accurately predicts properties derived from ensemble averages. However, the distinct nature of the calculation method necessary for determining the FES of the system, which requires a deep understanding of mechanisms and transition states, leaves questions about the model's applicability for FES determination.

Limited literature is currently available where EGNN is tested for predicting FES of molecular systems. Ple et al.⁶² employed the FENNIX (Force-field-Enhanced Neural Network Interactions)

model, which uses Allegro's representations of atomic pairs and then passed this data through an NN responsible for predicting the property of interest. Additionally, they trained a FENNIX model for alanine dipeptide in explicit water using data from classical MD and qualitatively recovered the FES but underestimated high free energy barriers. Similarly, Kovács et al.⁶³ used the MACE-OFF23 model to predict the various properties of a set of organic molecules. However, the predictions made from this message-passing neural network model for the FES of alanine-tripeptide in explicit solvent demonstrate the model's ability to predict the location of free energy minima but showed limitations with high free energy configurations. These results highlight the necessity of acquiring new knowledge to generate training data sets and models capable of recovering the FES of simple and complex molecules.

The quality of training data significantly influences the accuracy of the MLFFs for molecular simulations. Insufficient training data can lead to inaccurate predictions of energy and forces, especially when encountering untrained configurations, resulting in unstable physics. As systems become more complex, including diverse configurations in the training data becomes challenging. Efforts have been made to enhance configurational sampling in training data through methods like FLARE⁶⁴ and DP-GEN⁶⁵, which automate data preparation and model training using concurrent and active learning techniques. However, these approaches may still lack configurations representative of the underlying FES due to dependence solely on model deviations and uncertainties.

In this work, we aim to study if the distribution of CVs included in the training data and its representation of the system's FES affect the accuracy of the MLPs in predicting the system's FES via Metadynamics simulations. For this task, we used butane and alanine dipeptide molecules as examples. The rotation of butane's methyl groups around the central carbon-carbon bond gives

rise to various conformers mapped by the torsional angle of its carbon atoms⁶⁶. Moreover, the FES of butane has been extensively studied, providing a valuable reference to compare results⁶⁷⁻⁶⁹. We also studied alanine dipeptide (ADP) to highlight any effect resulting from higher energy barriers and a more complex configurational space. ADP has long been utilized as a fundamental model system in elucidating protein structures. Its significance lies in encapsulating essential elements of more complex polypeptides, enabling simplified yet insightful investigations⁷⁰⁻⁷². The configurational diversity of ADP stems from the rotation of its phi (ϕ) and psi (ψ) dihedral angles, which succinctly represent the molecule's configurational space^{73,74-76}. Widely studied for its FES⁷⁷⁻⁷⁹, ADP's FES makes it an ideal candidate for examining the interplay between structural transitions and energetic stability.

2. METHODS

The performance of MLPs relies significantly on the configurations present in the training dataset and those employed during testing for evaluating model accuracy. In many cases, the approach used to generate the test data is the same as the one used to create the training data. As a result, both data sets end up with configurations with similar distributions of CVs. In the ideal scenario, the distribution of CVs covers the entire space of configurations, but this is often not the case. Our datasets aim to replicate hypothetical scenarios of CV distributions that could be obtained if no information about the FES of the system is available. Butane and ADP were selected as test cases due to their relative simplicity and abundance of reference for their FES. The datasets were utilized to train Allegro MLPs, assess their accuracy in predicting free energy, and explore how the distribution of CVs in the training data impacts accuracy.

2.1 Database Construction

2.1.1 Butane

A. Classical Molecular Dynamics (CLMD)

Configurations for the butane datasets were generated using CLMD simulations using LAMMPS80 version 29Sep2021 and PLUMED281. A single butane molecule was inserted in a cubic box with sides of 4.0 nm. The interatomic interactions were modeled following the parameters presented by Sidky82 et al., which include using the Optimized Potentials for Liquid Simulations83 (OPLS) all-atom force field with a cutoff distance of 12.0 Å and treating Coulombic interactions using the particle-particle-particle-mesh (PPPM) and tolerance of 1E-8. An unbiased simulation was conducted for 5ns at 500 K using the NVT ensemble, saving frames every 20 ps. Configurations were extracted from this simulation to fill a distribution of interest. Eight distributions were studied, and each contained 500 samples. The distributions are named: Boltzmann (BD), Uniform (UD), Half-Uniform-Left (HULD), Half-Uniform-Right (HURD), Bias Left (BL), Bias Right (BR), Bias-Half-left (BHL), Bias-Half-right (BHR), and the code for their selection is accessible in the GitHub repository. An independent simulation with the same parameters and conditions was used to generate the test data set distributions. Histograms of the generated training and testing distributions are presented in **Figure 1**.

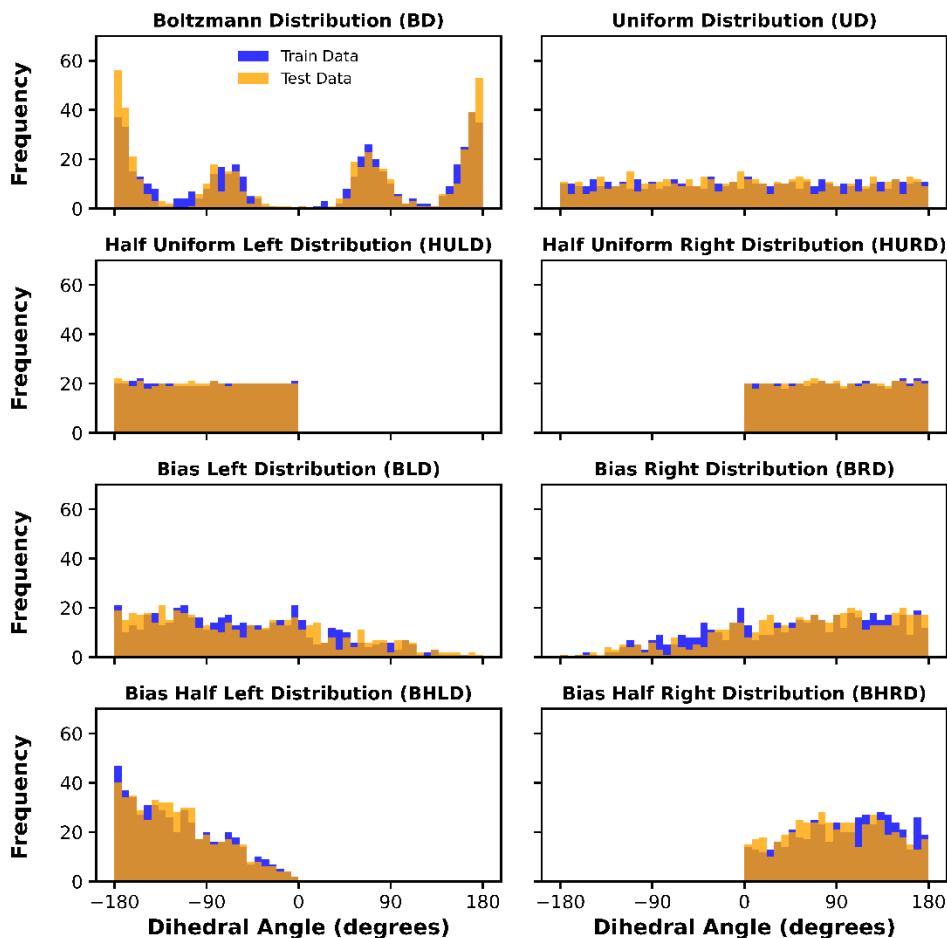


Figure 1. Distribution of butane conformers sampling in datasets used to train and test butane MLPs.

Two additional training data sets were generated to analyze further how the training data distribution affected the free energy predictions of the MLPs. The first will be referred to as case A and has configurations that only represent the local free energy minima of the butane FES. The second will be called case B, with configurations representing only the system's global free energy minimum. This data set aims to replicate a “typical” scenario in which an AIMD simulation is run for 20 ps and the system only explores one or few basins; the resulting trajectory is used as training, validation, and testing data. Consequently, the configurations were generated utilizing the parameters outlined in the subsequent section for *ab initio* single-point calculations. From the trajectory, 500 samples were chosen and employed as initial configurations for a single-step

unbiased CLMD simulation, utilizing the parameters above. The resulting histograms are presented in **Figure 2**.

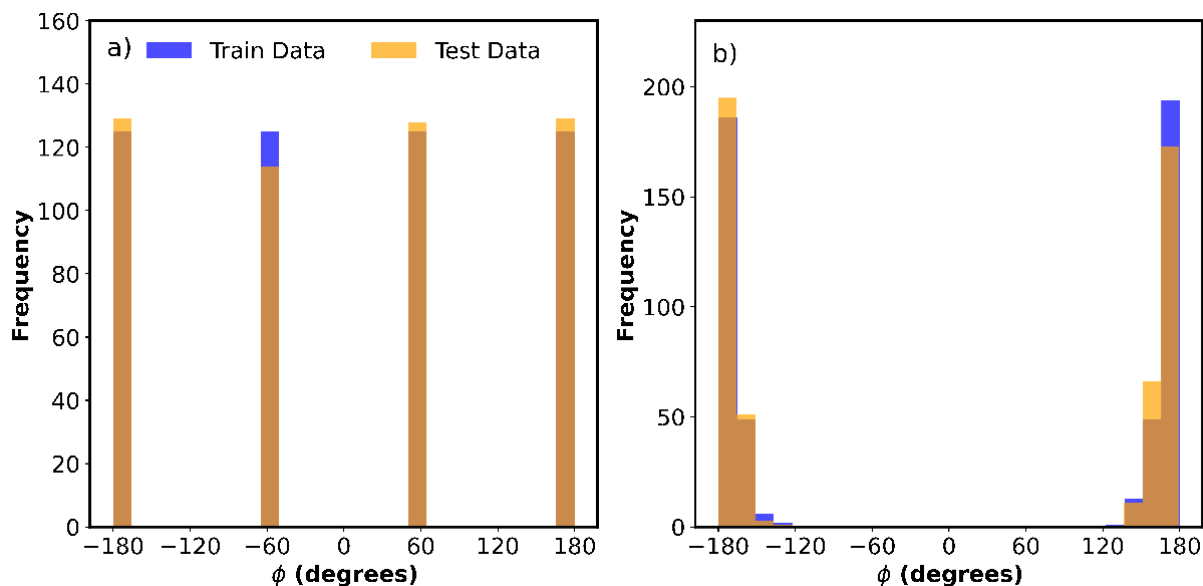


Figure 2. Histogram of sampled butane dihedrals in a) cases A and b) B.

After selecting configurations of interest based on the CV value, the coordinates, potential energy, atomic forces, and atomic types were stored in a *npz* format, marking the completion of the dataset generation. All the necessary code to accomplish this task is available in the GitHub repository (https://github.com/omendibleba/Considerations_for_MLPs_FES).

B. *Ab initio* single point calculations (SPC)

For the SPC training and test dataset, we used the same configurations that were generated using CLMD. The configurations in each data set were used as initial configurations for the SPCs. These were performed using the Quickstep module in CP2K⁸⁴ which employs a hybrid approach that combines Gaussian and plane waves techniques to calculate the potential energy surface and extract forces from the energy gradient. Calculation parameters were taken and modified from the works of Niemöller et al.⁸⁵, and they include the use of the revPBE⁸⁶ functional and corresponding

PBE Goedecker–Teter–Hutter pseudopotentials for core electrons^{87–89}, in combination with the molecularly optimized basis set (MOLOPT-DZVP-GTH)⁹⁰. The density CUTOFF was set to 800 Ry and a relative CUTOFF of 60 (REL_CUTOFF 60). Dispersion interactions were accounted for by applying the DFT-D3 correction^{91,92}. The self-consistent field (SCF) was set up with an accuracy threshold of 10^{-6} . The DIIS⁹³ (direct inversion in the iterative subspace) minimizer and FULL_SINGLE_INVERSE preconditioner were applied. These parameters were also used to perform *ab initio* molecular dynamic (AIMD) Metadynamics simulation as the reference for MLPs trained with SPC data. This simulation ran for 600 ps at 500 K using a time step of 1fs, and the optimal sampling GLE thermostat with a matrix size of 5 and scaling factor of 1 ps^{-1} . The Metadynamics parameters include the addition of Gaussian curves with height of 0.1 kcal/mol and width of 0.3 rad every 100 steps. The free energy was extracted from the biased simulation using the sum_hills tool provided by PLUMED2, and the estimation convergence was validated. All relevant files to this simulation are available in the GitHub repository. After calculating the potential energies and forces, they were extracted to generate the training and test datasets. The GitHub repository provides all the necessary code to accomplish this task.

2.1.2 Alanine dipeptide (ADP)

A. Classical Molecular Dynamics (CLMD)

Initial configurations of ADP were generated with CLMD. Since ADP has a higher free energy barrier than butane, enhanced sampling simulations were required to obtain sampling in all regions of the configurational space. The ADP molecule was put inside a cubic box with sides of 4.0 nm, and the atomic interactions were modeled by the AMBER99SB forcefield using a cutoff of 12.0 Å and the same parameters as Sidky et al.⁸² To achieve a uniform distribution of CVs across the

configurational space, a 2D grid consisting of 50 bins along each axis was generated. Subsequently, the center of each bin was utilized to conduct restrained simulations at the specified combinations of CV values. Each restrained simulation was performed for ten picoseconds at 500 K, employing a 100 kcal/(mol Å) spring constant. Following this, the CVs of the sampled configurations were scrutinized, and the one exhibiting the lowest error relative to the center value was selected. Finally, the chosen configuration underwent an unbiased single-step calculation to obtain its unbiased potential energy and forces, which conform to the final data set used to train and test the ADP MLPs. This approach created two training data sets: the Uniform distribution sets with 2500 and 5000 configurations. A two-dimensional histogram of the generated datasets is presented in **Figure 3**.

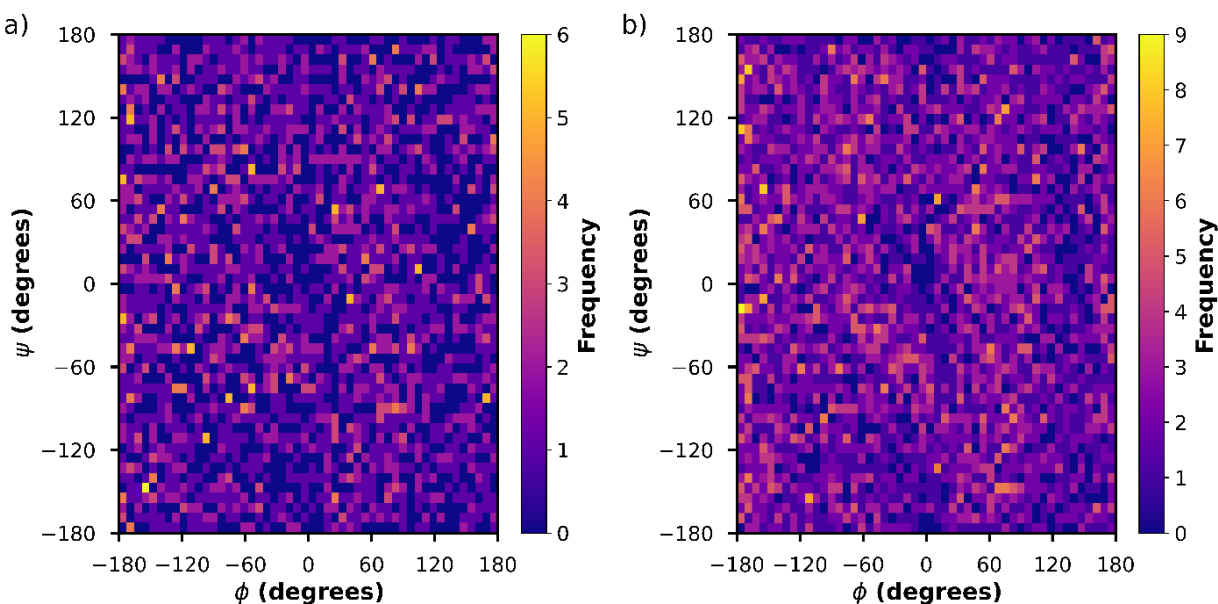


Figure 3. Histogram of sampled ϕ and ψ for alanine dipeptide uniform sampling distribution with a) 2500 frames and b) 5000 frames.

Training data sets for ADP were generated using a different approach than for butane. The Boltzmann distribution datasets were generated by first running a reference Metadynamics simulation of the ADP system, which ran at 500 K for 25 ns, using a 1 fs time step, and adding

Gaussian biases with a height of 0.28 kcal/mol and total width of 0.3 rad every 500 steps. The extracted free energy of this simulation was used as the reference for all ADP MLPs. The generated CVs were analyzed and selected to align with the probabilities dictated by the Boltzmann distribution of CVs, derived from an unbiased simulation at the same conditions and with the same simulation parameters. Finally, the selected configurations were used to run single-step unbiased simulations, extract the energies and forces, and create the datasets. Following this approach, two types of data sets were generated, and a 2-dimensional histogram of the selected configurations is presented in **Figure 4**.

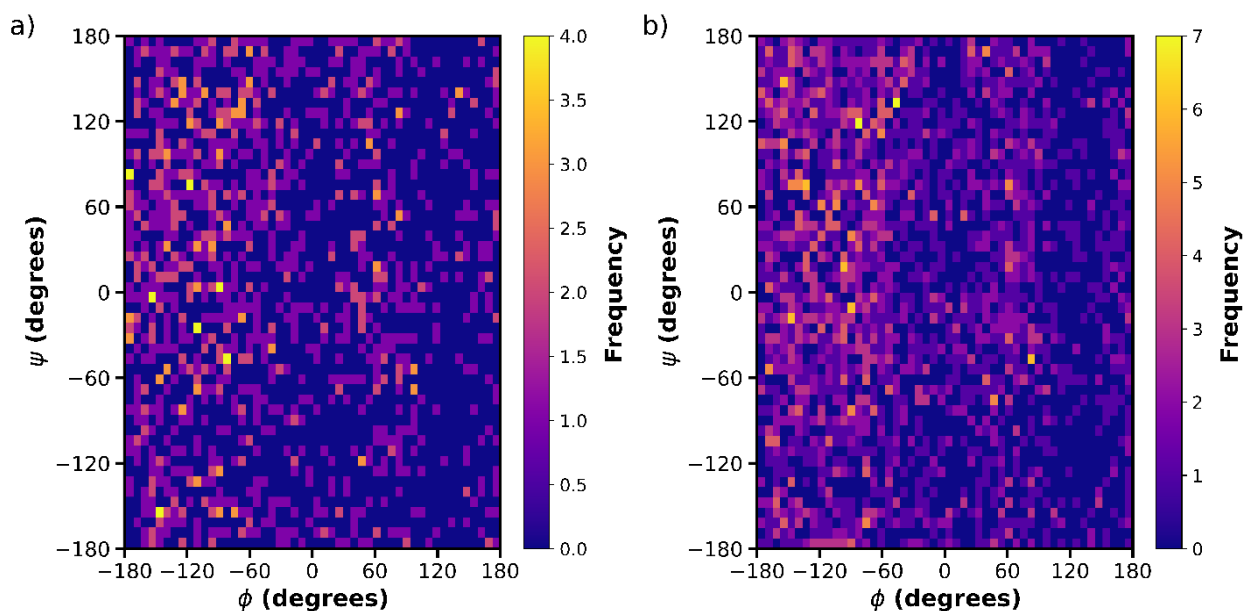


Figure 4. Histogram of sampled ϕ and ψ for alanine dipeptide Boltzmann sampling distribution with a) 2500 frames and b) 5000 frames.

To further explore the effect of the distribution of CVs in the training data on the accuracy of FES predictions of ADP, three additional classes of training data distribution were generated, namely, Unbiased, Only-Minima (Omin), and Characteristic Regions (CharReg). Each type of data set was generated with 500, 1000, and 2500 configurations. **Figure 5** shows the configuration in the 2500 variant of the Unbiased, Omin, and CharReg datasets, respectively.

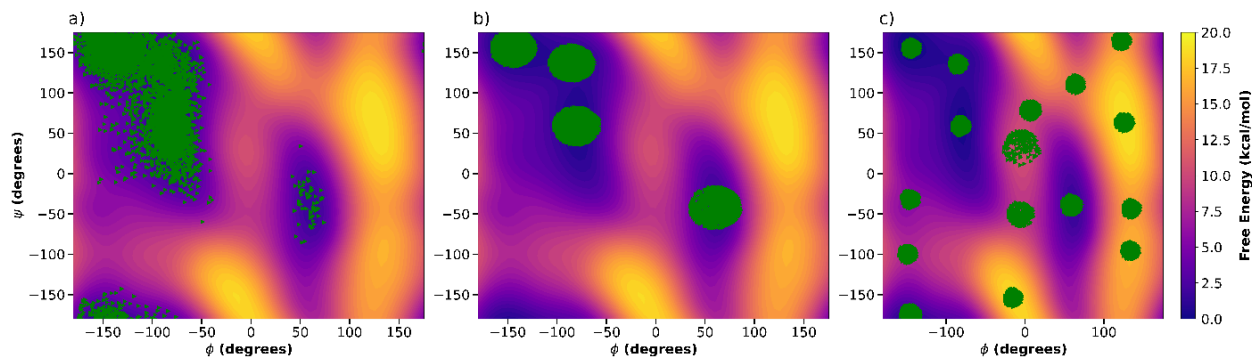


Figure 5. Alanine dipeptide included configurations in a) Unbiased, b) Omin, and c) CharReg datasets with 2500 samples on top of the FES of ADP. Green triangles represented included configurations.

The configurations for the Unbiased distribution were selected from the unbiased simulation used to obtain the Boltzmann distribution previously explained. This distribution aims to explore the behavior of the MLP when training with configurations that come directly from an unbiased simulation. The Omin distribution has configurations localized in the local free energy minima of the system. It intends to have a less diverse distribution of configurations near the global and local minima and analyze potential differences when the configurations do not come directly from a single molecular simulation. Finally, the CharReg distribution aims to include the characteristic locations of the FES in the training data configurations. In this way, the model has information about the CV values at which free energy minima and barriers occur.

B. *Ab initio* single point calculations (SPC)

SPCs of ADP were executed employing identical computational parameters delineated previously for the simulation of butane. The sole deviation across input files was incorporating oxygen and nitrogen basis sets and pseudopotentials. In addition, it is essential to highlight that due to the challenges of acquiring a converged Metadynamics simulation, the reference FES for ADP MLPs trained with *ab initio* SPCs comes from a Metadynamics classical MD simulation. Corresponding CP2K and LAMMPS input files are available in the GitHub repository.

2.2 Allegro Model

The initial model was selected with the suggested hyperparameters found in the examples of Allegro⁹⁴ configurations. Hyperparameter optimization was conducted using the Weight-and-Biases software⁹⁵, and more information can be found in the Supplemental Information (SI) section I. For all the training data sets, 80% of the data was used for training, and 20% was used for validation. The training process incorporated a local cutoff of 4.0 Å, and a polynomial envelope function with a parameter value of $p=6$ was employed for the Bessel functions. This function facilitated the decay of interactions as the interatomic distance increased. A maximum rotational number of $l_{\max}=3$ was also set for spherical harmonics. Three layers were used and for each the number of features was 32, the two-body latent dimension of the neural network architecture comprised five layers with dimensions [64, 128, 256, 512, 1024], and a latent multi-layer perceptron with dimension [1024, 1024, 1024]. SiLu nonlinearities were applied to the outputs of each hidden layer. Subsequently, the latent Multi-Layer Perceptron (MLP) consisted of three layers, each with a dimensionality of 1024. For the final edge energy MLP, a single hidden layer with a dimension of 128 was implemented without incorporating any nonlinearities. During training, a batch size of 5 and a learning rate of 0.002 were utilized to update the model parameters iteratively. The loss function of energies and forces to be minimized by the Allegro model architecture is presented in equation (1).

$$L = \frac{\lambda_E}{B} \sum_b^B (\hat{E}_b - E_b)^2 + \frac{\lambda_F}{3BN} \sum_{i=1}^{BN} \sum_{\alpha=1}^3 \left\| -\frac{\partial \hat{E}}{\partial r_{i,\alpha}} - F_{i,\alpha} \right\|^2 \quad (1)$$

Where $B, N, E_b, \hat{E}_b, F_{i,\alpha}$ refer to the batch size, number of atoms, batch of reference energies, batch of predicted energies and the force component on atom i in spatial direction α , respectively and λ_E, λ_F are the energy and force weights. The initial coefficients for the energy and forces in the loss function were set to 1.0. For more detailed information, visit the original publication for

Allegro⁹⁴. After training, the models were tested to predict the potential energy and forces of the configurations in the test data set.

2.3 Deep Potential Molecular Dynamics Simulations (DPMD)

2.3.1 Unbiased simulations

Trained models were employed to conduct deep potential molecular dynamics (DPMD) utilizing LAMMPS coupled with Allegro and PLUMED2. The systems for these simulations were identical to those constructed for the reference data, consisting of a single molecule enclosed within a cubic box with sides measuring 4 nm. The trained Allegro MLPs were used to describe the interactions of atoms in the system and PLUMED2 was used to track the sampling of CVs. The unbiased simulations ran for two nanoseconds at 500 K using a time step of 1 fs and storing frames every 500 fs. The CVs sampled during this simulation allowed a direct comparison to those sampled in the reference trajectory used to generate the training data.

2.3.2 Metadynamics simulations

DPMD-biased simulations allowed the evaluation of the MLP's accuracy in predicting the FES of butane and ADP. Metadynamics simulations were conducted at 300 K for ten nanoseconds using the systems discussed in the previously discussed sections. For butane simulations, Gaussian biases were added every 500 steps with a height of 0.28 kcal/mol, a width of 0.3 rad, and a bias factor of 5. While ADP simulations were conducted at 300 K, Gaussian biases were added every 100 steps with a height of 0.3 kcal/mol, a width of 0.3 rad, and a bias factor of 3.

3. Results and discussions

In this section, we present the results related to training and validating the MLPs. Moreover, we report on the model's capabilities to recover the dihedrals of butane and alanine dipeptide in unbiased simulations and the FES of the systems using Metadynamics simulations.

3.1 Training and testing the MLPs

3.1.1 Butane

Figure 6 presents the evolution of the loss function and its energy and force components for the MLP trained with the Boltzmann distribution (BD) data at the classical level of theory. Similar plots for all other models trained in this study can be found in Section II of the SI.

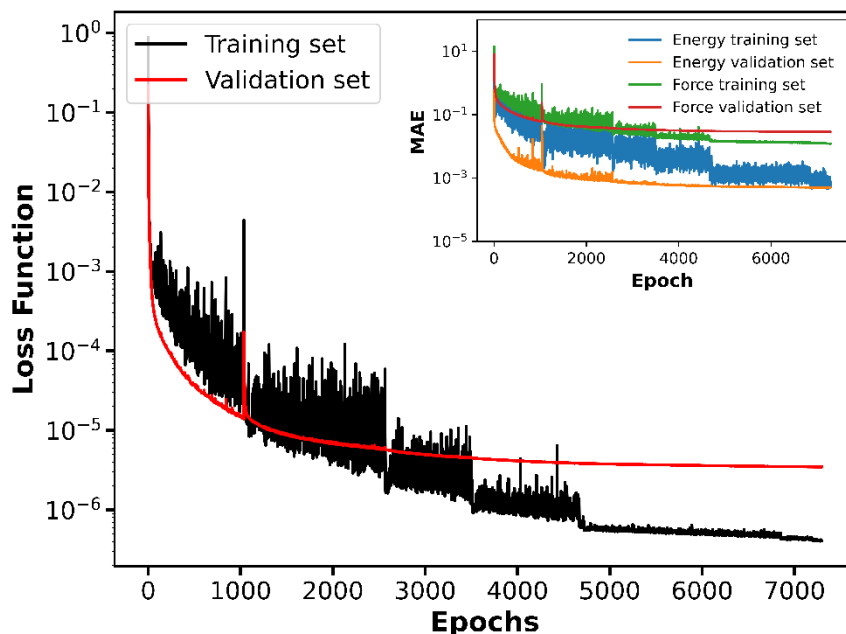


Figure 6. The logarithm of the loss function was calculated using the training and validation sets during the butane MLP training with the Boltzmann distribution (BD) data at the classical level of theory. The energy and force components of the loss function are documented in the inset.

During the training procedure, the loss function of both training and validation datasets was minimized, reaching values of 10^{-5} after approximately 3500 epochs. The model continued

training until 7200 epochs and the training loss function continued decreasing, achieving values of 10^{-6} . Given the magnitude of the loss functions being smaller than 10^{-5} , the results demonstrate good agreement and indicate the absence of overfitting. The analysis of the component of the loss function, presented in the inset of **Figure 6** as MAE, shows that the contributions of forces are higher than energy contributions at the beginning of training. While training continues, the force contributions remain constant, and the energy contributions remain minimized during the remaining epochs. The trained MLP was tested to predict potential energy and the force components of atoms included in the test dataset. The results are displayed in **Figure 7**.

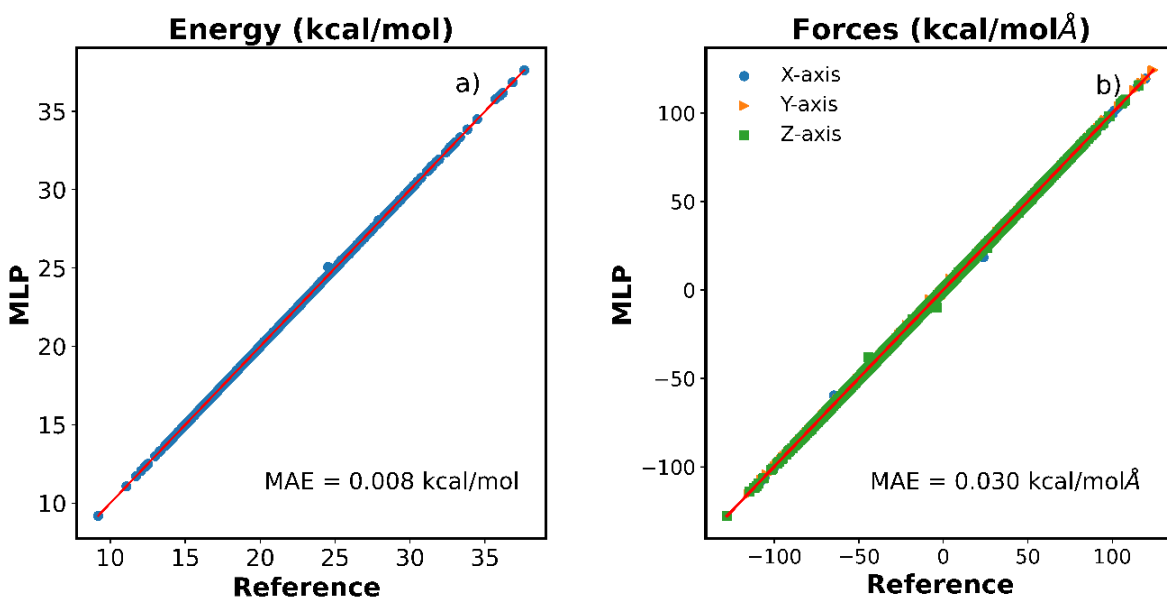


Figure 7. Scatter plot for a) potential energy and b) forces for the x, y, and z axes computed at the classical level of theory and predicted by the MLP of butane trained with the Boltzmann distribution (BD) data.

The predicted energies for the test set agree with the potential energies calculated with CLMD. The mean absolute error (MAE) is 0.008 kcal/mol, corresponding to 0.571×10^{-3} kcal/(mol atom). Similarly, the force predictions show good accuracy, evident with a 0.034 kcal/(mol Å). These results are comparable to MAE obtained in other works training MLPs for organic molecules using graph neural networks⁹⁶ and better accuracy than other machine learning

approaches for force field development.^{97,98} The same prediction test was conducted for all the MLPs for butane, the MAE results are summarized in **Table 1**, and additional plots are available in section III of the SI.

Table 1. MAE results of energy and force prediction tests for butane MLPs trained at the classical and *ab initio* level of theory. Energies are in kcal/mol, and forces are in kcal/(mol Å).

Distribution	Energy MAE (Classical)	Energy MAE (<i>ab initio</i>)	Force MAE (Classical)	Force MAE (<i>ab initio</i>)
Boltzmann	0.008	0.027	0.030	0.116
Uniform	0.008	0.032	0.031	0.133
Half-Left-Uni	0.008	0.030	0.031	0.127
Half-Right-Uni	0.006	0.030	0.034	0.132
Bias-Left	0.008	0.030	0.032	0.128
Bias-Right	0.008	0.034	0.032	0.134
Bias Half Left	0.010	0.028	0.043	0.125
Bias Half Right	0.007	0.028	0.030	0.122
Case A	0.006	0.023	0.025	0.099
Case B	0.002	0.015	0.012	0.086

Results obtained from MLPs trained with data from classical MD are approximately one order of magnitude smaller than their *ab initio* counterparts. The main reason is the difference in magnitudes of the energy values used to calculate the loss function during training. For example, suppose we select the configuration with the highest potential energy value in the training data with the Boltzmann distribution. In that case, we find its value to be 37.62 kcal/mol, while the same configuration had a value of -17,956.16 kcal/mol when calculated with the *ab initio* approach. Similarly, the standard deviation (STD) for the potential energies predicted by the MLP trained with classical and *ab initio* data is 4.23 kcal/mol and 5.74 kcal/mol, respectively.

Therefore, although the magnitudes of the MAE are smaller for MLPs trained with classical data, models trained with *ab initio* data are more accurate for a more extensive range of values.

The results also suggest that focusing the training and testing data on specific regions of the configurational space has a slight positive effect on the prediction accuracy of the models. This is evident when comparing the MAE of potential energy made with the more dispersed Uniform distribution, and the more localized Case B distributions, which resulted in 0.032 and 0.015 kcal/mol, respectively. A reduction in MAE is expected given the increased amount of training data on a specific region of the configurational space, this implies a more specialized model for this area. A similar reduction is observed for models trained with the classical molecular dynamics approach. Overall, the agreement of predictions with reference values suggests that the predictions of the MLPs are not significantly affected by the distribution of configurations in the training data and support reliable prediction power from the trained models.

3.1.2 Alanine dipeptide (ADP)

Plots of the logarithm of the loss function during the training of ADP MLPs are available in Section IV of the SI. In most cases, the loss functions of models trained with data from CLMD showed signs of overfitting. That was not the case for models trained with *ab initio* calculations. Thus, the cause of overfitting is attributed to the values of CLMD compared to *ab initio* calculations. In CLMD, different configurations could have similar potential energies and atomic force values, while the accuracy of *ab initio* calculations allows for better differentiation of the configuration's energetic and force values. As a result, the model trained with the broader range of values has a better capacity to discern between different configurations. All trained models were tested to predict the energy and forces included in the test data set, and the results in terms of MAE are presented in **Table 2**. Additional plots are available in section V of the SI.

Table 2. MAE results of energy and force prediction tests for alanine dipeptide MLPs trained at the classical and *ab initio* level of theory. Energies are in kcal/mol, and forces are in kcal/(mol Å).

Distribution	Energy MAE(Classical)	Energy MAE (<i>ab initio</i>)	Force MAE (Classical)	Force MAE (<i>ab initio</i>)
Boltzmann-2500	8.399	0.140	40.796	0.284
Boltzmann-5000	4.679	0.098	40.44	0.319
Uniform-2500	0.982	0.115	8.195	0.233
Uniform-5000	0.744	0.160	8.627	0.395
Unbiased-500	4.540	3.393	40.575	1.424
Unbiased-1000	4.078	3.111	40.590	1.374
Unbiased-2500	3.307	2.802	40.479	1.269
OnlyMin-500	6.042	2.205	41.284	1.334
OnlyMin-1000	3.920	1.812	31.623	1.214
OnlyMin-2500	6.785	1.644	40.854	1.023
CharReg-500	5.432	0.837	41.166	1.022
CharReg-1000	5.230	0.686	41.000	0.698
CharReg-2500	4.419	0.558	40.685	0.678

The disparities in performance between MLPs trained using classical data and those trained with *ab initio* are apparent, as demonstrated by the significant MAE observed during the assessment of energy and force predictions. These differences are attributed to the inherent limitations of CLMD compared to *ab initio* calculations. The complexity of the ADP molecule relative to butane exacerbates this issue, as the data derived from CLMD simulations lacks the necessary granularity to discern subtle variations in energies and forces among similar configurations. Consequently, the predictive model encounters difficulties in accurately estimating these values during evaluation tests. For this reason, the focus of the analysis of the MLPs for ADP will be performed using the models trained with *ab initio* accuracy.

The results for the MLP trained with the Boltzmann distributions suggest the model's prediction accuracy increases when the amount of training data is duplicated from 2500 to 5000 frames. The increment in accuracy from 0.140 kcal/mol to 0.098 kcal/mol is insignificant compared to the computational cost required to train the model with such a larger data set. Moreover, the MAE for the force predictions of these same models shows that increasing configurations in the training data set negatively affected the model's accuracy since the MAE rose from 0.284 to 0.319 kcal/(mol Å). The increment of the force prediction MAE suggests that the model can become prone to overfitting with the increment in training data size, implying that increasing the amount of training data with this distribution will not necessarily result in a more accurate MLP.

The MLP trained with uniform distribution and 2500 frames exhibited the lowest MAE among all tested distributions, which aligns with expectations. This outcome stems from the fact that uniform distributions encompass the most diverse array of configurations compared to other generated distributions. Consequently, the model trained on such data achieves greater robustness due to its exposure to a broader spectrum of configurations during training. However, the results suggest that duplicating the training data in this distribution negatively affects the model's prediction accuracy for both potential energy and atomic forces. Once more, this behavior can be attributed to the potential overfitting of the model, particularly when augmented with additional training. This result also suggests that increasing the amount of training data in this distribution will not have a significant positive effect on model accuracy but, on the contrary, can affect the performance of the MLP.

Results from the models trained with the unbiased distributions (**Figure 5a**) showed these models could not accurately predict the energies and forces from the test data. Similar results are observed for the models trained with configurations that only represent the minima of ADP's FES

(**Figure 5b**). The MAE for these MLPs ranged from 3.393 to 1.644 kcal/mol, which is not considered accurate enough for most applications.

Finally, results from models trained with the data in characteristic regions (**Figure 5c**) indicate the model predictions agreed with reference values for all MLPs. The potential energy MAE was 0.837, 0.686, and 0.558 for the models trained with 500, 1000, and 2500 configurations. In addition to the good level of accuracy, these models showcase the expected trend, which is that incrementing the amount of training data should reduce the MAE of prediction for energies and forces. The trend indicates that augmenting the training data volume with this distribution may enhance model accuracy. Nonetheless, escalating the number of configurations in the training dataset poses computational resource challenges for training MLPs. Furthermore, this surge in data volume diminishes the advantages conferred by equivariant graph neural networks, which advocate for a reduced number of training configurations.

3.2 Unbiased deep potential molecular dynamics (DPMD)

In this section, we first validate the stability of the trained and tested MLPs in unbiased MD simulations. After this, we report an analysis of the sampled CVs during the simulations and the effects of the distribution of CVs in the training data on the accuracy of sampled dihedrals.

3.2.1 Butane

All butane MLPs demonstrate good stability across the unbiased simulations by maintaining physical integrity without displaying unphysical configurations throughout the two ns of simulation time. **Figure 8** illustrates the sampled dihedral angles of the butane molecule during unbiased DPMD with models trained with distributions presented as cases A and B, respectively.

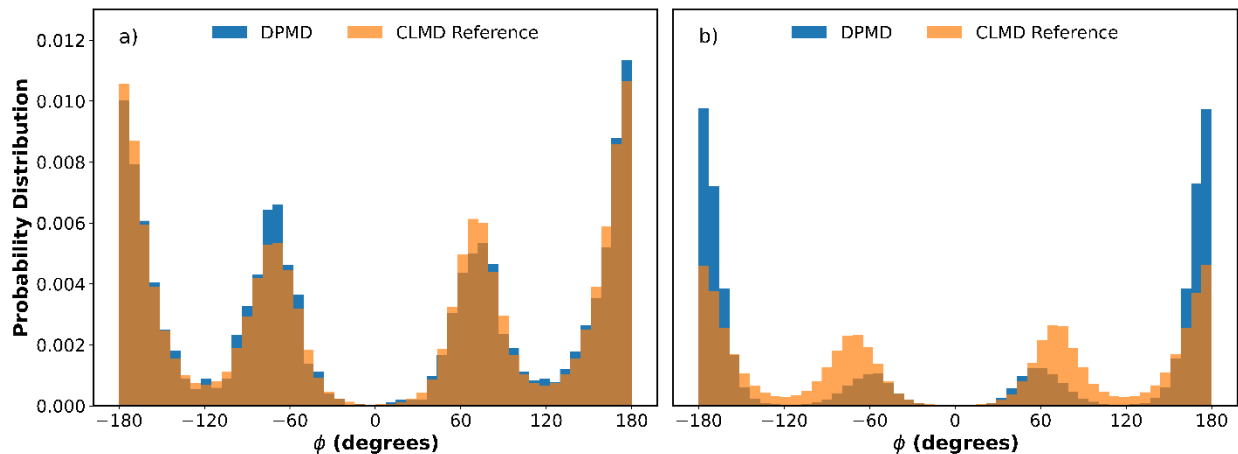


Figure 8. Sampled ϕ dihedrals of butane during a two ns unbiased simulation with a) butane case A training data and b) butane case B training data compared to the reference sampled dihedrals.

Butane MLPs trained with the distributions presented in **Figure 1** had similar results to those depicted in **Figure 8a**, and the plots are available in Section VI of the SI. These results suggest that the accuracy and stability of the butane MLPs are not affected by the dihedral distribution included in the training data. It is important to mention that the dihedral of butane is a symmetric CV and the FES is also symmetric. Therefore, the energies and forces of configurations in which CV goes from -180 to 0 are the mirror image of configurations in which CV goes from 0 to 180. The symmetry of the CV combined with the equivariance of the Allegro model significantly helps the model during training since, with one configuration of the training data, the model is learning the information of 2 configurations. On the one hand, results in Figure 3a highlight the extrapolation capabilities of the Allegro model since the model trained with case B data (configuration only in free energy minima of the system) could recover the expected distribution of sampled CVs. This implies that the model could accurately predict the energies and forces of configuration out of the training data, which had higher free energies than those included in the training set. On the other hand, results from Figure 3b highlight the limitations of the Allegro model to extrapolate energies and forces of configurations out of the training data when it does not

include configurations near all characteristic regions of the FES of the system (i.e., free energy peaks and basins). This is evident by increased sampling in the training data's focus regions, around -180 and 180 degrees. This was followed by a lack of sampling of configurations around the -60 and 60 dihedrals compared to the reference. Additionally, the results suggest that the MLP has identified a local minimum around -60 and 60 degrees, which is qualitatively correct but shifted towards zero compared to the reference. These results imply that for simple systems like butane, the model can accurately extrapolate the potential energies and forces of configurations out of the training data if configurations near all the characteristic regions of the FES are included. Additionally, they show that when the model lacks sufficient information on the system's configurational space, the MLPs can qualitatively recover the distribution of CVs, but quantitative deviations are evident.

3.2.2 Alanine Dipeptide

From the ADP MLPs, the most accurate in predicting potential energy and forces was the MLP trained with a uniform distribution and 2500 frames at the *ab initio* level of theory. For this reason, the analysis of this section is focused on this MLP. **Figure 9** displays the ϕ and ψ dihedral angle distributions sampled using the mentioned model.

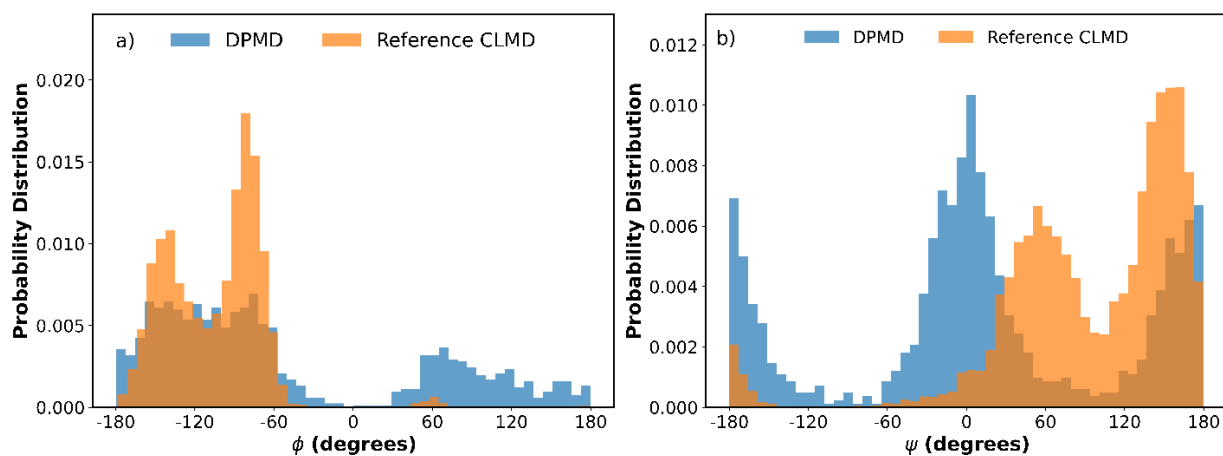


Figure 9. Sampled a) ϕ and a) ψ dihedrals of alanine dipeptide sampled during deep potential molecular dynamics simulation with a model trained with 2500 frames, uniform distribution, and at the *ab initio* level of theory.

The histogram analysis of the sampled ϕ and ψ dihedrals indicate a discrepancy in the model's ability to replicate the distribution observed during AIMD simulations. Specifically, the ϕ dihedrals displayed a higher sampling frequency than expected, between -180° and -60° , while exhibiting lower sampling than anticipated, around 60° . Notably, there was excess sampled data near 40° to 180° for ϕ dihedrals. Similarly, the ψ dihedrals revealed an increased sampling between -180° and 0° , with a reduced sampling frequency observed between 0° and 180° . Conversely, there was a notably increased occurrence of sampled data around the 0° for the ψ dihedrals. These discrepancies suggest a lack of fidelity in replicating the expected distribution of dihedral angles, highlighting limitations in the model's accuracy in representing the full range of ϕ and ψ dihedral conformations observed in unbiased molecular dynamics simulations. The other models, unfortunately, encountered significant challenges in completing the unbiased simulations reliably. Several instances revealed these models presented unphysical configurations during the simulation process, like the one illustrated in **Figure 10**.

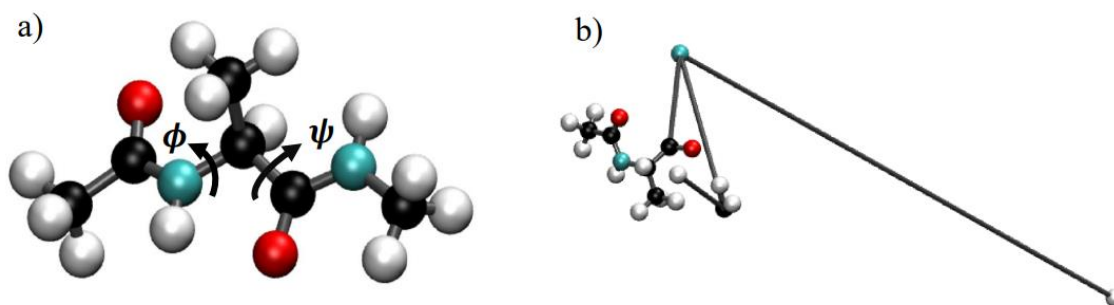


Figure 10. A) Starting Alanine dipeptide configuration. B) Unphysical alanine dipeptide configuration caused failure on the model's deep potential molecular dynamics trained with Boltzmann Distribution and 2500 frames. Black is carbon, white is hydrogen, red is oxygen, and cyan is nitrogen.

These unphysical configurations suggest limitations within the less accurate models, potentially indicating flaws in their parameterization or underlying representations. Such instances of instability and unphysical behavior during simulations raise questions regarding the robustness

and reliability of these models in accurately capturing the dynamics and conformations of ADP. This type of issue has been previously reported in the literature⁹⁹ and is attributed to a lack of configurations in the training data that were observed during a molecular simulation. In some cases, the model can predict the potential energy and forces with a reasonable degree of accuracy. Still, the error adds up with every step until a threshold is passed and the system becomes unphysical. To optimize the model's hyperparameters, we performed a hyperparameter optimization using Weights and Biases, where we changed the batch size, learning rate, local cutoff, embedding multiplicity, and the number of layers. However, these changes did not result in a significant improvement in the model accuracy. Additional information can be found in Section I of the SI.

These results imply that for more complex systems like ADP, the model has trouble extrapolating the potential energies and forces for configurations which lie outside the training data. The multiple configurations of this molecule can result in the same CV values. However, these configurations could have very different potential energies and forces due to the different distances between atoms in the different configurations. As a result, it is possible that analyzing the sampled CVs of the training data gives us a good idea about the accuracy of the model to accurately describe the interactions within atomic environments. Still, it lacks resolution about the multiple configurations that result in the same CV value. Therefore, for systems like ADP or others more complex, there is the possibility of lacking coordinates that result in the same CV value but have different potential energy values. When the model is trained with this data, the model is expected to be accurate throughout all the configurational space of the system. However, it has challenges in high-free energy regions where it is hard to obtain training samples. Increasing the training data can alleviate this problem, but the increased computational resources needed to

perform training can be a limiting factor. Additionally, increasing the training data would diminish one of the main benefits of equivariant graph neural networks: the need for small training data sets compared to other NN approaches.

4. Deep Potential Metadynamics Simulations

This section presents the FES predicted by the trained MLPs of butane and ADP, it also discusses the causes of failure and success of the models. Additionally, we report the predictions' residuals and additional details supporting the discussion.

4.1 Butane

The predicted FES results for the butane MLPs trained with the eight distributions and the *ab initio* level of theory depicted in Figure 1 are presented in **Figure 11**. The results generally suggest good agreement of the predictions with the reference free energy values. The results indicate that the model with the highest MAE was the one trained with the Bias-Half-Left distribution, which value corresponds to 0.215 kcal/mol. These MAEs correspond to accuracies of to 7.64×10^{-3} kcal/(mol atom) and to 15.36×10^{-3} kcal/(mol atom), which is considered a good degree of accuracy for this test. Additional plots and information about these results and those obtained with models trained with classical data are available in Section VII of the SI.

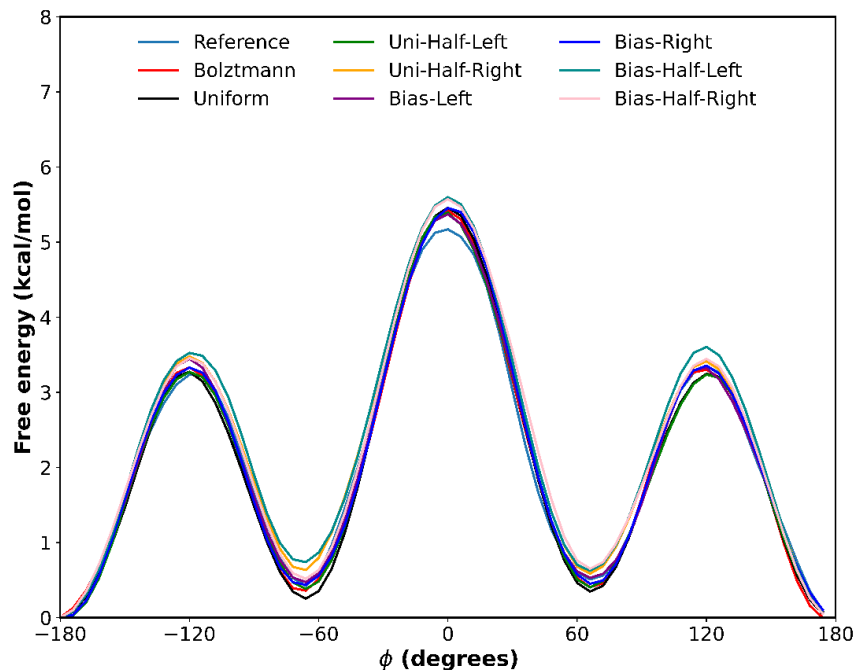


Figure 11. Free energy surface of butane as a function of the rotation of the dihedral angle predictions with models trained with distributions presented in Figure 1 at the *ab initio* level of theory.

The Metadynamics results derived from the butane models trained using the case A distribution effectively reconstructed the FES of the system at both classical and *ab initio* levels of theory, as showcased in **Figure 12**. The free energy surface of butane as a function of the rotation of its dihedral angle was predicted by the Allegro model trained with case A training at a) classical and b) *ab initio* level of theory. **Figure 12**. These results emphasize the model's proficiency in reconstructing the FES at both levels of theory using the training data from case A.

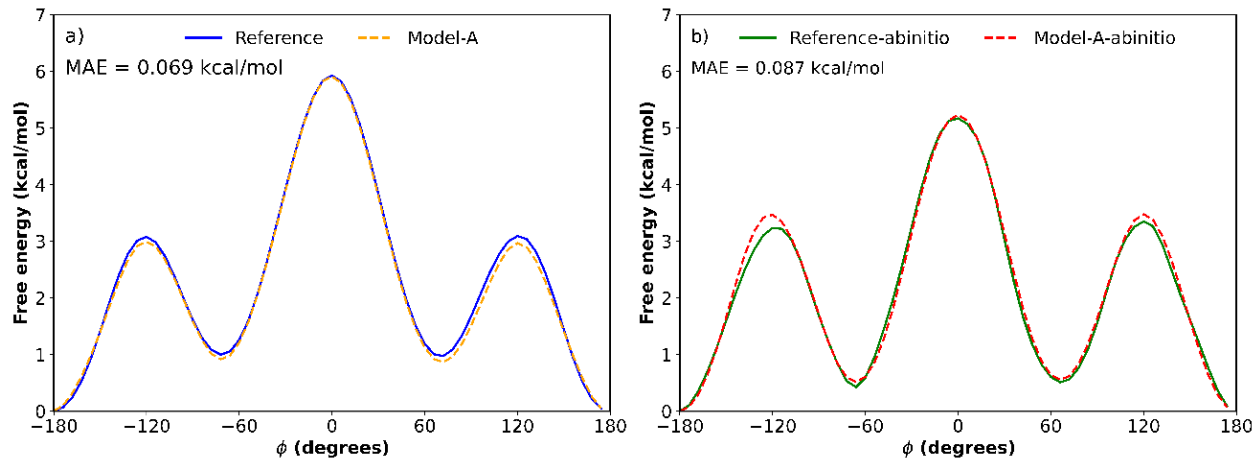


Figure 12. The free energy surface of butane as a function of the rotation of its dihedral angle was predicted by the Allegro model trained with case A training at a) classical and b) *ab initio* level of theory.

Panel a) presents the FES prediction results for the MLP trained with classical data, which generally agree well with the reference FES obtained from classical molecular dynamics. Slight deviations are observed near the free energy peak at 120° and the free energy valley at 60° . The model's accuracy is supported by the MAE of 0.069 kcal/mol which corresponds to 4.93×10^{-3} kcal/(mol atom). Similarly, results from the MLP trained with *ab initio* data presented in panel b) suggest the model predictions were less accurate near the free energy peak near -120° and 120° . However, the accuracy of the predictions remains acceptable with a MAE of 6.21×10^{-3} kcal/(mol atom). These results highlight the extrapolation capabilities of the Allegro model since training MLP with potential energies and forces of configurations that correspond only to the free energy minima of the system was sufficient to have a model that accurately describes the FES of the molecule. Conversely, MLPs trained with case B distribution, configurations representing only the global minimum of the FES, exhibited a notable lack of accuracy in predicting the location of free energy basins and the values of energy barriers at classical and *ab initio* theory levels, as evidenced in **Figure 13**. Despite both models qualitatively capturing the shape of the FES, the mean absolute error (MAE) for the model trained with classical data (panel a) was 32.43×10^{-3}

kcal/(mol atom), while for the model trained with ab initio data (panel b) it was 33.36×10^{-3} kcal/(mol atom).

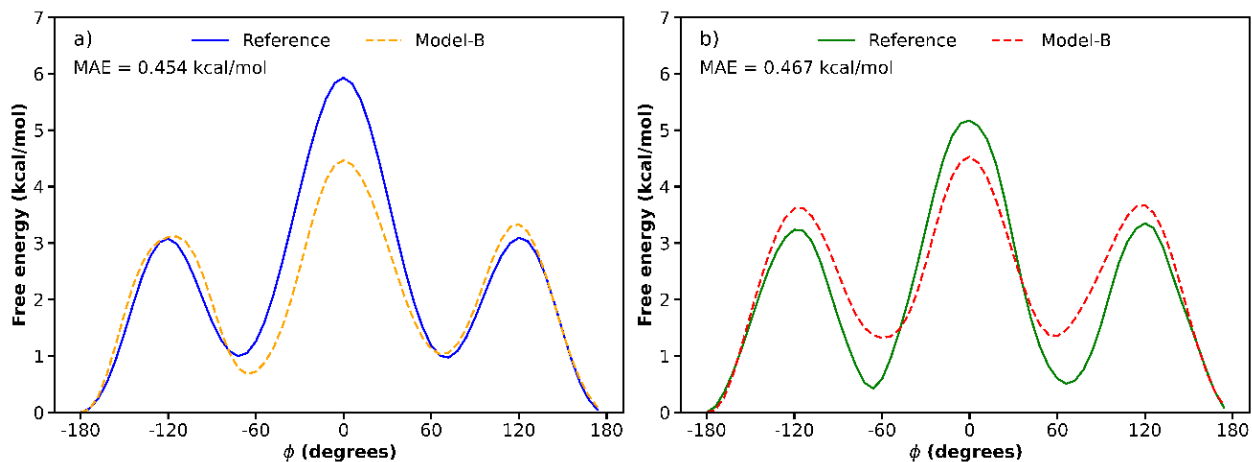


Figure 13. The free energy surface of butane as a function of the rotation of its dihedral angle was predicted by the Allegro model trained with case B training at a) classical and b) ab initio level of theory.

The inaccuracies of these models suggest that the training data was insufficient to allow the models to fully and accurately describe the energies of configurations not included in the training data. The accuracy difference between **Figure 12's** and **Figure 13's** results highlights the model's limitations to extrapolate the energy of configurations not observed during training. When the training data includes configurations that represent the characteristic minima of the molecule, the model shows good accuracy. Still, when training data lacks representations of distinct regions of the FES of the system, the model presents significant inaccuracies. This analysis implies that prior knowledge of the system FES is important when generating training data for a robust MLP capable of recovering the FES of the system through enhanced sampling simulations. It shows that a lack of data on characteristic regions of the FES will cause model inaccuracies. Additionally, the results imply that trained MLPs can have accurate prediction results for energies and forces, such as those presented in **Figure 7**, and lack accuracy in other tests related to the system's free energy, such as those in **Figure 8** and **Figure 13**. To obtain a better visualization of the regions in which the model

was less accurate, we plotted the residuals of the predictions as a function of the dihedral value, shown in **Figure 14**.

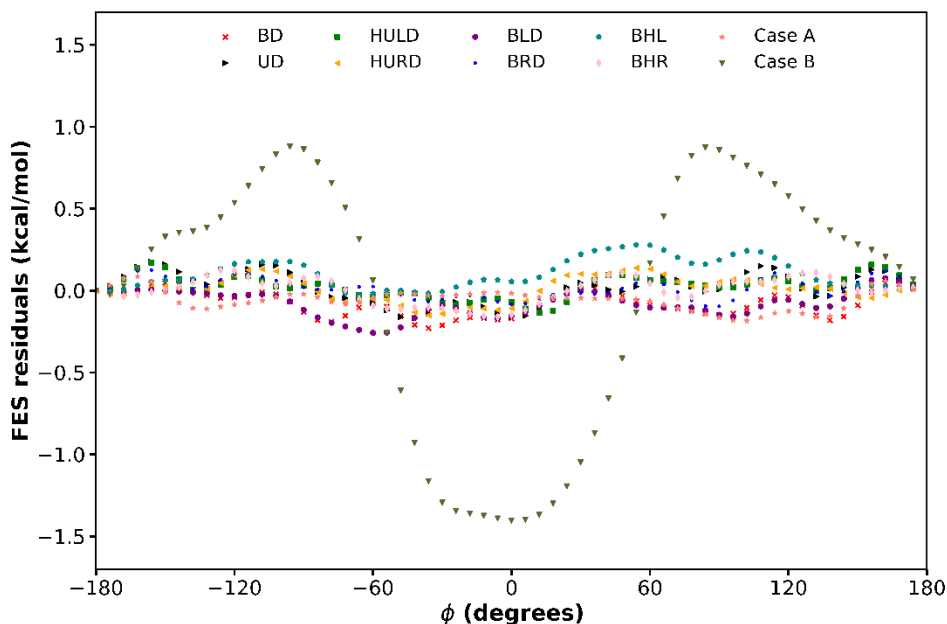


Figure 14. Residuals of free energy predictions with butane training data distribution at the classical level of theory.

The results indicate that all models, except for the one trained with Case B data, provided accurate predictions of the FES, as evidenced by the residuals being uniformly distributed around zero. As expected from the FES prediction in **Figure 13 a**), the residual for the MLP trained with case B data is significant in regions far from the global minimum (180°), where the training data was focused. Moreover, the extrapolation accuracy is also affected by the height of the free energy barrier, as confirmed by a higher residual magnitude at 0, where the highest free energy peak is located.

A similar plot for the models trained with *ab initio* accuracy are included in Section VIII of the SI, and they suggest that most models predicted the system's FES with good accuracy. However, predictions from MLPs trained with the bias-half-left (BHL), bias-half-right (BHR), and case A showed higher inaccuracies and variance in residuals than their counterparts trained with classical

data. This is attributed to the underlying accuracy of *ab initio* approaches compared to classical calculations. As a result, in classical MD, different configurations could have similar energetic values, while in AIMD, these configurations will have very different potential energies, resulting in a better energetic resolution between configurations. This allows MLPs trained with classical data to do a shorter extrapolation than MLPs trained with *ab initio* data when they encounter a configuration not included in the training set. To better illustrate this point, we calculated the error percentage of potential energy. We plotted as the second y-axis of the free energy vs dihedral value plot, presented in **Figure 15**.

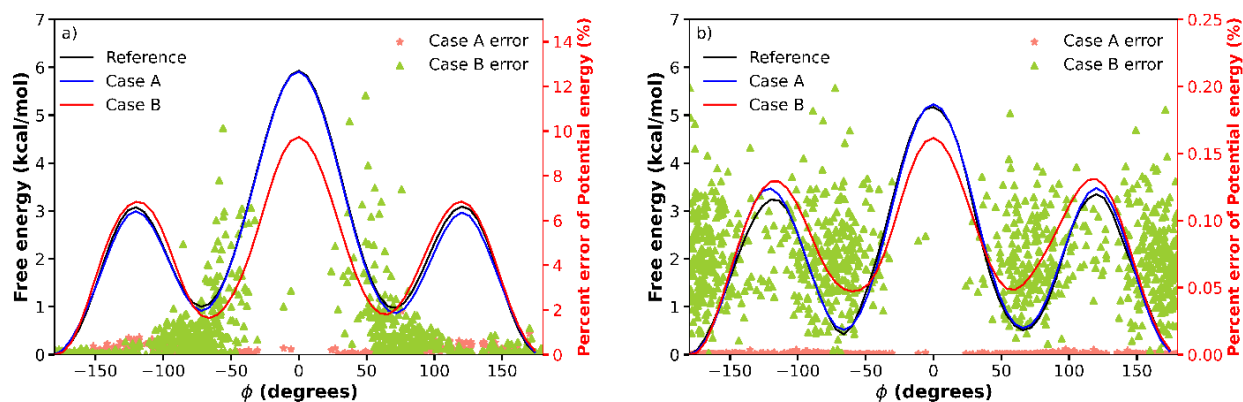


Figure 15. Butane's predicted FES with MLPs trained on Case A and Case B data versus dihedral angle, with the second y-axis displaying potential energy error percentage for MLPs trained on a) classical and b) *ab initio* data.

The markers in **Figure 15** indicate the percent error of potential energy predictions at different dihedral values. Results in panel a) suggest that the model trained with case A data successfully recovered the FES of the system, and the percentage error for the potential energy stayed under 1% in all the configurational space. However, results from the model trained with case B data indicate the model was more accurate near the global minimum of the system, which is expected since training data was focused on this region. Additionally, the free energy accuracy decreases as the value of the dihedral approaches zero. Similarly, the percentage error for potential energy increases as we get close to the region of maximum free energy, achieving values near 12%.

Results in panel b) suggest that models trained with *ab initio* accuracy maintained the percentage error for potential energy predictions under 0.25%. Results from the MLP trained with case A data showed good accuracy in predicting the FES of butane but showed error percentages under 0.05% across the configurational space. Predictions made by the MLP trained with case A data had minor deviations predicting the FES in regions of high free energy, and the error for potential energy was small. However, results from the model trained with case B data demonstrate a significant lack of accuracy when predicting the FES as we get away from the global minimum where the training data was focused. Independent of the accuracy of FES prediction, the percent error for potential energy predictions for this model did not follow the expected pattern observed for the MLP trained with classical, as seen in panel a) of **Figure 15**. These results imply that the model could predict the potential energy of configurations not included in the training data with high accuracy. Still, this accuracy is not reflected in FES prediction accuracy. Moreover, it is interesting to see that for these models, there is no significant difference between the error percentages in regions where there was training data and areas where there was not.

Overall, the results for butane MLPs have three principal implications. First, knowledge of the FES of the system is required to generate training data that will produce a robust model capable of predicting potential and free energy across all the configurational spaces of the system. For simple systems like butane, giving the model training data in the characteristic regions of the system's FES was sufficient to train accurate MLPs across all the configurational space. However, this can be a significant challenge for more complex systems where the FES is difficult to obtain. Second, the extrapolation accuracy of the model is reduced as the free energy of the configurations not included in the training data set increases. Again, it emphasized the need for prior knowledge of the FES to know the value of a CV at which there are free energy peaks, valleys, and transitions

in between. Finally, MLPs trained with ab initio data can show signs of reasonable accuracy in predicting energies and forces, but this does not necessarily reflect in the model's accuracy in predicting the FES of the system. Given the intrinsic importance of the free energy of a system for thermodynamic and dynamic properties, these implications leave open questions about the applicability of MLPs for such systems.

4.2 Alanine dipeptide (ADP)

The Allegro MLPs for ADP trained with uniform distribution and 2500 configurations were used to describe the atomic interactions in Metadynamics simulations aimed at reconstructing the system's FES. The predicted 2D FES was compared to the reference to obtain a heatmap of the MAEs, which is presented in Figure 16 a. These results indicate that the model had near zero MAE in regions of low free energy. Additionally, it is evident that the higher MAE was focused on regions of high free energy, corresponding to phi values higher than 100° for the ψ dihedral. The predicted free energy of ADP was plotted against the values of its ϕ dihedral in Figure 16 b. The converged outcome of the 2D and 1D FES are presented in **Figure 16**. Panel A illustrates the predicted free energy plotted against ϕ and ψ dihedrals, and Panel B only shows the free energy of the ϕ dihedral CV.

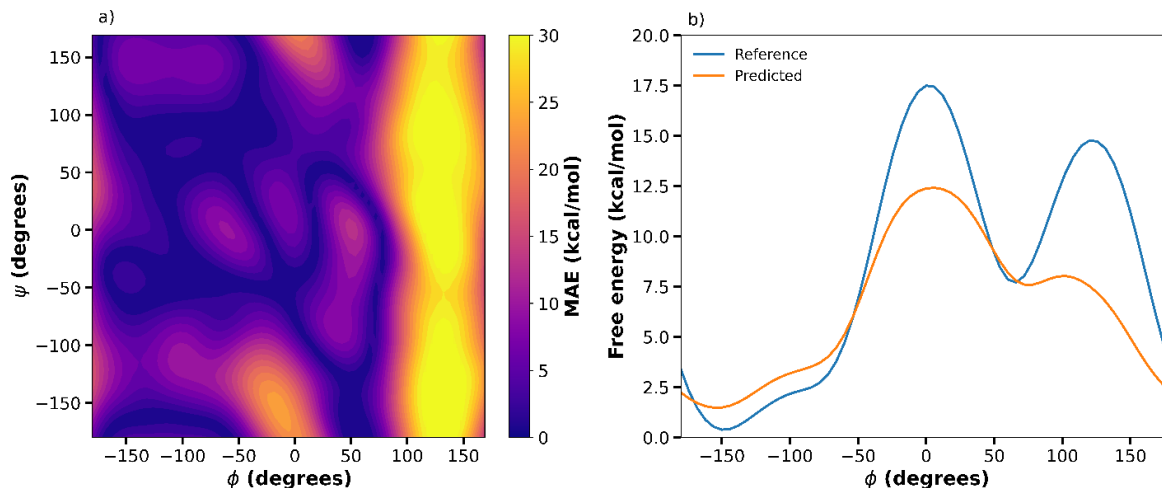


Figure 16. a) MAE heatmap of FES model predictions of alanine dipeptide as a function of its ϕ and ψ dihedral rotation. b) Predicted FES of alanine dipeptide as a function of the rotation of its ϕ dihedral. Both plots were obtained with the model trained with 2500 frames, a uniform distribution, and at the ab initio level of theory.

These results indicate that the model prediction of a global free energy minimum around -160° and two free energy peaks around 0° and 120° . Additionally, the model prediction of a local free energy minimum near 60° was shifted towards the larger angles. The lack of accuracy is further substantiated by the model's prediction MAE value of 2.59 kcal/mol, emphasizing significant discrepancies between the model's predictions and the ground truth values for ADP's FES. Similar results were achieved for the ADP MLPs trained with unbiased, only minima, and characteristic region distributions. FES predictions from the MLP trained solely with minima closely resembled those from the unbiased model. See Section IX of the SI for predictions from this model, while results for the other two models are depicted in **Figure 17**.

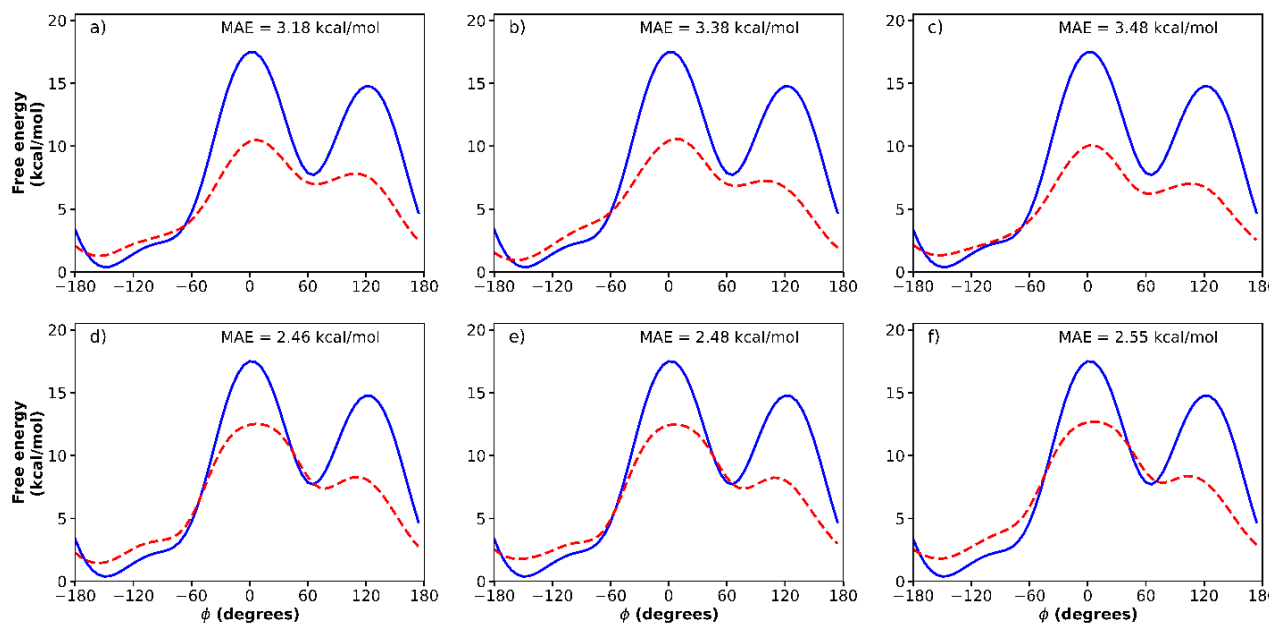


Figure 17. Free energy of alanine dipeptide as a function of the ϕ dihedral angle predicted by Allegro models trained with unbiased data including A) 500, B) 1000, and C) 2500 samples, and characteristic region (CharReg) data D) 500, E) 1000 and F) 2500 samples.

Panels a to c in **Figure 17** show the predicted FES and MAE for the models trained with the unbiased distribution using 500, 1000, and 2500 configurations, respectively. Meanwhile, panels d to f present the FES and MAE for models trained with 500, 1000, and 2500 configurations, respectively. Two key observations are derived from these results. First, the accuracy of FES predictions decreases when the number of configurations in the training data using each distribution increases. This goes against the expected trend, which suggests that the model's accuracy should improve with the amount of training data, as was observed for the energy and force prediction tests shown in **Table 2**. This is attributed to the training and test data configurations and those observed during Metadynamics simulations. In typical scenarios, such as in this study, the configurations encompassed within both the training and test datasets correspond to overlapping regions within the configurational space of the system. Ideally, these configurations would encompass the entirety of possible configurations, but for complex systems like ADP,

achieving this comprehensiveness presents a significant challenge. Consequently, the datasets often represent similar regions of FES, resulting in increased model accuracy within these regions as the quantity of training data grows. However, when MLPs are employed for Metadynamics simulations, the accuracy of predictions for the FES diminishes. This decline stems from slight overfitting of the models to the regions included in the training data, leading to more significant errors in areas not adequately represented in the training dataset.

The second key observation is that even though the ADP model trained with the uniform distribution and 2500 configurations had the smallest MAE in the energy and force evaluation test (Table 2), this was not the model with the smallest error for FES predictions. The most accurate FES prediction was done by the ADP MLP trained with the characteristic region distribution and 2500 configurations. The difference in MAE with the MLP trained with the uniform distribution and 2500 configurations was previously believed to be the most accurate, is of 0.04 kcal/mol. This difference provides insights into the model extrapolation capabilities since the uniform distribution has more dispersed configurations across the configurational space, and the characteristic region's distribution has more localized configurations in specific areas. This result implies that the model does not require information on all the configurational space, only on the characteristic regions of the FES. However, with more complex molecules, the possibility of having multiple configurations with similar CV values but very different energies and forces increases. As a result, one may think that the training data covers the whole configurational space, which might be accurate, but this does not equal having all the configurations that result in the same CV value.

The implications of these results are significant: they suggest that MLPs can show good prediction accuracy for potential energy and atomic forces and still fail to recover the FES of the system. This was the case with the butane MLPs trained with case B distribution and ADP MLPs

trained with the uniform and CharReg distributions. These results highlight the need for a more robust metric to assess the absolute accuracy of a model to describe the interactions in the entire configurational space of a system of interest. Additionally, the results highlight the need for prior knowledge of the system FES to generate the training data and validate the model's accuracy beyond its capacity to predict potential energy. This requirement raises significant questions about the usability and accuracy of MLPs for systems where the FES and corresponding CVs are not well defined. In such cases, a model could be trained and tested with configurations that fall in similar regions of the configurational space, giving the illusion of accuracy. Still, if this model were tested in an enhanced simulation, it would likely show inaccuracies and instabilities. The chance for this increases as the system and its FES become more complex. Additional efforts are required to develop new methodologies to enhance the robustness of training data sets and to develop metrics that ensure an MLP is accurate for a system in multiple tasks, including the prediction of the FES through enhanced sampling simulations.

5. Conclusions

Twenty MLPs were trained for the molecule butane, employing five distinct distributions of CVs within the training dataset. Additionally, twenty-six MLPs were trained for the more complex molecule ADP, utilizing thirteen distributions of CVs. Half of these models were trained with energies and forces computed at the classical level of theory, while the remaining half utilized identical configurations but with energies and forces calculated at the *ab initio* level of theory. After training, the MLPs were evaluated through energy and force prediction tests, analysis of sampled CVs in unbiased simulations, and accuracy of FES prediction via Metadynamics simulations.

The MLPs trained for butane exhibited consistent and satisfactory accuracy in predicting energy and forces across the test datasets, regardless of the specific distribution of CVs and level of theory used for model training. However, when CVs were localized in the global minimum, the accuracy of this prediction did not reflect the model's accuracy in describing the atoms' interactions in an unbiased simulation. The lack of accuracy is further evidenced by the failure of the model to recover the FES of butane.

For the case of ADP, the accuracy of energy and force predictions during testing was notably influenced by both the distribution of CVs and the level of theory utilized for training. MLPs trained with energies and forces derived from classical calculations for ADP demonstrated a reduced capacity to discern subtle variations in energies and forces among structurally similar configurations compared to models trained with *ab initio* calculations. This discrepancy ultimately led to diminished accuracy in the predictions of these models. The models trained with more dispersed datasets showed better accuracy overall. However, this accuracy was not reflected in unbiased and biased simulations. Several simulations presented unphysical structures for ADP. None of the ADP models could recover the FES of the system, which highlights the challenges in generating a robust training dataset for complex systems and the need for prior knowledge about the system FES.

Failure to accurately describe saddle points and free energy barriers will lead to inaccurate description of the system transition states which will result in inaccurate estimation of various thermodynamic and dynamic properties. Moreover, these inaccuracies are not necessarily identifiable in current evaluation approaches which test the model's capacity to recover the potential energy and atomic forces of a test set. EGNN models, such as Allegro, provide a new methodology to perform MD simulations with *ab initio* accuracy at a reduced computational cost,

but improved evaluation methodologies must be developed to ensure the accuracy and robustness of the model through all its configurational space.

Substantial limitations may emerge if the underlying FES of the system is either unknown or inadequately studied. Such circumstances can result in the development of MLPs that potentially provide a misleading perception of accuracy through current evaluation methodologies. Consequently, there is a pressing need for additional endeavors to optimize both the process of generating training data and the methods used for evaluation. These efforts should extend beyond the scope of potential energy and atomic force prediction capabilities to encompass a broader range of assessments, including free energy.

Code Availability

All the inputs and code required and used to obtain the results presented in this work are available in the following GitHub repository.

https://github.com/omendibleba/Considerations_for_MLPs_FES

Acknowledgments

This work was supported by the Department of Education via grant number P200A210048, and the University of Notre Dame. Computational resources were provided by the Notre Dame Center for Research Computing.

Conflicts of interest

The authors have no conflicts to disclose.

References

- (1) Wales, D. J.; Bogdan, T. V. Potential Energy and Free Energy Landscapes. *J. Phys. Chem. B* **2006**, *110* (42), 20765–20776. DOI: 10.1021/jp0680544.
- (2) Fiorin, G.; Klein, M. L.; Hénin, J. Using Collective Variables to Drive Molecular Dynamics Simulations. *Mol. Phys.* **2013**, *111* (22–23), 3345–3362. DOI: 10.1080/00268976.2013.813594.
- (3) Steele, J. A.; Lai, M.; Zhang, Y.; Lin, Z.; Hofkens, J.; Roeffaers, M. B. J.; Yang, P. Phase Transitions and Anion Exchange in All-Inorganic Halide Perovskites. *Accounts Mater. Res.* **2020**, *1* (1), 3–15. DOI: 10.1021/accountsmr.0c00009.
- (4) Walsh, A.; Catlow, C. R. A.; Smith, A. G. H.; Sokol, A. A.; Woodley, S. M. Strontium Migration Assisted by Oxygen Vacancies in SrTiO₃ from Classical and Quantum Mechanical Simulations. *Phys. Rev. B* **2011**, *83* (22), 220301. DOI: 10.1103/PhysRevB.83.220301.
- (5) Bousquet, D.; Coudert, F.-X.; Boutin, A. Free Energy Landscapes for the Thermodynamic Understanding of Adsorption-Induced Deformations and Structural Transitions in Porous Materials. *J. Chem. Phys.* **2012**, *137* (4), 44118. DOI: 10.1063/1.4738776.
- (6) Costa, M. G. S.; Batista, P. R.; Bisch, P. M.; Perahia, D. Exploring Free Energy Landscapes of Large Conformational Changes: Molecular Dynamics with Excited Normal Modes. *J. Chem. Theory Comput.* **2015**, *11* (6), 2755–2767. DOI: 10.1021/acs.jctc.5b00003.
- (7) Dutta, S.; Chandra, A. Free Energy Landscape of the Adenylation Reaction of the Aminoacylation Process at the Active Site of Aspartyl TRNA Synthetase. *J. Phys. Chem. B* **2022**, *126* (31), 5821–5831. DOI: 10.1021/acs.jpcc.2c03843.
- (8) Seibert, M. M.; Patriksson, A.; Hess, B.; van der Spoel, D. Reproducible Polypeptide Folding and Structure Prediction Using Molecular Dynamics Simulations. *J. Mol. Biol.* **2005**, *354* (1), 173–183. DOI: 10.1016/j.jmb.2005.09.030.
- (9) Altis, A.; Otten, M.; Nguyen, P. H.; Hegger, R.; Stock, G. Construction of the Free Energy Landscape of Biomolecules via Dihedral Angle Principal Component Analysis. *J. Chem. Phys.* **2008**, *128* (24), 245102. DOI: 10.1063/1.2945165.
- (10) Barducci, A.; Bonomi, M.; Parrinello, M. Metadynamics. *WIREs Comput. Mol. Sci.* **2011**, *1* (5), 826–843. DOI: 10.1002/wcms.31.
- (11) Kästner, J. Umbrella Sampling. *Wiley Interdiscip. Rev. Comput. Mol. Sci.* **2011**, *1* (6), 932–942. DOI: 10.1002/wcms.66.

- (12) Comer, J.; Gumbart, J. C.; Hénin, J.; Lelièvre, T.; Pohorille, A.; Chipot, C. The Adaptive Biasing Force Method: Everything You Always Wanted To Know but Were Afraid To Ask. *J. Phys. Chem. B* **2015**, *119* (3), 1129–1151. DOI: 10.1021/jp506633n.
- (13) Ren, W.; Vanden-Eijnden, E.; Maragakis, P.; E, W. Transition Pathways in Complex Systems: Application of the Finite-Temperature String Method to the Alanine Dipeptide. *J. Chem. Phys.* **2005**, *123* (13), 134109. DOI: 10.1063/1.2013256.
- (14) Lazim, R.; Suh, D.; Choi, S. Advances in Molecular Dynamics Simulations and Enhanced Sampling Methods for the Study of Protein Systems. *Int. J. Mol. Sci.* **2020**, *21* (17). DOI: 10.3390/ijms21176339.
- (15) Kumar, H.; Maiti, P. K. Introduction to Molecular Dynamics Simulation. **2011**, *23*, 161–197. DOI: 10.1007/978-93-86279-50-7_6.
- (16) Marx, D.; Grotendorst, J.; Blugel, S. *An Introduction to Ab Initio Molecular Dynamics Simulations*; Computational Nanoscience: Do It Yourself, Vol. 31, Citeseer, 2006; pp 195-244.
- (17) Car, R. Introduction to Density-Functional Theory and Ab-Initio Molecular Dynamics. *Quant. Struct. Relationships* **2002**, *21* (2), 97–104. doi: 10.1002/1521-3838(200207)21:2<97::AID-QSAR97>3.0.CO;2-6.
- (18) Friesner, R. A. *Ab Initio* Quantum Chemistry: Methodology and Applications. *Proc. Natl. Acad. Sci.* **2005**, *102* (19), 6648–6653. DOI: 10.1073/pnas.0408036102.
- (19) Piccini, G.; Lee, M. S.; Yuk, S. F.; Zhang, D.; Collinge, G.; Kollias, L.; Nguyen, M. T.; Glezakou, V. A.; Rousseau, R. Ab Initio Molecular Dynamics with Enhanced Sampling in Heterogeneous Catalysis. *Catal. Sci. Technol.* **2022**, *12* (1), 12–37. DOI: 10.1039/d1cy01329g.
- (20) Bailleul, S.; Dedecker, K.; Cnudde, P.; Vanduyfhuys, L.; Waroquier, M.; Van Speybroeck, V. Ab Initio Enhanced Sampling Kinetic Study on MTO Ethene Methylation Reaction. *J. Catal.* **2020**, *388*, 38–51. DOI: 10.1016/j.jcat.2020.04.015.
- (21) Schilling, M.; Cunha, R. A.; Luber, S. Zooming in on the O–O Bond Formation—An Ab Initio Molecular Dynamics Study Applying Enhanced Sampling Techniques. *J. Chem. Theory Comput.* **2020**, *16* (4), 2436–2449. DOI: 10.1021/acs.jctc.9b01207.
- (22) Shehu, A. An Ab-Initio Tree-Based Exploration to Enhance Sampling of Low-Energy Protein Conformations. *Robot. Sci. Syst.* **2010**, *5*, 241–248. DOI: 10.15607/rss.2009.v.031.

- (23) McCarty, J.; Parrinello, M. A Variational Conformational Dynamics Approach to the Selection of Collective Variables in Metadynamics. *J. Chem. Phys.* **2017**, *147* (20), 204109. DOI: 10.1063/1.4998598.
- (24) Coutinho, N. D.; Machado, H. G.; Carvalho-Silva, V. H.; da Silva, W. A. Topography of the Free Energy Landscape of Claisen–Schmidt Condensation: Solvent and Temperature Effects on the Rate-Controlling Step. *Phys. Chem. Chem. Phys.* **2021**, *23* (11), 6738–6745. DOI: 10.1039/D0CP05659F.
- (25) Baidya, A. T. K.; Kumar, A.; Kumar, R.; Darreh-Shori, T. Allosteric Binding Sites of Aβ Peptides on the Acetylcholine Synthesizing Enzyme ChAT as Deduced by In Silico Molecular Modeling. *Int. J. Mol. Sci.* **2022**, *23* (11). DOI: 10.3390/ijms23116073.
- (26) Wang, E.; Sun, H.; Wang, J.; Wang, Z.; Liu, H.; Zhang, J. Z. H.; Hou, T. End-Point Binding Free Energy Calculation with MM/PBSA and MM/GBSA: Strategies and Applications in Drug Design. *Chem. Rev.* **2019**, *119* (16), 9478–9508. DOI: 10.1021/acs.chemrev.9b00055.
- (27) Školáková, A.; Leitner, J.; Salvetr, P.; Novák, P.; Deduytsche, D.; Kopeček, J.; Detavernier, C.; Vojtěch, D. Kinetic and Thermodynamic Description of Intermediary Phases Formation in Ti-Al System during Reactive Sintering. *Mater. Chem. Phys.* **2019**, *230*, 122–130. DOI: 10.1016/j.matchemphys.2019.03.062.
- (28) Zhang, L.; Han, J.; Wang, H.; Car, R.; Weinan, E. Deep Potential Molecular Dynamics: A Scalable Model with the Accuracy of Quantum Mechanics. *Physical Review Letters*. 2018. DOI: 10.1103/PhysRevLett.120.143001.
- (29) Behler, J. Constructing High-Dimensional Neural Network Potentials: A Tutorial Review. *Int. J. Quantum Chem.* **2015**, *115* (16), 1032–1050. DOI: 10.1002/qua.24890.
- (30) Mueller, T.; Hernandez, A.; Wang, C. Machine Learning for Interatomic Potential Models. *J. Chem. Phys.* **2020**, *152* (5), 50902. DOI: 10.1063/1.5126336.
- (31) Manzhos, S.; Carrington, T. J. Neural Network Potential Energy Surfaces for Small Molecules and Reactions. *Chem. Rev.* **2021**, *121* (16), 10187–10217. DOI: 10.1021/acs.chemrev.0c00665.
- (32) Saucedo, H. E.; Vassilev-Galindo, V.; Chmiela, S.; Müller, K.-R.; Tkatchenko, A. Dynamical Strengthening of Covalent and Non-Covalent Molecular Interactions by Nuclear Quantum Effects at Finite Temperature. *Nat. Commun.* **2021**, *12* (1), 442. DOI: 10.1038/s41467-020-20212-1.

- (33) Zhang, W.; Weng, M.; Zhang, M.; Ye, Y.; Chen, Z.; Li, S.; Li, S.; Pan, F.; Wang, L. Revealing Morphology Evolution of Lithium Dendrites by Large-Scale Simulation Based on Machine Learning Force Field. *Adv. Energy Mater.* **2023**, *13* (4), 2202892. DOI: 10.1002/aenm.202202892.
- (34) Graser, J.; Kauwe, S. K.; Sparks, T. D. Machine Learning and Energy Minimization Approaches for Crystal Structure Predictions: A Review and New Horizons. *Chem. Mater.* **2018**, *30* (11), 3601–3612. DOI: 10.1021/acs.chemmater.7b05304.
- (35) Kang, Y.; Li, L.; Li, B. Recent Progress on Discovery and Properties Prediction of Energy Materials: Simple Machine Learning Meets Complex Quantum Chemistry. *J. Energy Chem.* **2021**, *54*, 72–88. DOI: 10.1016/j.jechem.2020.05.044.
- (36) Evans, R.; Hovan, L.; Tribello, G. A.; Cossins, B. P.; Estarellas, C.; Gervasio, F. L. Combining Machine Learning and Enhanced Sampling Techniques for Efficient and Accurate Calculation of Absolute Binding Free Energies. *J. Chem. Theory Comput.* **2020**, *16* (7), 4641–4654. DOI: 10.1021/acs.jctc.0c00075.
- (37) Yang, M.; Bonati, L.; Polino, D.; Parrinello, M. Using Metadynamics to Build Neural Network Potentials for Reactive Events: The Case of Urea Decomposition in Water. *Catal. Today* **2022**, *387*, 143–149. DOI: 10.1016/j.cattod.2021.03.018.
- (38) Deringer, V. L.; Caro, M. A.; Csányi, G. A General-Purpose Machine-Learning Force Field for Bulk and Nanostructured Phosphorus. *Nat. Commun.* **2020**, *11* (1), 5461. DOI: 10.1038/s41467-020-19168-z.
- (39) Johansson, A.; Xie, Y.; Owen, C. J.; Lim, J. S.; Sun, L.; Vandermause, J.; Kozinsky, B. Micron-Scale Heterogeneous Catalysis with Bayesian Force Fields from First Principles and Active Learning. **2022**, DOI: 10.48550/arXiv.2204.12573.
- (40) Galvelis, R.; Doerr, S.; Damas, J. M.; Harvey, M. J.; De Fabritiis, G. A Scalable Molecular Force Field Parameterization Method Based on Density Functional Theory and Quantum-Level Machine Learning. *J. Chem. Inf. Model.* **2019**, *59* (8), 3485–3493. DOI: 10.1021/acs.jcim.9b00439.
- (41) Behler, J.; Csányi, G. Machine Learning Potentials for Extended Systems: A Perspective. *Eur. Phys. J. B* **2021**, *94* (7), 1–11. DOI: 10.1140/epjb/s10051-021-00156-1.
- (42) Das Sarma, S.; Deng, D.-L.; Duan, L.-M. Machine Learning Meets Quantum Physics. *Phys. Today* **2019**, *72* (3), 48–54. DOI: 10.1063/PT.3.4164.
- (43) Wu, J.; Zhang, Y.; Zhang, L.; Liu, S. Deep Learning of Accurate Force Field of Ferroelectric HfO₂. *Phys. Rev. B* **2021**, *103* (2), 1–12. DOI: 10.1103/PhysRevB.103.024108.

- (44) Bartók, A. P.; Kondor, R.; Csányi, G. On Representing Chemical Environments. *Phys. Rev. B - Condens. Matter Mater. Phys.* **2013**, *87* (18), 1–19. DOI: 10.1103/PhysRevB.87.184115.
- (45) Ortner, C. On the Atomic Cluster Expansion: Interatomic Potentials and Beyond. **2023**, *1*, 1–5. DOI: 10.25950/c7f24234.
- (46) Kühne, R.; Ebert, R.-U.; Schüürmann, G. Chemical Domain of QSAR Models from Atom-Centered Fragments. *J. Chem. Inf. Model.* **2009**, *49* (12), 2660–2669. DOI: 10.1021/ci900313u.
- (47) Unke, O. T.; Chmiela, S.; Sauceda, H. E.; Gastegger, M.; Poltavsky, I.; Schütt, K. T.; Tkatchenko, A.; Müller, K.-R. Machine Learning Force Fields. *Chem. Rev.* **2021**, *121* (16), 10142–10186. DOI: 10.1021/acs.chemrev.0c01111.
- (48) Kocer, E.; Ko, T. W.; Behler, J. Neural Network Potentials: A Concise Overview of Methods. *Annu. Rev. Phys. Chem.* **2022**, *73*, 163–186. DOI: 10.1146/annurev-physchem-082720-034254.
- (49) Kolb, B.; Marshall, P.; Zhao, B.; Jiang, B.; Guo, H. Representing Global Reactive Potential Energy Surfaces Using Gaussian Processes. *J. Phys. Chem. A* **2017**, *121* (13), 2552–2557. DOI: 10.1021/acs.jpca.7b01182.
- (50) Deringer, V. L.; Bartók, A. P.; Bernstein, N.; Wilkins, D. M.; Ceriotti, M.; Csányi, G. Gaussian Process Regression for Materials and Molecules. *Chem. Rev.* **2021**, *121* (16), 10073–10141. DOI: 10.1021/acs.chemrev.1c00022.
- (51) Wang, H.; Zhang, L.; Han, J.; E, W. DeePMD-Kit: A Deep Learning Package for Many-Body Potential Energy Representation and Molecular Dynamics. *Comput. Phys. Commun.* **2018**, *228*, 178–184. DOI: 10.1016/j.cpc.2018.03.016.
- (52) Schütt, K. T.; Kindermans, P.-J.; Sauceda, H. E.; Chmiela, S.; Tkatchenko, A.; Müller, K.-R. SchNet: A Continuous-Filter Convolutional Neural Network for Modeling Quantum Interactions. **2017**. DOI: 10.48550/arXiv.1706.08566
- (53) Thölke, P.; De Fabritiis, G. *TorchMD-NET: Equivariant Transformers for Neural Network based Molecular Potentials*. **2022**. DOI: 10.48550/arXiv.2202.02541
- (54) Chmiela, S.; Sauceda, H. E.; Poltavsky, I.; Müller, K.-R.; Tkatchenko, A. SGDML: Constructing Accurate and Data Efficient Molecular Force Fields Using Machine Learning. *Comput. Phys. Commun.* **2019**, *240*, 38–45. DOI: 10.1016/j.cpc.2019.02.007.
- (55) Batzner, S.; Musaelian, A.; Sun, L.; Geiger, M.; Mailoa, J. P.; Kornbluth, M.; Molinari, N.; Smidt, T. E.; Kozinsky, B. E(3)-Equivariant Graph Neural Networks for Data-Efficient and Accurate Interatomic Potentials. **2021**. DOI: 10.1038/s41467-022-29939-5.

- (56) Gkeka, P.; Stoltz, G.; Barati Farimani, A.; Belkacemi, Z.; Ceriotti, M.; Chodera, J. D.; Dinner, A. R.; Ferguson, A. L.; Maillet, J.-B.; Minoux, H.; Peter, C.; Pietrucci, F.; Silveira, A.; Tkatchenko, A.; Trstanova, Z.; Wiewiora, R.; Lelièvre, T. Machine Learning Force Fields and Coarse-Grained Variables in Molecular Dynamics: Application to Materials and Biological Systems. *J. Chem. Theory Comput.* **2020**, *16* (8), 4757–4775. DOI: 10.1021/acs.jctc.0c00355.
- (57) Reiser, P.; Neubert, M.; Eberhard, A.; Torresi, L.; Zhou, C.; Shao, C.; Metni, H.; van Hoesel, C.; Schopmans, H.; Sommer, T.; Friederich, P. Graph Neural Networks for Materials Science and Chemistry. *Commun. Mater.* **2022**, *3* (1), 1–18. DOI: 10.1038/s43246-022-00315-6.
- (58) Musaelian, A.; Batzner, S.; Johansson, A.; Sun, L.; Owen, C. J.; Kornbluth, M.; Kozinsky, B. Learning Local Equivariant Representations for Large-Scale Atomistic Dynamics. **2022**. DOI: 10.1038/s41467-023-36329-y.
- (59) Musaelian, A.; Johansson, A.; Batzner, S.; Kozinsky, B. Scaling the Leading Accuracy of Deep Equivariant Models to Biomolecular Simulations of Realistic Size. **2023**. DOI: 10.48550/arXiv.2304.10061.
- (60) Lee, S.-H.; Li, J.; Olevano, V.; Sklénard, B. Equivariant Graph Neural Network Interatomic Potential for Green-Kubo Thermal Conductivity in Phase Change Materials. **2023**. DOI: 10.48550/arXiv.2307.02327.
- (61) Owen, C. J.; Torrissi, S. B.; Xie, Y.; Batzner, S.; Coulter, J.; Musaelian, A.; Sun, L.; Kozinsky, B. Complexity of Many-Body Interactions in Transition Metals via Machine-Learned Force Fields from the TM23 Data Set. **2023**. DOI: 10.48550/arXiv.2302.12993.
- (62) Plé, T.; Lagardère, L.; Piquemal, J.-P. Force-Field-Enhanced Neural Network Interactions: From Local Equivariant Embedding to Atom-in-Molecule Properties and Long-Range Effects. *Chem. Sci.* **2023**, *14*, 12554-12569. DOI: 10.1039/D3SC02581K
- (63) Kovács, D. P.; Moore, J. H.; Browning, N. J.; Batatia, I.; Horton, J. T.; Kapil, V.; Witt, W. C.; Magdău, I.-B.; Cole, D. J.; Csányi, G. MACE-OFF23: Transferable Machine Learning Force Fields for Organic Molecules. **2023**. DOI: 10.48550/arXiv.2312.15211
- (64) Vandermause, J.; Torrissi, S. B.; Batzner, S.; Xie, Y.; Sun, L.; Kolpak, A. M.; Kozinsky, B. On-the-Fly Active Learning of Interpretable Bayesian Force Fields for Atomistic Rare Events. *npj Comput. Mater.* **2020**, *6* (1). DOI: 10.1038/s41524-020-0283-z.

- (65) Zhang, Y.; Wang, H.; Chen, W.; Zeng, J.; Zhang, L.; Wang, H.; E, W. DP-GEN: A Concurrent Learning Platform for the Generation of Reliable Deep Learning Based Potential Energy Models. *Comput. Phys. Commun.* **2020**, *253*, 107206. DOI: 10.1016/j.cpc.2020.107206.
- (66) Daldrop, J. O.; Kappler, J.; Brünig, F. N.; Netz, R. R. Butane Dihedral Angle Dynamics in Water Is Dominated by Internal Friction. *Proc. Natl. Acad. Sci.* **2018**, *115* (20), 5169–5174. DOI: 10.1073/pnas.1722327115.
- (67) OTTER, W. K. D. E. N.; BRIELS, W. J. Free Energy from Molecular Dynamics with Multiple Constraints. *Mol. Phys.* **2000**, *98* (12), 773–781. DOI: 10.1080/00268970009483348.
- (68) Jorgensen, W. L.; Buckner, J. K. Use of Statistical Perturbation Theory for Computing Solvent Effects on Molecular Conformation. Butane in Water. *J. Phys. Chem.* **1987**, *91* (24), 6083–6085. DOI: 10.1021/j100308a003.
- (69) Beveridge, D. L.; DiCapua, F. M. Free Energy via Molecular Simulation: Applications to Chemical and Biomolecular Systems. *Annu. Rev. Biophys. Biophys. Chem.* **1989**, *18*, 431–492. DOI: 10.1146/annurev.bb.18.060189.002243.
- (70) Lau, W. F.; Montgomery Pettitt, B. Conformations of the Glycine Dipeptide. *Biopolymers* **1987**, *26* (11), 1817–1831. DOI: 10.1002/bip.360261102.
- (71) Ösabay, K.; Young, W. S.; Bashford, D.; Brooks, C. L.; Case, D. A. Dielectric Continuum Models for Hydration Effects on Peptide Conformational Transitions. *J. Phys. Chem.* **1996**, *100* (7), 2698–2705. DOI: 10.1021/jp9527315.
- (72) Rosso, L.; Abrams, J. B.; Tuckerman, M. E. Mapping the Backbone Dihedral Free-Energy Surfaces in Small Peptides in Solution Using Adiabatic Free-Energy Dynamics. *J. Phys. Chem. B* **2005**, *109* (9), 4162–4167. DOI: 10.1021/jp045399i.
- (73) Smith, P. E. The Alanine Dipeptide Free Energy Surface in Solution. *J. Chem. Phys.* **1999**, *111* (12), 5568–5579. DOI: 10.1063/1.479860.
- (74) Bohner, M. U.; Kästner, J. An Algorithm to Find Minimum Free-Energy Paths Using Umbrella Integration. *J. Chem. Phys.* **2012**, *137* (3), 34105. DOI: 10.1063/1.4736317.
- (75) Yao, S.; Van, R.; Pan, X.; Park, J. H.; Mao, Y.; Pu, J.; Mei, Y.; Shao, Y. Machine Learning Based Implicit Solvent Model for Aqueous-Solution Alanine Dipeptide Molecular Dynamics Simulations. *RSC Adv.* **2023**, *13* (7), 4565–4577. DOI: 10.1039/d2ra08180f.
- (76) Branduardi, D.; Gervasio, F. L.; Parrinello, M. From A to B in Free Energy Space. *J. Chem. Phys.* **2007**, *126* (5), 54103. DOI: 10.1063/1.2432340.

- (77) Prada-Gracia, D.; Gómez-Gardeñes, J.; Echenique, P.; Falo, F. Exploring the Free Energy Landscape: From Dynamics to Networks and Back. *PLoS Comput. Biol.* **2009**, *5* (6), e1000415. DOI: 10.1371/journal.pcbi.1000415.
- (78) Drozdov, A. N.; Grossfield, A.; Pappu, R. V. Role of Solvent in Determining Conformational Preferences of Alanine Dipeptide in Water. *J. Am. Chem. Soc.* **2004**, *126* (8), 2574–2581. DOI: 10.1021/ja039051x.
- (79) Poblete, H.; Miranda-Carvajal, I.; Comer, J. Determinants of Alanine Dipeptide Conformational Equilibria on Graphene and Hydroxylated Derivatives. *J. Phys. Chem. B* **2017**, *121* (15), 3895–3907. DOI: 10.1021/acs.jpcc.7b01130.
- (80) Thompson, A. P.; Aktulga, H. M.; Berger, R.; Bolintineanu, D. S.; Brown, W. M.; Crozier, P. S.; in 't Veld, P. J.; Kohlmeyer, A.; Moore, S. G.; Nguyen, T. D.; Shan, R.; Stevens, M. J.; Tranchida, J.; Trott, C.; Plimpton, S. J. LAMMPS - a Flexible Simulation Tool for Particle-Based Materials Modeling at the Atomic, Meso, and Continuum Scales. *Comput. Phys. Commun.* **2022**, *271*. DOI: 10.1016/J.CPC.2021.108171.
- (81) Tribello, G. A.; Bonomi, M.; Branduardi, D.; Camilloni, C.; Bussi, G. PLUMED 2: New Feathers for an Old Bird. *Comput. Phys. Commun.* **2014**, *185* (2), 604–613. DOI: 10.1016/j.cpc.2013.09.018.
- (82) Sidky, H.; Colón, Y. J.; Helfferich, J.; Sikora, B. J.; Bezik, C.; Chu, W.; Giberti, F.; Guo, A. Z.; Jiang, X.; Lequieu, J.; Li, J.; Moller, J.; Quevillon, M. J.; Rahimi, M.; Ramezani-Dakhel, H.; Rathee, V. S.; Reid, D. R.; Sevgen, E.; Thapar, V.; Webb, M. A.; Whitmer, J. K.; De Pablo, J. J. SSAGES: Software Suite for Advanced General Ensemble Simulations. *J. Chem. Phys.* **2018**, *148* (4). DOI: 10.1063/1.5008853.
- (83) Jorgensen, W. L.; Maxwell, D. S.; Tirado-Rives, J. Development and Testing of the OPLS All-Atom Force Field on Conformational Energetics and Properties of Organic Liquids. *J. Am. Chem. Soc.* **1996**, *118* (45), 11225–11236. DOI: 10.1021/ja9621760.
- (84) VandeVondele, J.; Krack, M.; Mohamed, F.; Parrinello, M.; Chassaing, T.; Hutter, J. Quickstep: Fast and Accurate Density Functional Calculations Using a Mixed Gaussian and Plane Waves Approach. *Comput. Phys. Commun.* **2005**, *167* (2), 103–128. DOI: 10.1016/j.cpc.2004.12.014.
- (85) Niemöller, H.; Blasius, J.; Hollóczki, O.; Kirchner, B. How Do Alternative Amino Acids Behave in Water? A Comparative Ab Initio Molecular Dynamics Study of Solvated α -Amino Acids and α -Amino Amidines. *J. Mol. Liq.* **2022**, *367*, 120282. DOI: 10.1016/j.molliq.2022.120282.
- (86) Zhang, Y.; Yang, W. Comment on “Generalized Gradient Approximation Made Simple”. *Phys. Rev. Lett.* **1998**, *80* (4), 890. DOI: 10.1103/PhysRevLett.80.890.

- (87) Goedecker, S.; Teter, M.; Hutter, J. Separable Dual-Space Gaussian Pseudopotentials. *Phys. Rev. B* **1996**, *54* (3), 1703–1710. DOI: 10.1103/PhysRevB.54.1703.
- (88) Hartwigsen, C.; Goedecker, S.; Hutter, J. Relativistic Separable Dual-Space Gaussian Pseudopotentials from H to Rn. *Phys. Rev. B* **1998**, *58* (7), 3641–3662. DOI: 10.1103/PhysRevB.58.3641.
- (89) Krack, M. Pseudopotentials for H to Kr Optimized for Gradient-Corrected Exchange-Correlation Functionals. *Theor. Chem. Acc.* **2005**, *114* (1), 145–152. DOI: 10.1007/s00214-005-0655-y.
- (90) VandeVondele, J.; Hutter, J. Gaussian Basis Sets for Accurate Calculations on Molecular Systems in Gas and Condensed Phases. *J. Chem. Phys.* **2007**, *127* (11), 114105. DOI: 10.1063/1.2770708.
- (91) Grimme, S.; Antony, J.; Ehrlich, S.; Krieg, H. A Consistent and Accurate Ab Initio Parametrization of Density Functional Dispersion Correction (DFT-D) for the 94 Elements H-Pu. *J. Chem. Phys.* **2010**, *132* (15), 154104. DOI: 10.1063/1.3382344.
- (92) Grimme, S.; Ehrlich, S.; Goerigk, L. Effect of the Damping Function in Dispersion Corrected Density Functional Theory. *J. Comput. Chem.* **2011**, *32* (7), 1456–1465. DOI: 10.1002/jcc.21759.
- (93) Kühne, T. D.; Iannuzzi, M.; Del Ben, M.; Rybkin, V. V.; Seewald, P.; Stein, F.; Laino, T.; Khaliullin, R. Z.; Schütt, O.; Schiffmann, F.; Golze, D.; Wilhelm, J.; Chulkov, S.; Bani-Hashemian, M. H.; Weber, V.; Borštnik, U.; Taillefumier, M.; Jakobovits, A. S.; Lazzaro, A.; Pabst, H.; Müller, T.; Schade, R.; Guidon, M.; Andermatt, S.; Holmberg, N.; Schenter, G. K.; Hehn, A.; Bussy, A.; Belleflamme, F.; Tabacchi, G.; Glöß, A.; Lass, M.; Bethune, I.; Mundy, C. J.; Plessl, C.; Watkins, M.; VandeVondele, J.; Krack, M.; Hutter, J. CP2K: An Electronic Structure and Molecular Dynamics Software Package - Quickstep: Efficient and Accurate Electronic Structure Calculations. *J. Chem. Phys.* **2020**, *152* (19), 194103. DOI: 10.1063/5.0007045.
- (94) Musaelian, A.; Batzner, S.; Johansson, A.; Sun, L.; Owen, C. J.; Kornbluth, M.; Kozinsky, B. Learning Local Equivariant Representations for Large-Scale Atomistic Dynamics. **2022**, 1–21. DOI: 10.1038/s41467-023-36329-y.
- (95) Biewald, L. Experiment Tracking with Weights and Biases. *Softw. available from wandb. com* **2020**, *2*, 233.
- (96) Wang, X.; Xu, Y.; Zheng, H.; Yu, K. A Scalable Graph Neural Network Method for Developing an Accurate Force Field of Large Flexible Organic Molecules. *J. Phys. Chem. Lett.* **2021**, *12* (33), 7982–7987. DOI: 10.1021/acs.jpcclett.1c02214.
- (97) Chmiela, S.; Sauceda, H. E.; Müller, K.-R.; Tkatchenko, A. Towards Exact Molecular Dynamics Simulations with Machine-Learned Force Fields. *Nat. Commun.* **2018**, *9* (1), 3887. DOI: 10.1038/s41467-018-06169-2.

- (98) Poltavsky, I.; Tkatchenko, A. Machine Learning Force Fields: Recent Advances and Remaining Challenges. *J. Phys. Chem. Lett.* **2021**, *12* (28), 6551–6564. DOI: 10.1021/acs.jpcllett.1c01204.
- (99) Fu, X.; Wu, Z.; Wang, W.; Xie, T.; Keten, S.; Gomez-Bombarelli, R.; Jaakkola, T. Forces Are Not Enough: Benchmark and Critical Evaluation for Machine Learning Force Fields with Molecular Simulations. **2022**. DOI: 10.48550/arXiv.2210.07237

Supporting Information
Considerations in the use of ML interaction potentials for free energy calculations

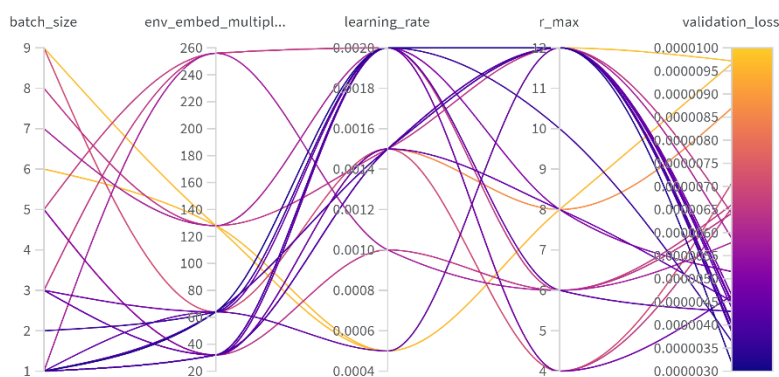
Orlando A. Mendible, Jonathan K. Whitmer, and Yamil J. Colón*
University of Notre Dame, IN 46556, USA
Corresponding author: ycolon@nd.edu

Table of Contents

Section I: Hyperparameter Optimization	2
Section II: Butane MLPs training and validation loss functions	3
Section III: Energy and force prediction results of butane MLPs.....	7
Section IV: Alanine dipeptide (ADP) MLPs training and validation loss functions	11
Section V: Energy and force prediction results of ADP MLPs	16
Section VI: Butane dihedral sampled in deep potential simulations.	24
Section VII. Butane FES predicted by Allegro models trained with Classical level of theory	26
Section VIII. Residuals of FES predicted by Allegro model trained with <i>ab initio</i> level of theory.	27
References.....	28

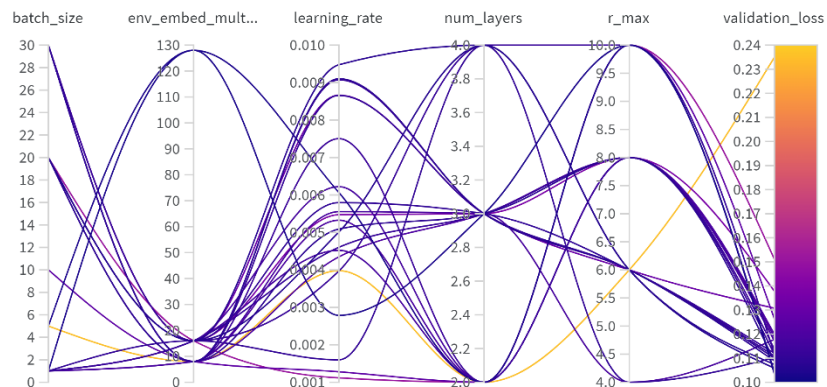
Section I: Hyperparameter Optimization

Hyperparameter optimization was conducted for butane and alanine dipeptide using the Weight-and-Biases¹ software. The selected parameters to be optimized were the batch size (i.e., an integer between 1 and 10), learning rate (0.0005,0.001,0.0015,0.002), maximum cutoff (r_max, 4, 6, 8, 10, 12), and neurons of the embedding multiplicity layer (env_embed_multiplicity, 32, 64, 128, 256). In the case of butane, 25 models were trained using the Boltzmann Distribution dataset with 5000 configurations and *ab initio* level of accuracy until early stopping was achieved using different combinations of parameters to select the one with the lowest validation loss value. The results for butane are presented in the Supplementary Figure 1.



Supplementary Figure 1. Hyperparameter optimization results for butane.

Results suggest that variations in the selected parameters do not significantly affect the achievable validation loss value. For alanine dipeptide, the optimization was conducted using the same hyperparameters previously described using the training dataset containing 2500 samples and a uniform distribution at the *ab initio* level of theory. The results of this optimization are presented in Supplementary Figure 2.

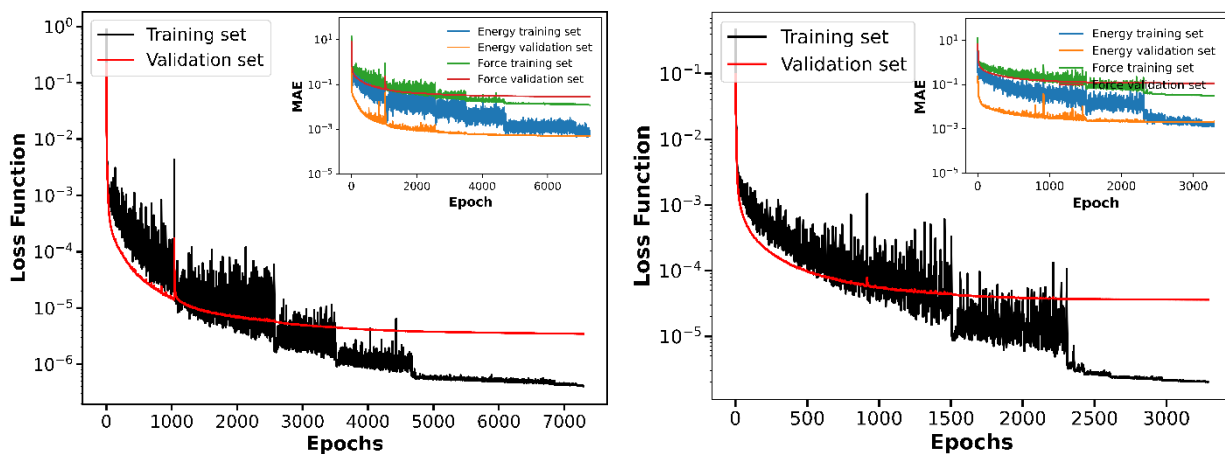


Supplementary Figure 2. Hyperparameter optimization results for alanine dipeptide.

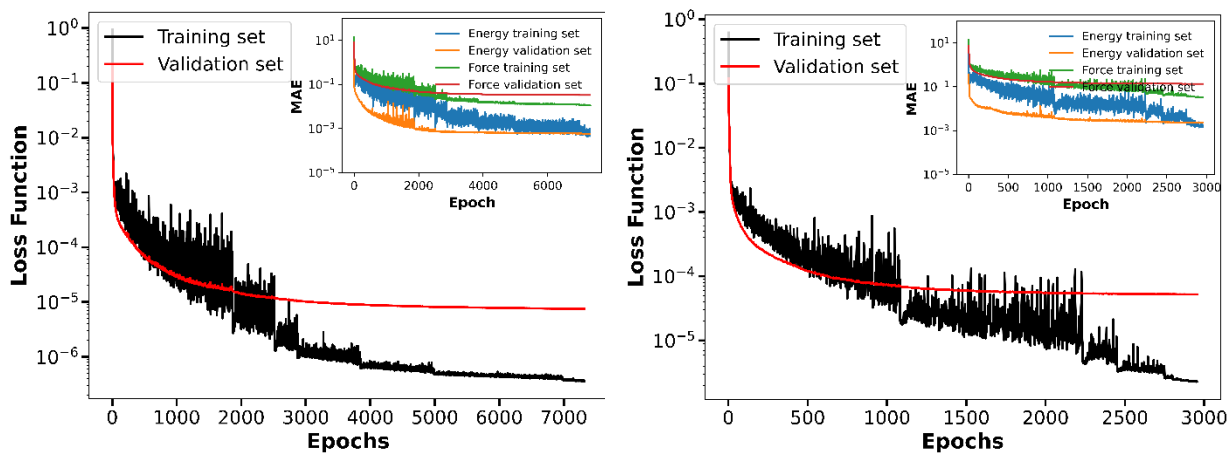
A more significant effect is observed for the ADP models, therefore the setting leading to the lower validation loss was selected and presented in the main paper.

Section II: Butane MLPs training and validation loss functions

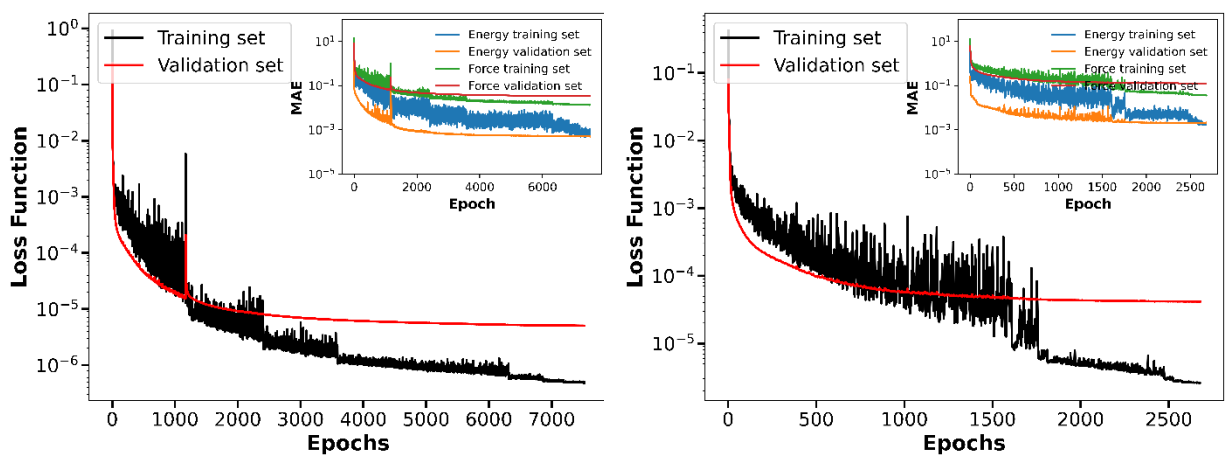
This section presents the logarithm of the loss function for the trained MLPs for butane using all the distributions presented in the paper at the classical and *ab initio* levels of theory.



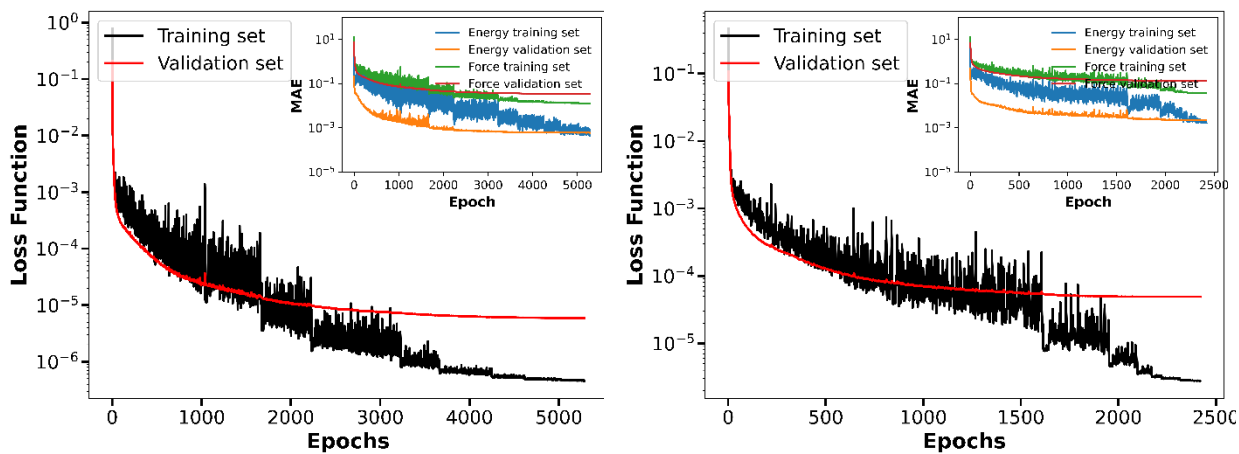
Supplementary Figure 3. Loss function of butane MLPs trained with Boltzmann distribution at the a) classical and b) *ab initio* levels of theory.



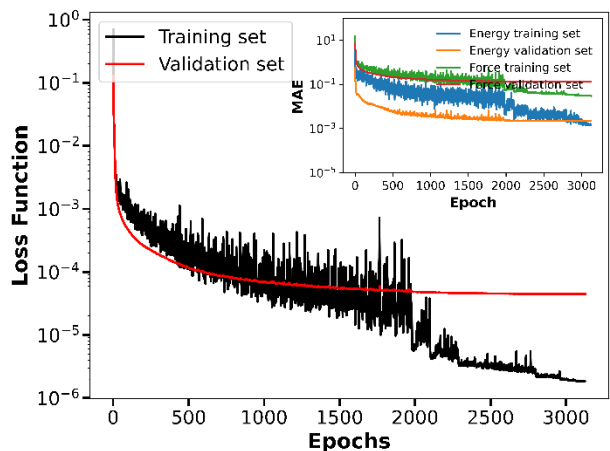
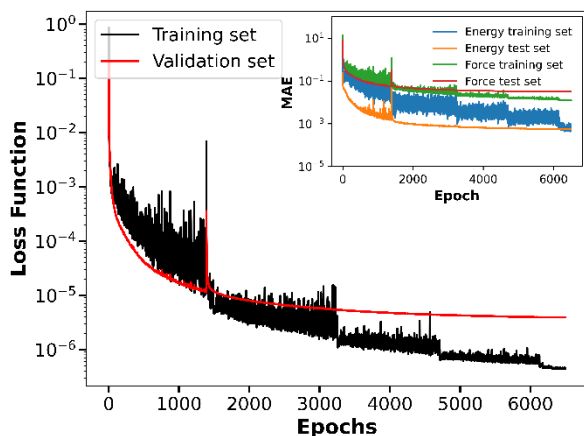
Supplementary Figure 4. Loss function of butane MLPs trained with uniform distribution at the a) classical and b) *ab initio* levels of theory.



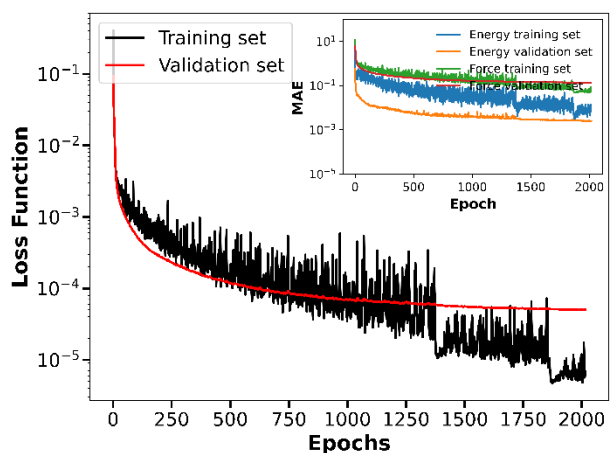
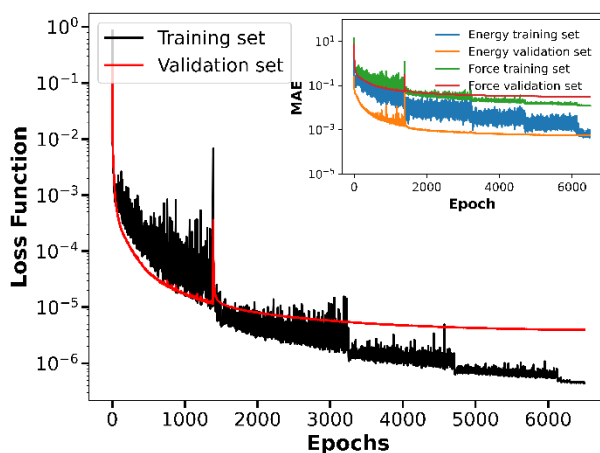
Supplementary Figure 5. Loss function of butane MLPs trained with half left uniform distribution at the a) classical and b) *ab initio* levels of theory.



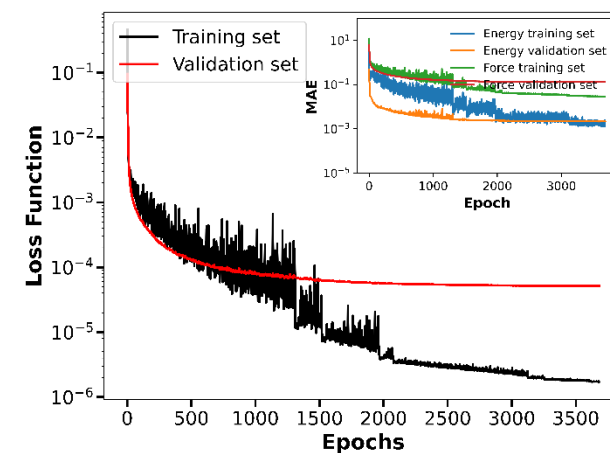
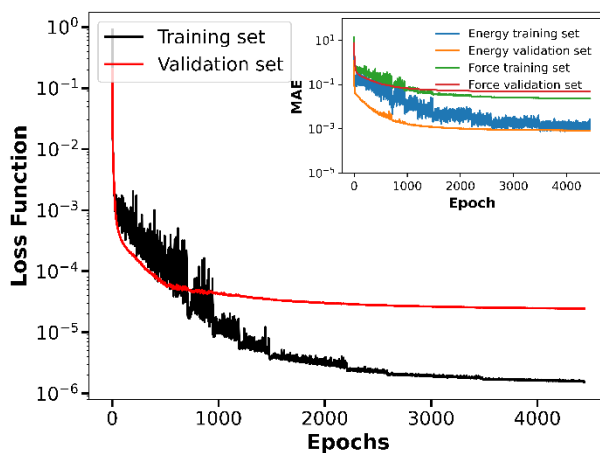
Supplementary Figure 6. Loss function of butane MLPs trained with half right uniform distribution at the a) classical and b) *ab initio* levels of theory.



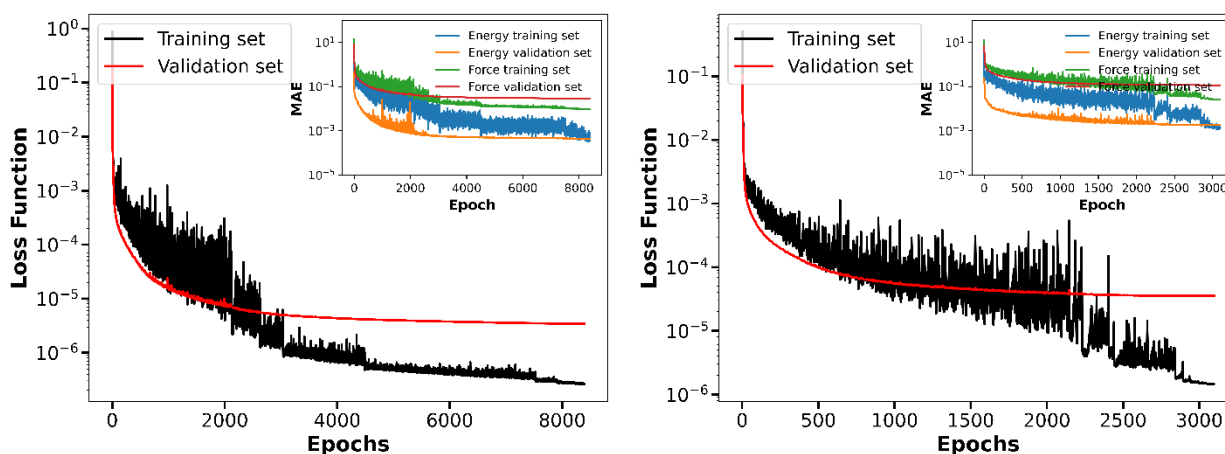
Supplementary Figure 7. Loss function of butane MLPs trained with bias left distribution at the a) classical and b) *ab initio* levels of theory.



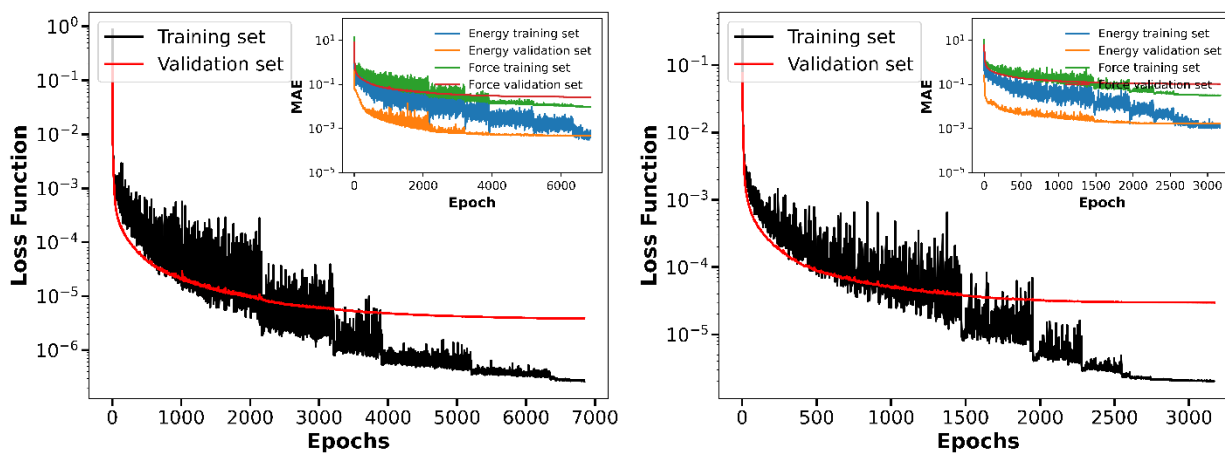
Supplementary Figure 8. Loss function of butane MLPs trained with bias right distribution at the a) classical and b) *ab initio* levels of theory.



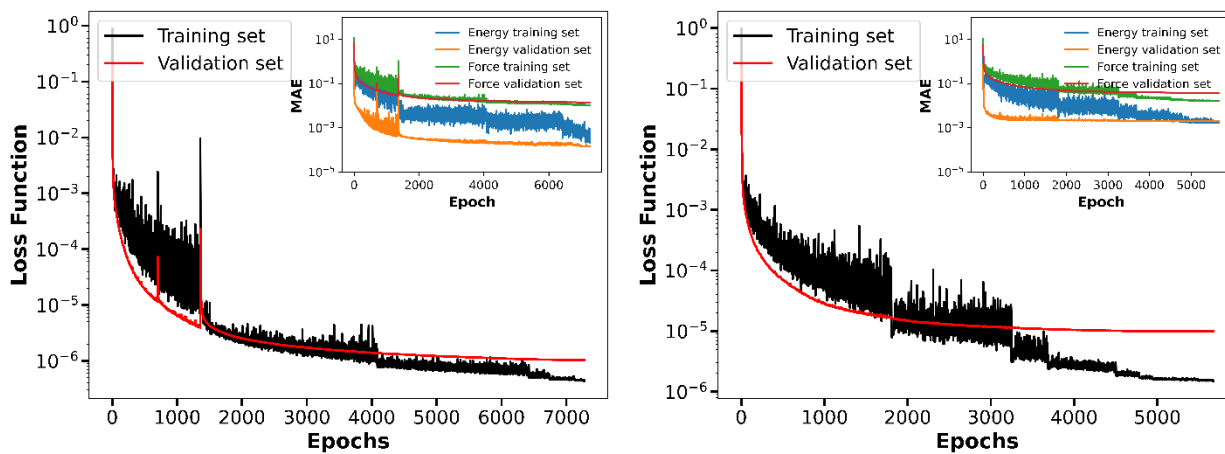
Supplementary Figure 9. Loss function of butane MLPs trained with bias half left distribution at the a) classical and b) *ab initio* levels of theory.



Supplementary Figure 10. Loss function of butane MLPs trained with bias half right distribution at the a) classical and b) *ab initio* levels of theory.

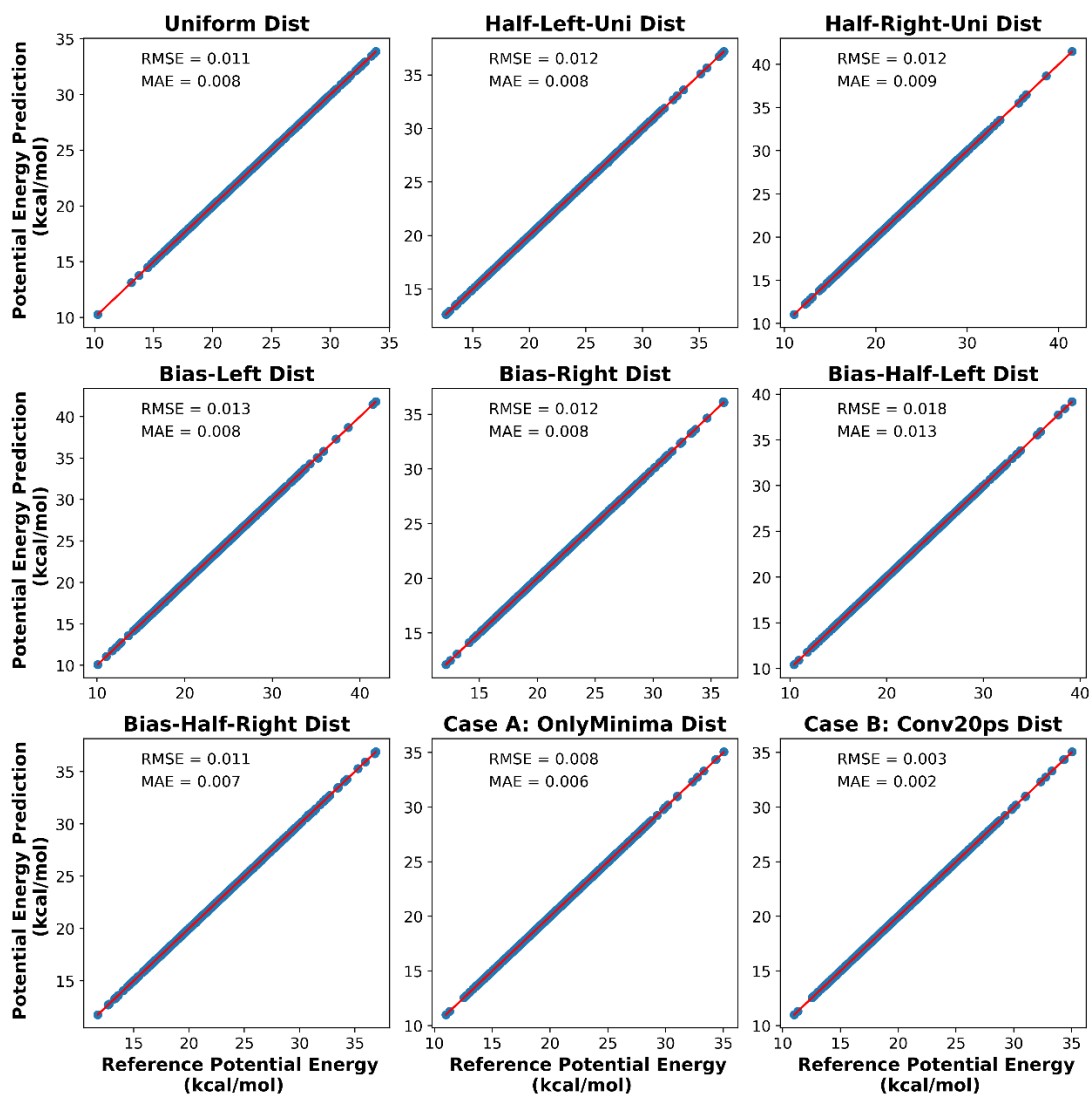


Supplementary Figure 11. Loss function of butane MLPs trained with case A (Only minima) distribution at the a) classical and b) *ab initio* levels of theory.

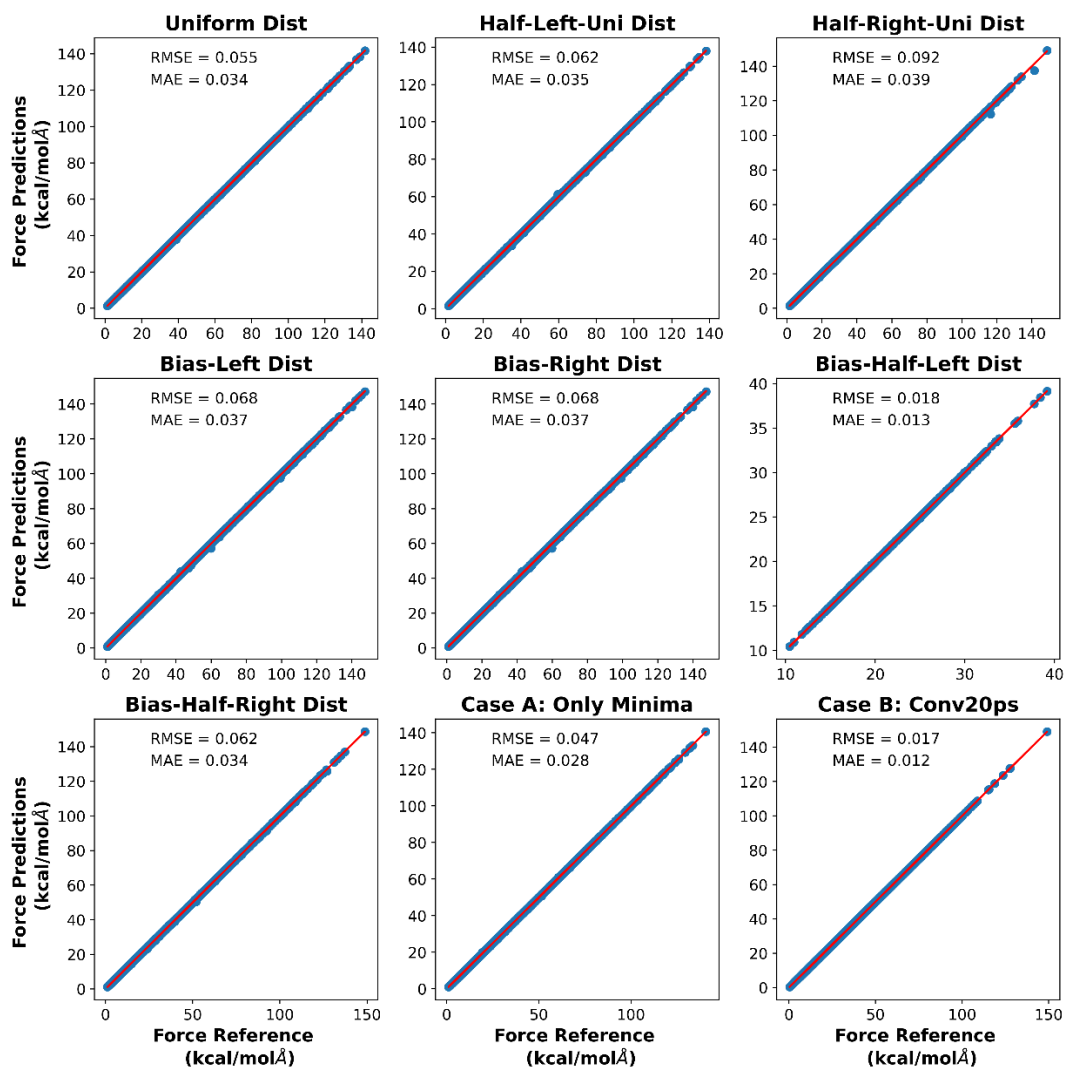


Supplementary Figure 12. Loss function of butane MLPs trained with case B (global minimum) distribution at the a) classical and b) *ab initio* levels of theory.

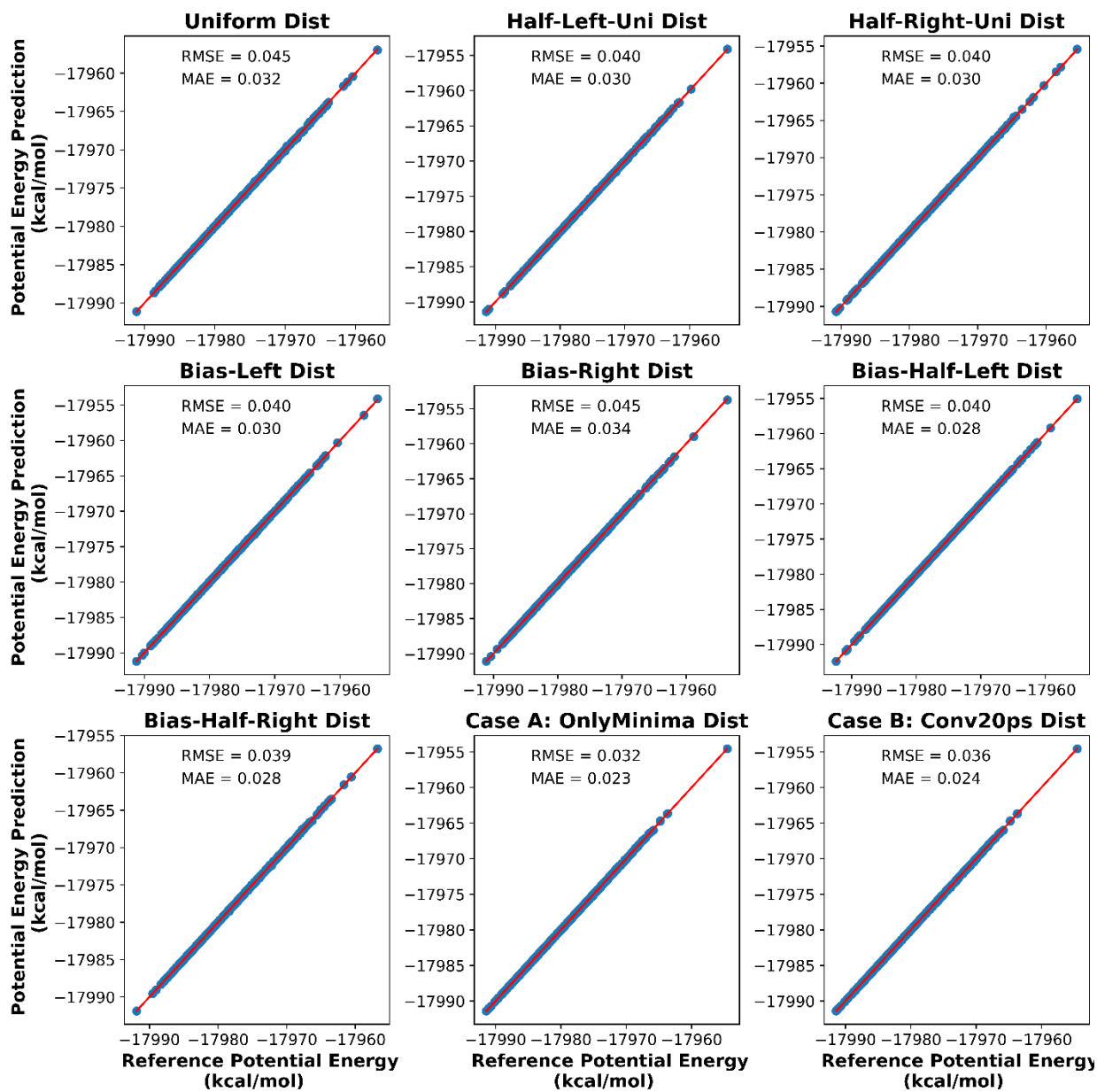
Section III: Energy and force prediction results of butane MLPs



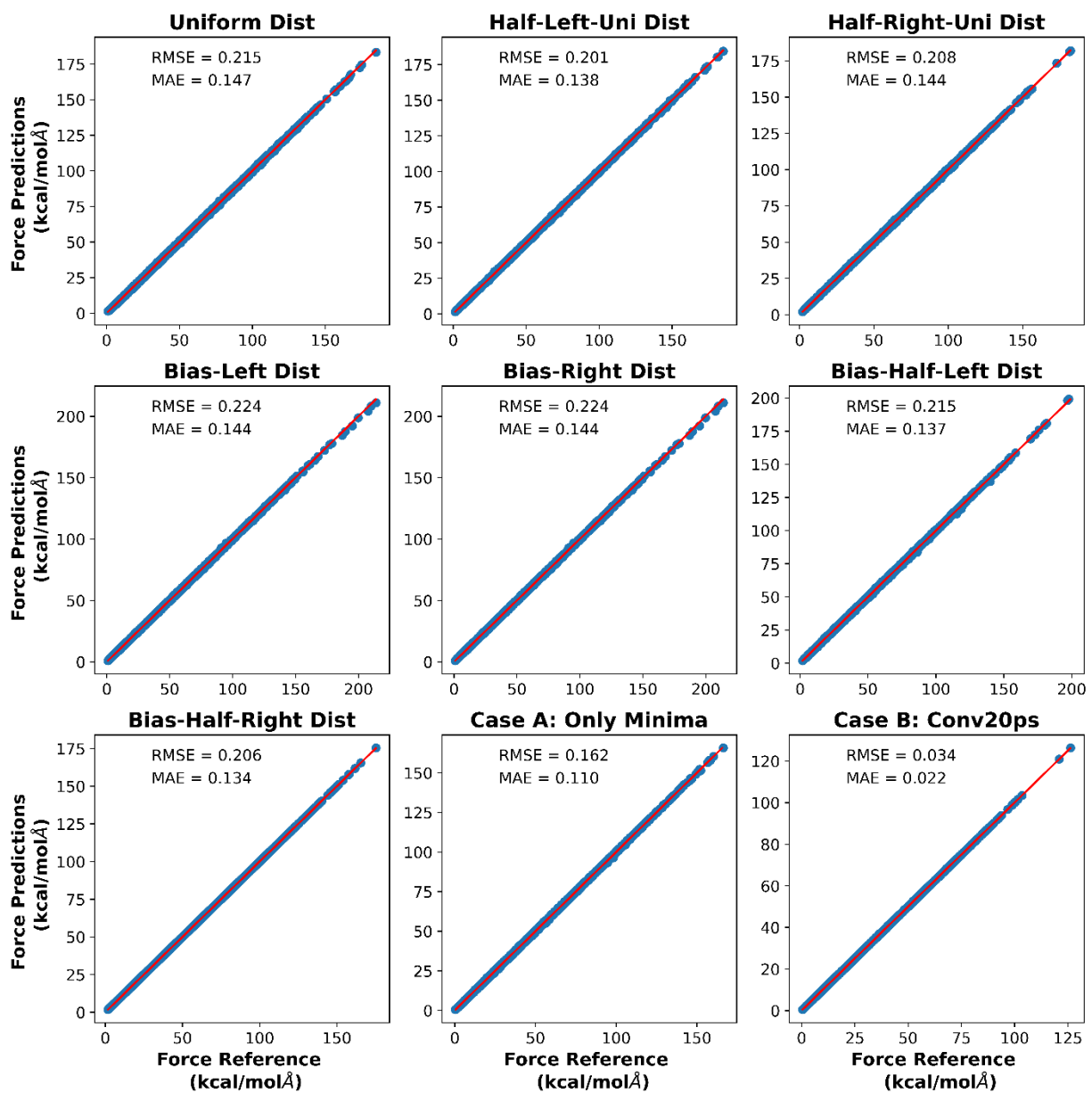
Supplementary Figure 13. Butane potential energy predictions made by trained Allegro models vs reference test values at the classical level of theory.



Supplementary Figure 14. Atomic force predictions made by trained Allegro models vs reference test values at the classical level of theory.



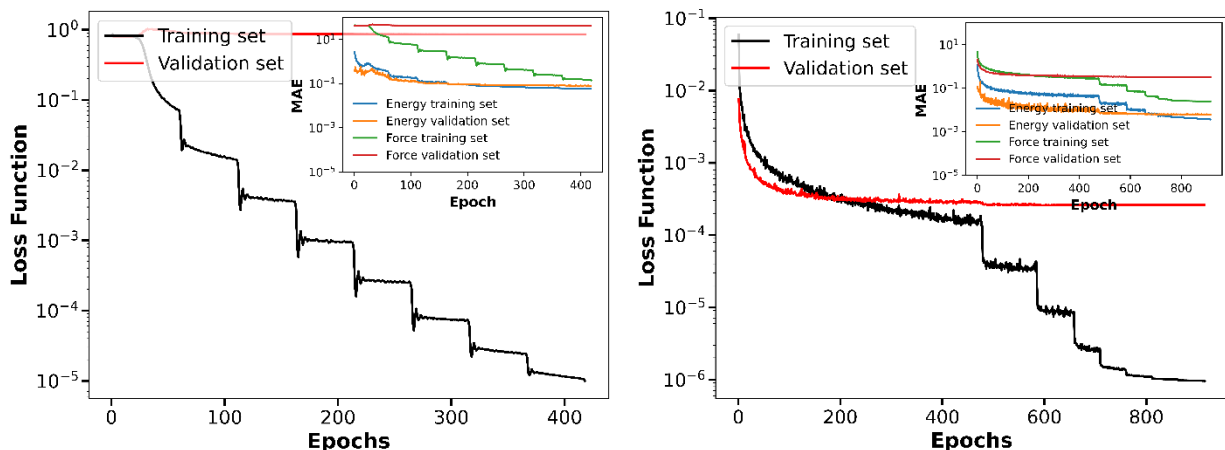
Supplementary Figure 15. Butane potential energy predictions made by trained Allegro models vs reference test values at the *ab initio* level of theory.



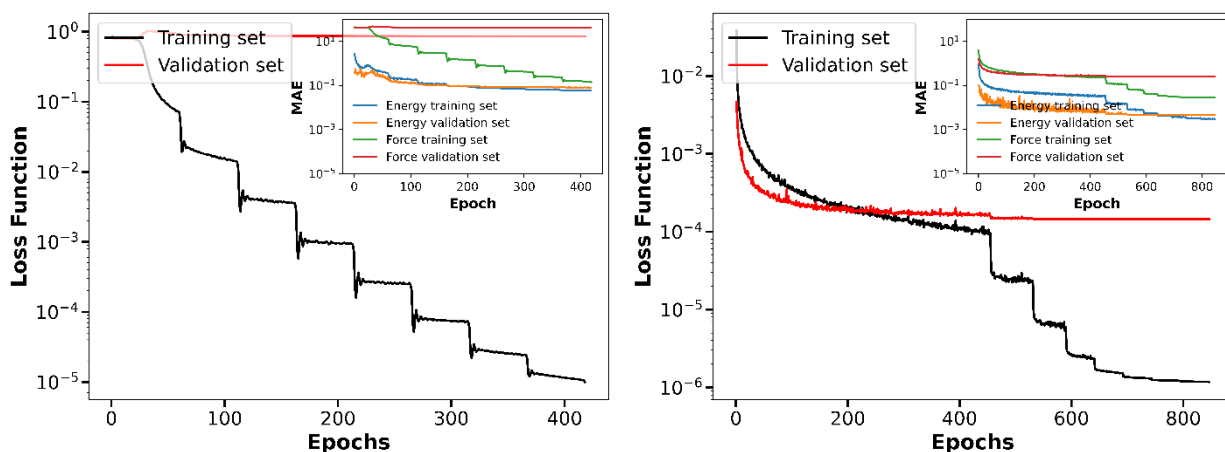
Supplementary Figure 16. Atomic force predictions made by trained Allegro models vs reference test values at the *ab initio* level of theory.

Section IV: Alanine dipeptide (ADP) MLPs training and validation loss functions

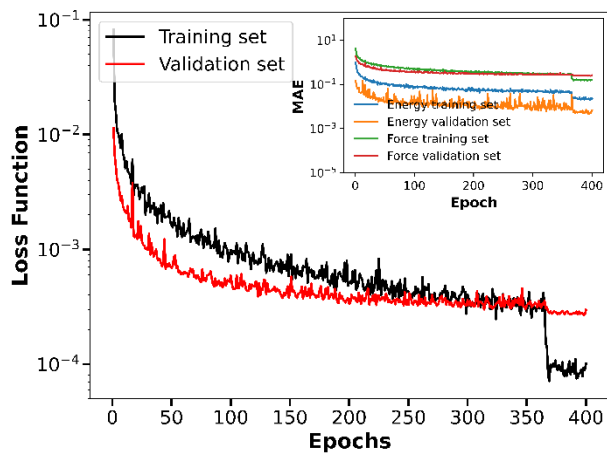
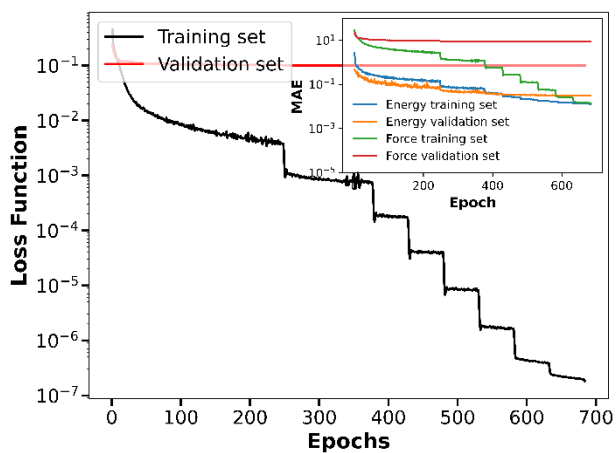
This section presents the logarithm of the loss function for the trained MLPs for ADP using all the distributions presented in the paper at the classical and *ab initio* levels of theory.



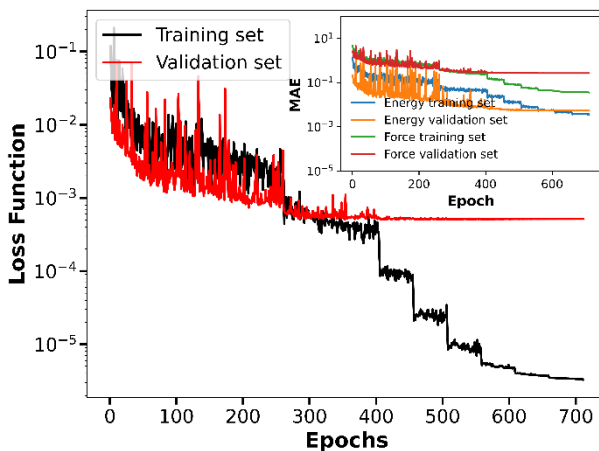
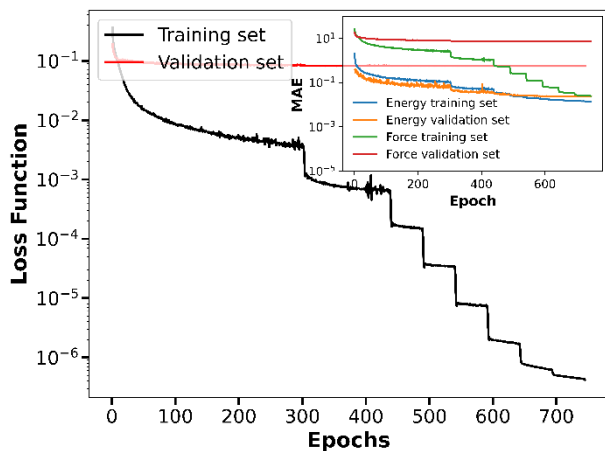
Supplementary Figure 17. Loss function of ADP MLPs trained with 2500 configurations and the Boltzmann distribution at the a) classical and b) *ab initio* levels of theory.



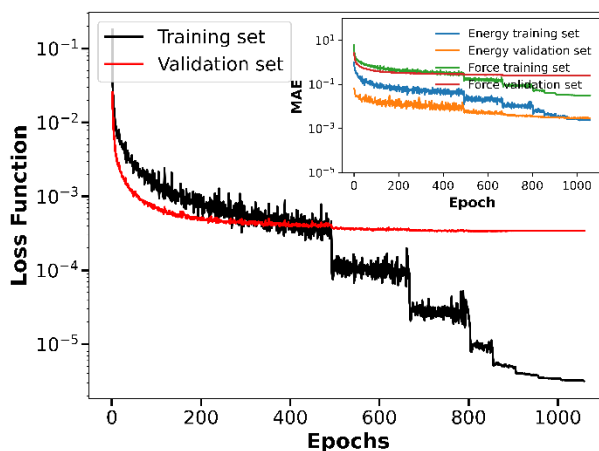
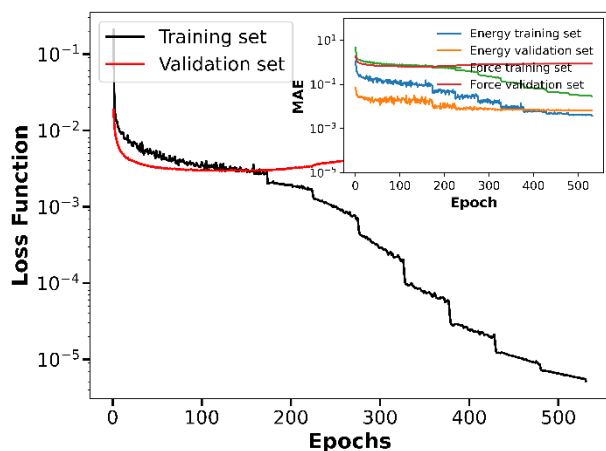
Supplementary Figure 18. Loss function of ADP MLPs trained with 5000 configurations and the Boltzmann distribution at the a) classical and b) *ab initio* levels of theory.



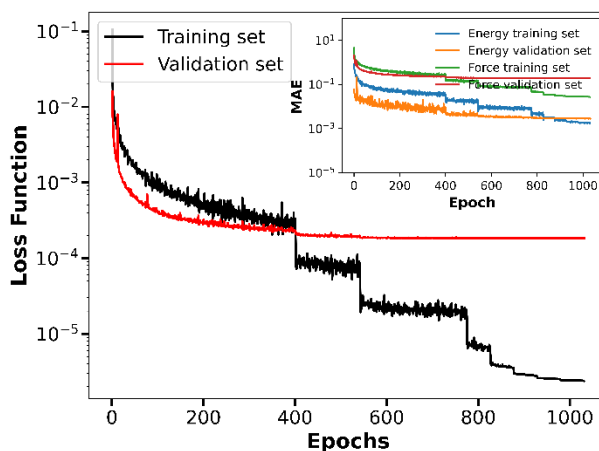
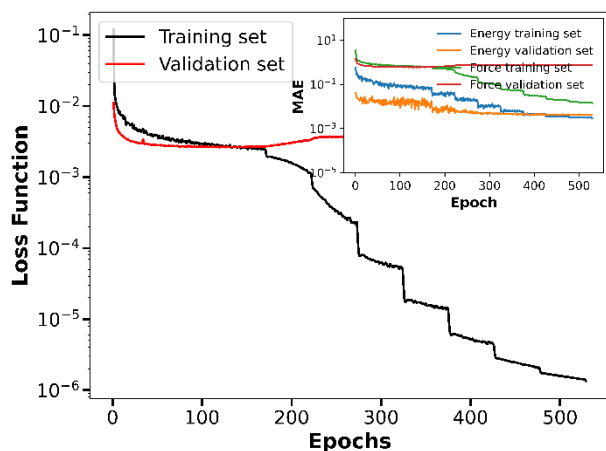
Supplementary Figure 19. Loss function of ADP MLPs trained with 2500 configurations and the uniform distribution at the a) classical and b) *ab initio* levels of theory.



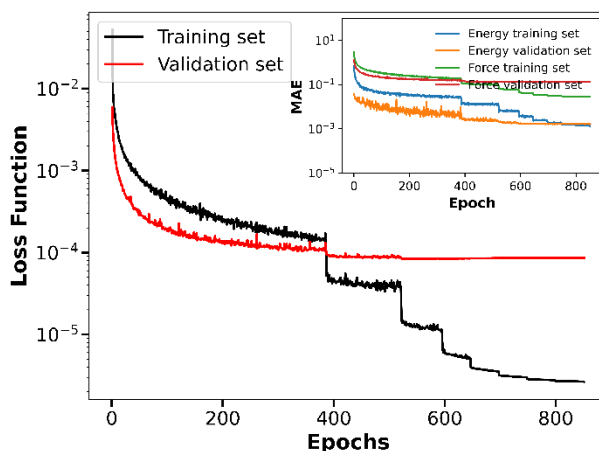
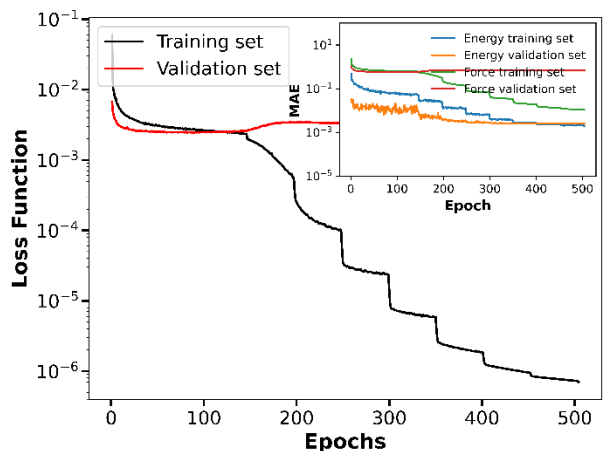
Supplementary Figure 20. Loss function of ADP MLPs trained with 5000 configurations and the uniform distribution at the a) classical and b) *ab initio* levels of theory.



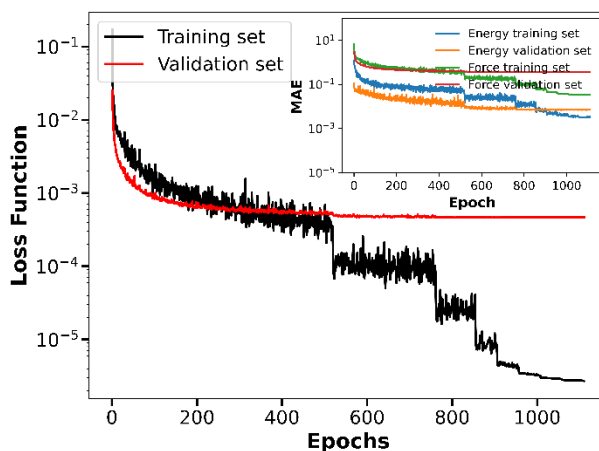
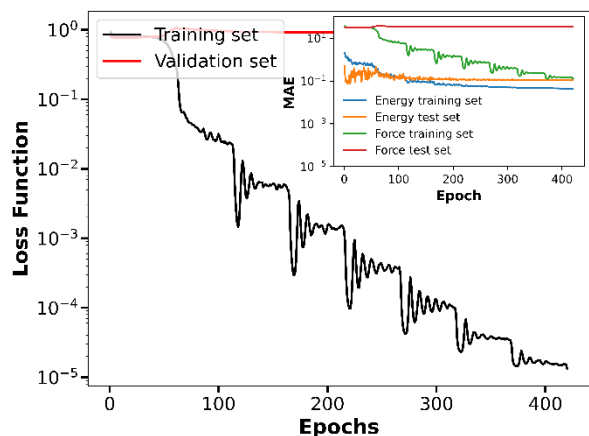
Supplementary Figure 21. Loss function of ADP MLPs trained with 500 configurations and the unbiased distribution at the a) classical and b) *ab initio* levels of theory.



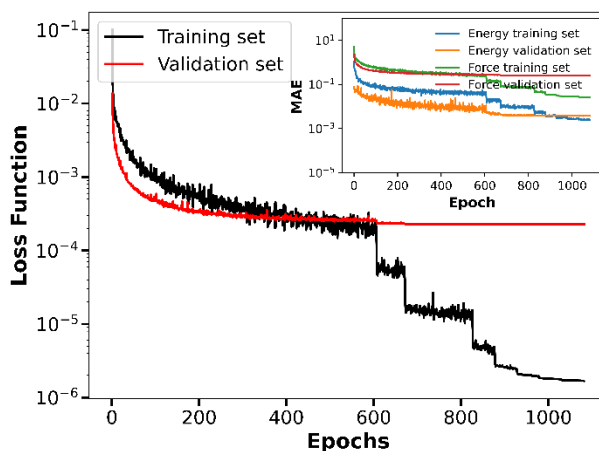
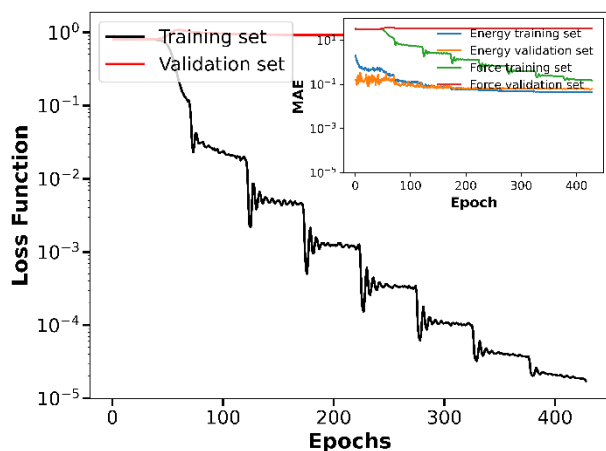
Supplementary Figure 22. Loss function of ADP MLPs trained with 1000 configurations and the unbiased distribution at the a) classical and b) *ab initio* levels of theory.



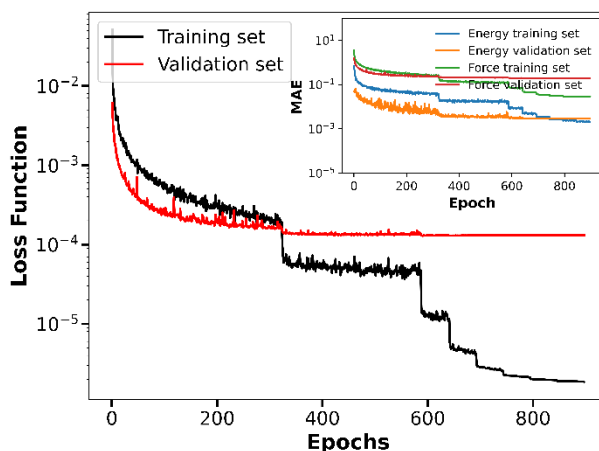
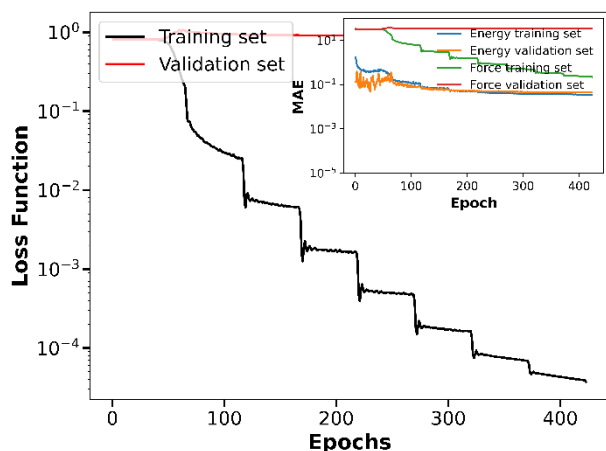
Supplementary Figure 23. Loss function of ADP MLPs trained with 2500 configurations and the unbiased distribution at the a) classical and b) *ab initio* levels of theory.



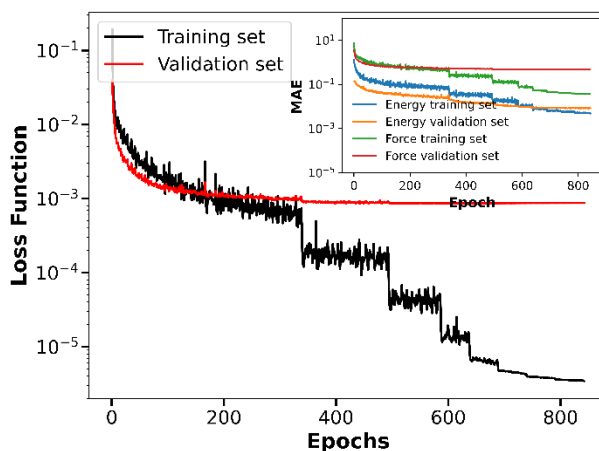
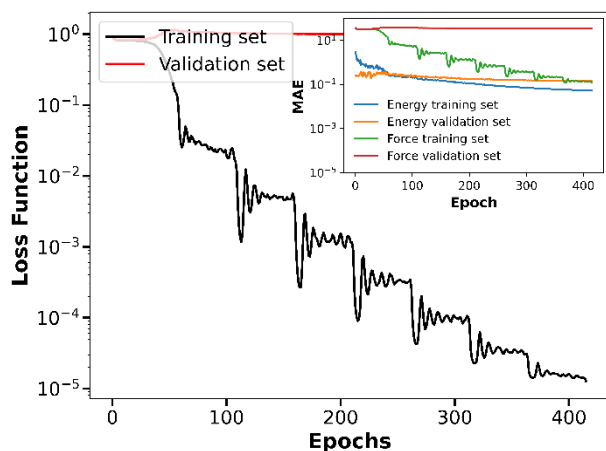
Supplementary Figure 24. Loss function of ADP MLPs trained with 500 configurations and the only minima distribution at the a) classical and b) *ab initio* levels of theory.



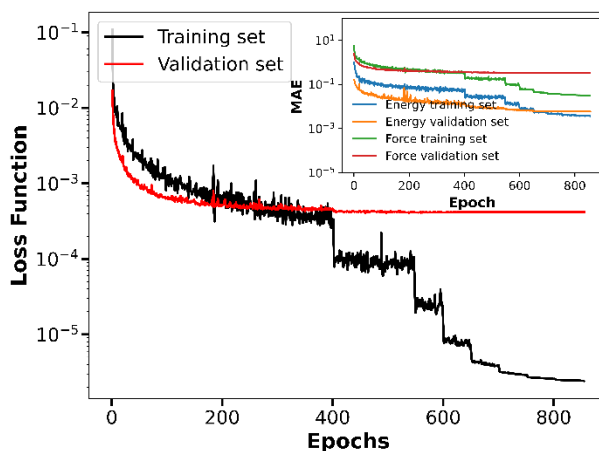
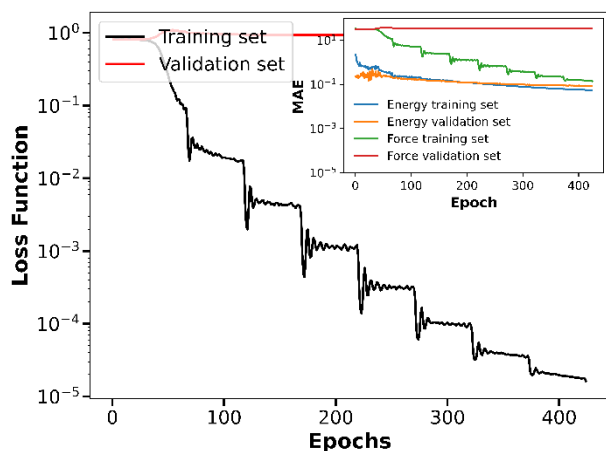
Supplementary Figure 25. Loss function of ADP MLPs trained with 1000 configurations and the only minima distribution at the a) classical and b) *ab initio* levels of theory.



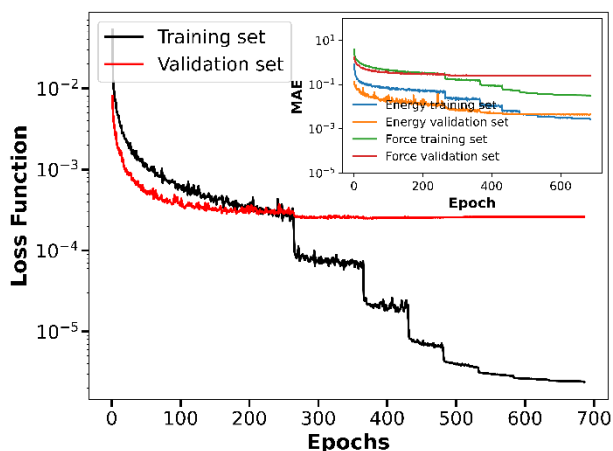
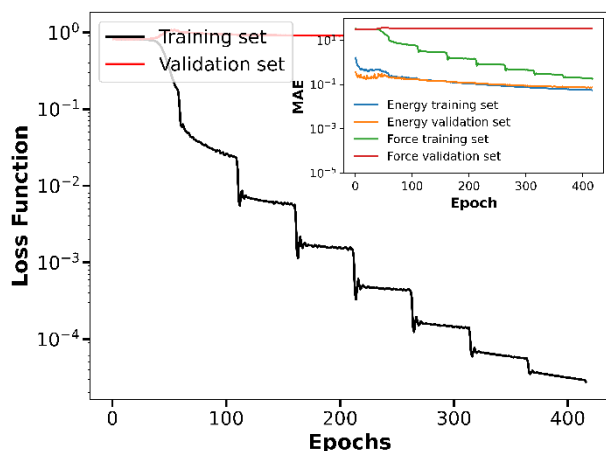
Supplementary Figure 26. Loss function of ADP MLPs trained with 2500 configurations and the only minima distribution at the a) classical and b) *ab initio* levels of theory.



Supplementary Figure 27. Loss function of ADP MLPs trained with 500 configurations and the characteristic regions distribution at the a) classical and b) *ab initio* levels of theory.

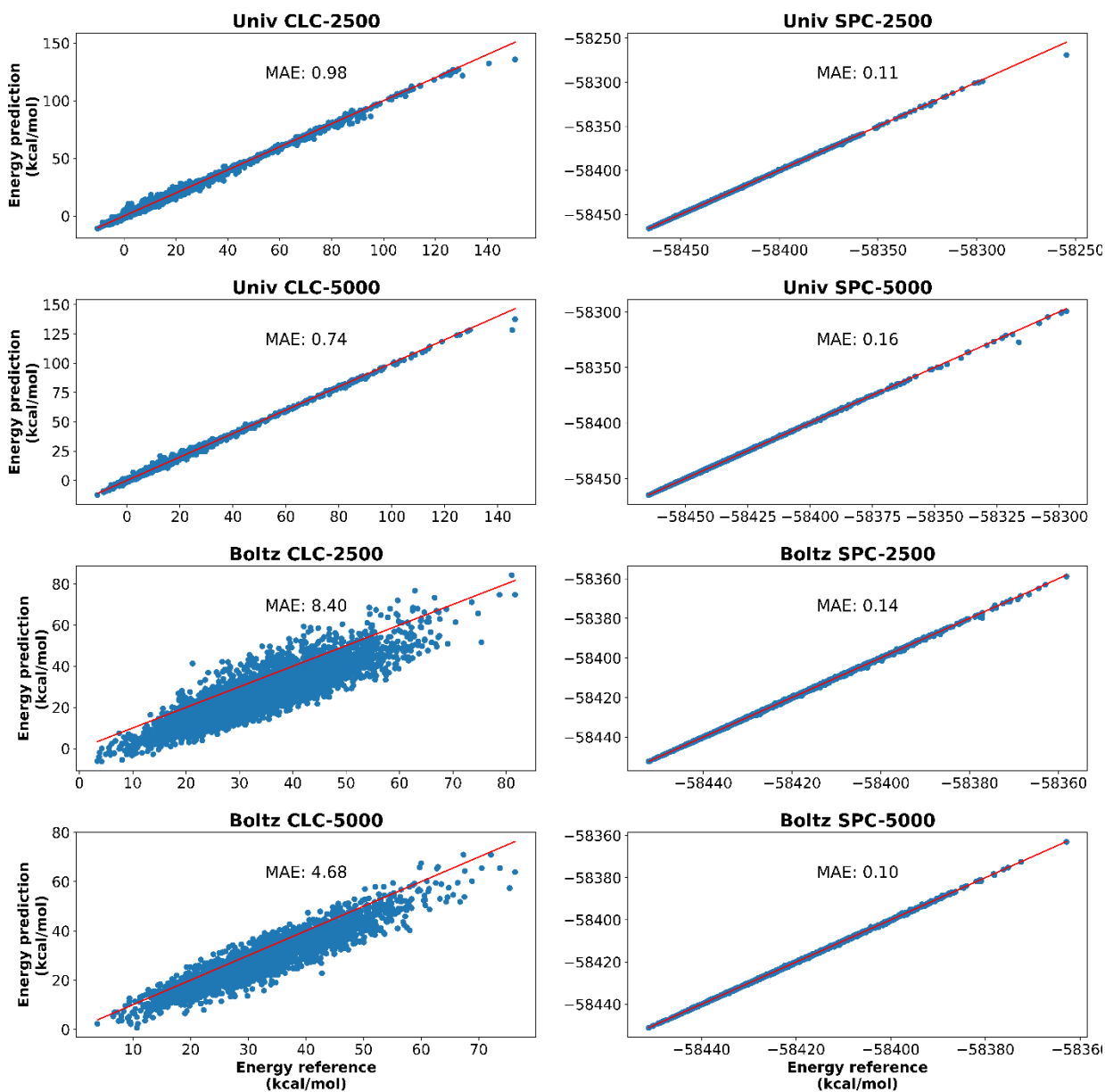


Supplementary Figure 28. Loss function of ADP MLPs trained with 1000 configurations and the characteristic regions distribution at the a) classical and b) *ab initio* levels of theory.

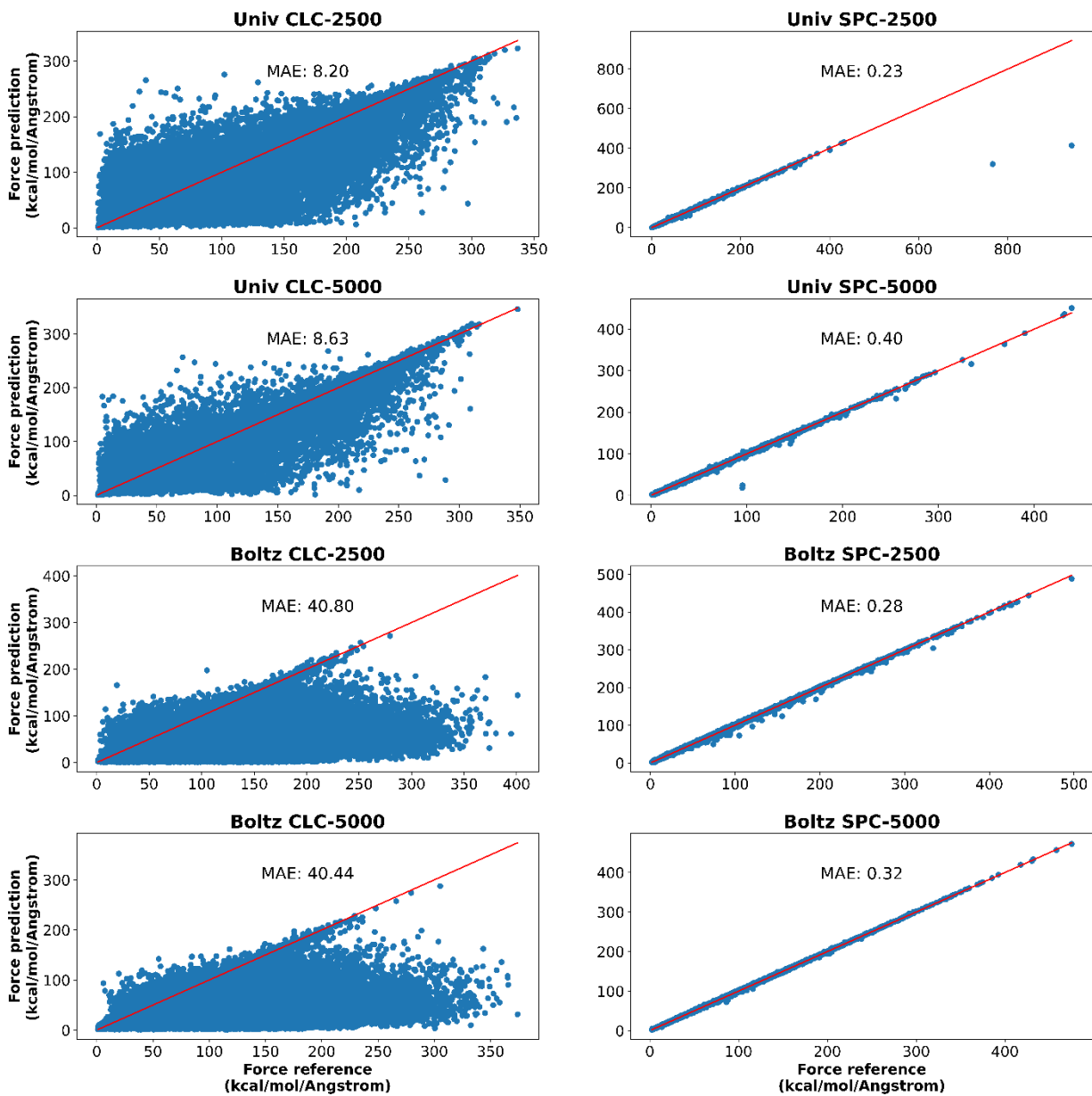


Supplementary Figure 29. Loss function of ADP MLPs trained with 2500 configurations and the characteristic regions distribution at the a) classical and b) *ab initio* levels of theory.

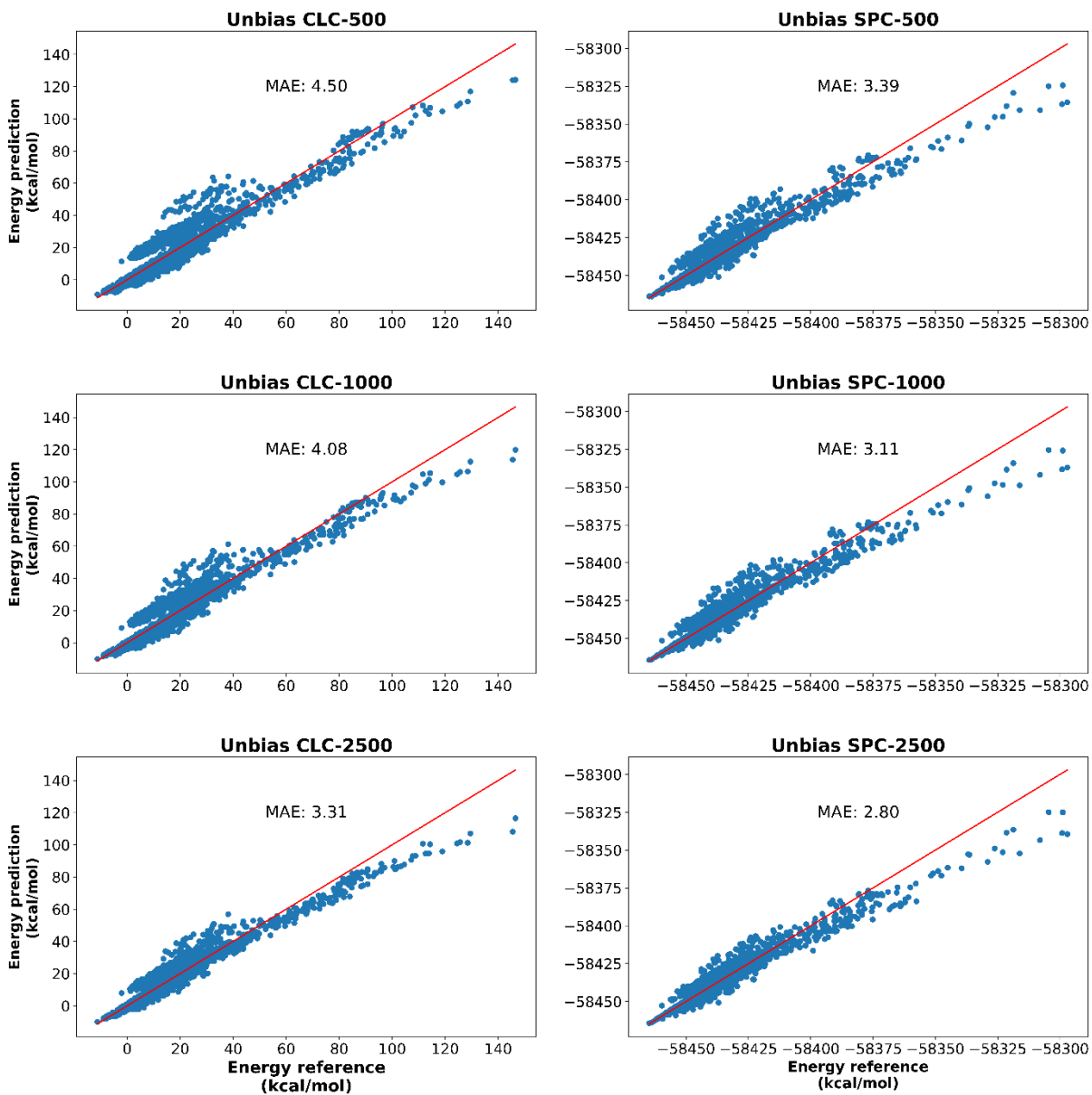
Section V: Energy and force prediction results of ADP MLPs



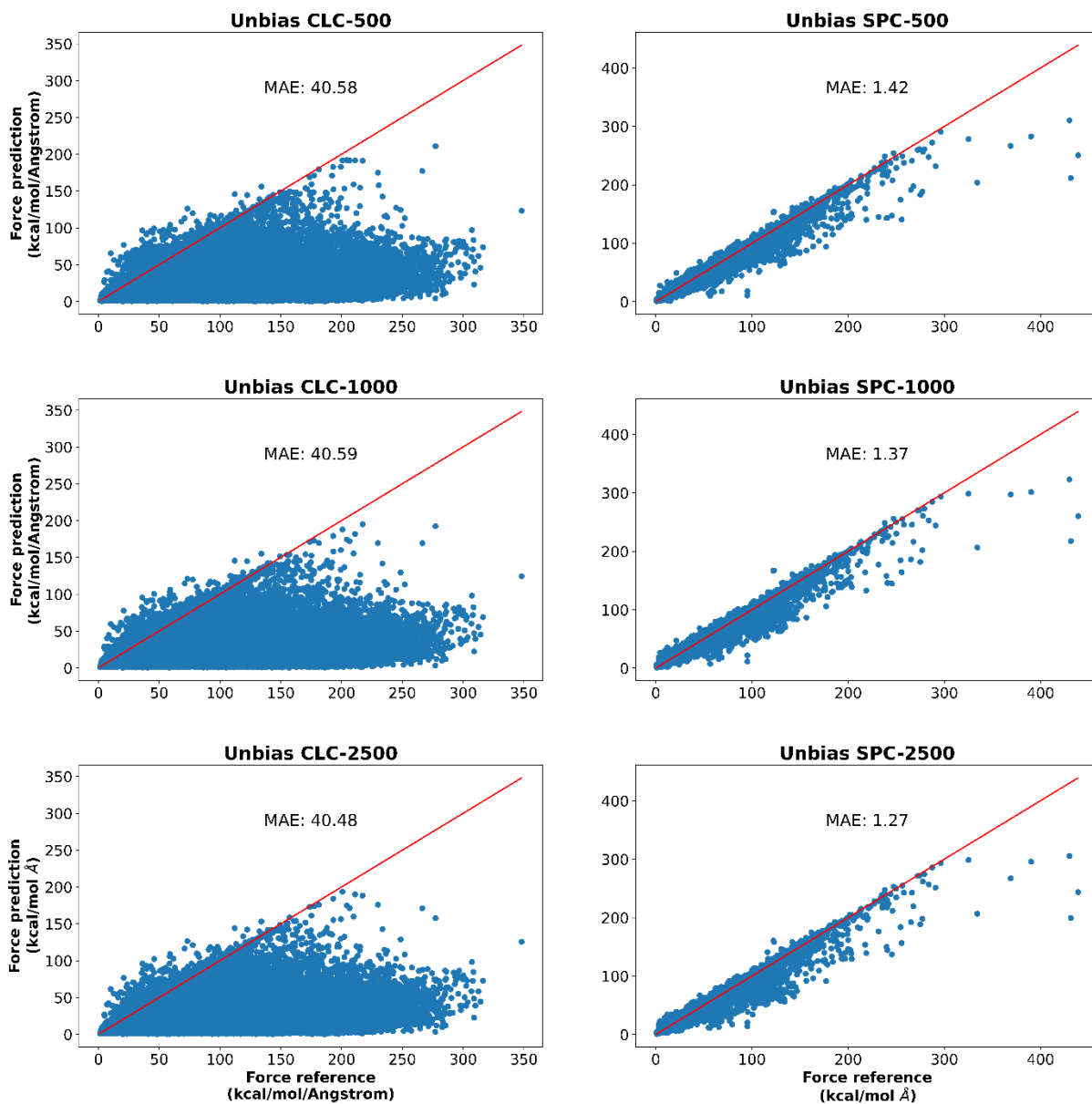
Supplementary Figure 30. ADP potential energy predictions made by trained MLPs with the Uniform and Boltzmann distributions vs reference test values at the classical and *ab initio* level of theory.



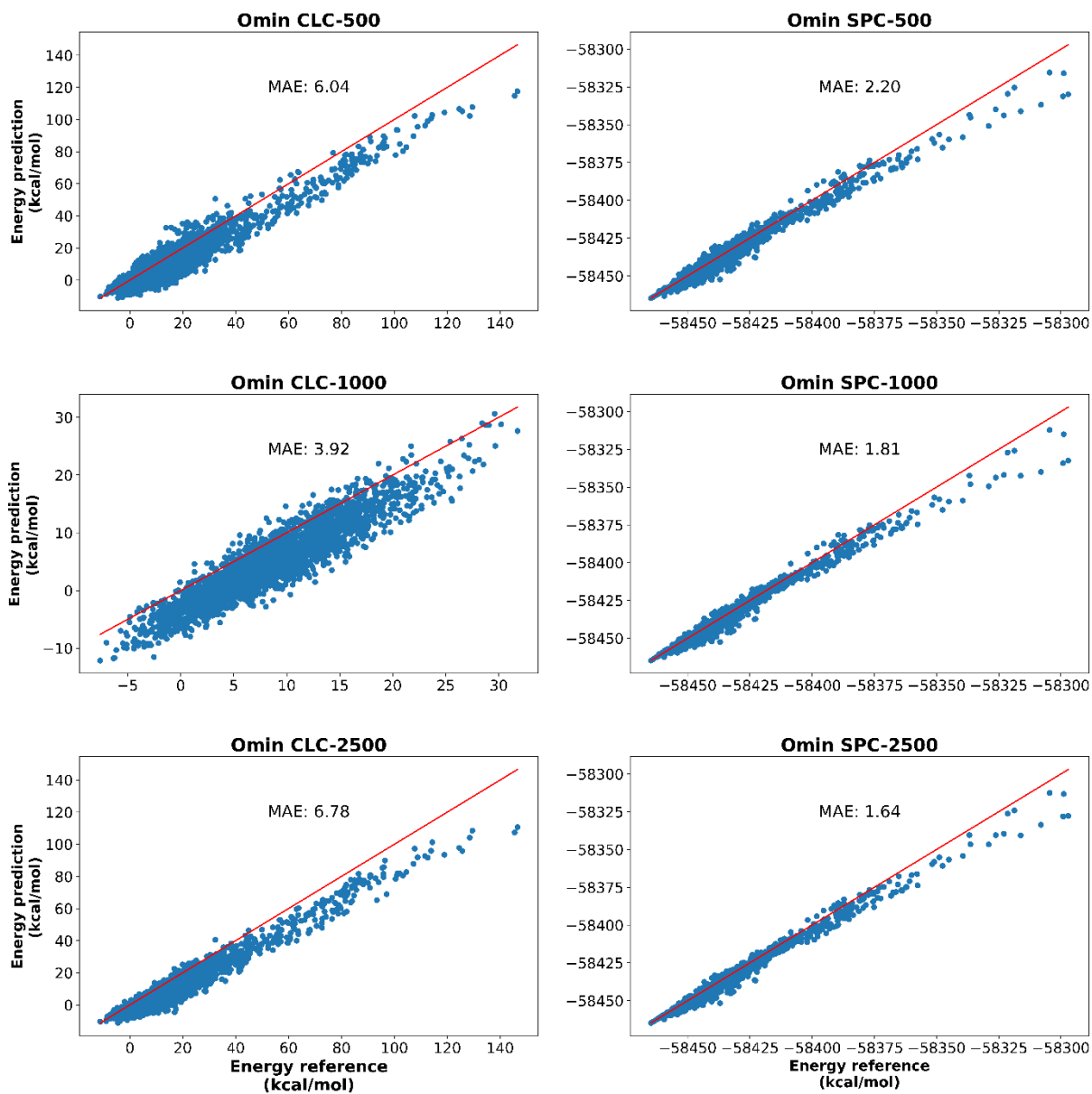
Supplementary Figure 31. ADP atomic forces predictions made by trained MLPs with the Uniform and Boltzmann distributions vs reference test values at the classical and *ab initio* level of theory.



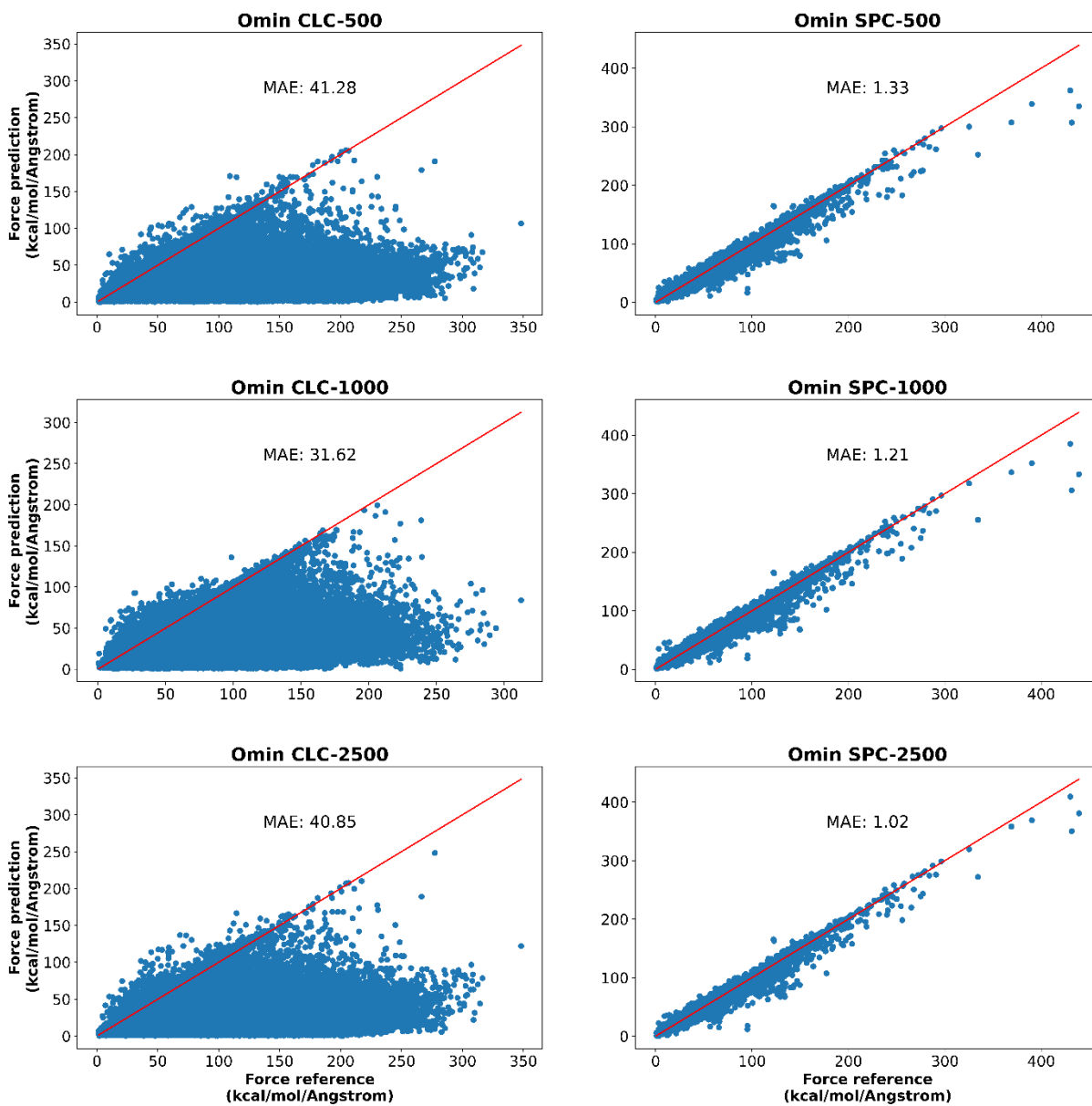
Supplementary Figure 32. ADP potential energy predictions made by trained MLPs with the unbiased distributions vs reference test values at the classical and *ab initio* level of theory.



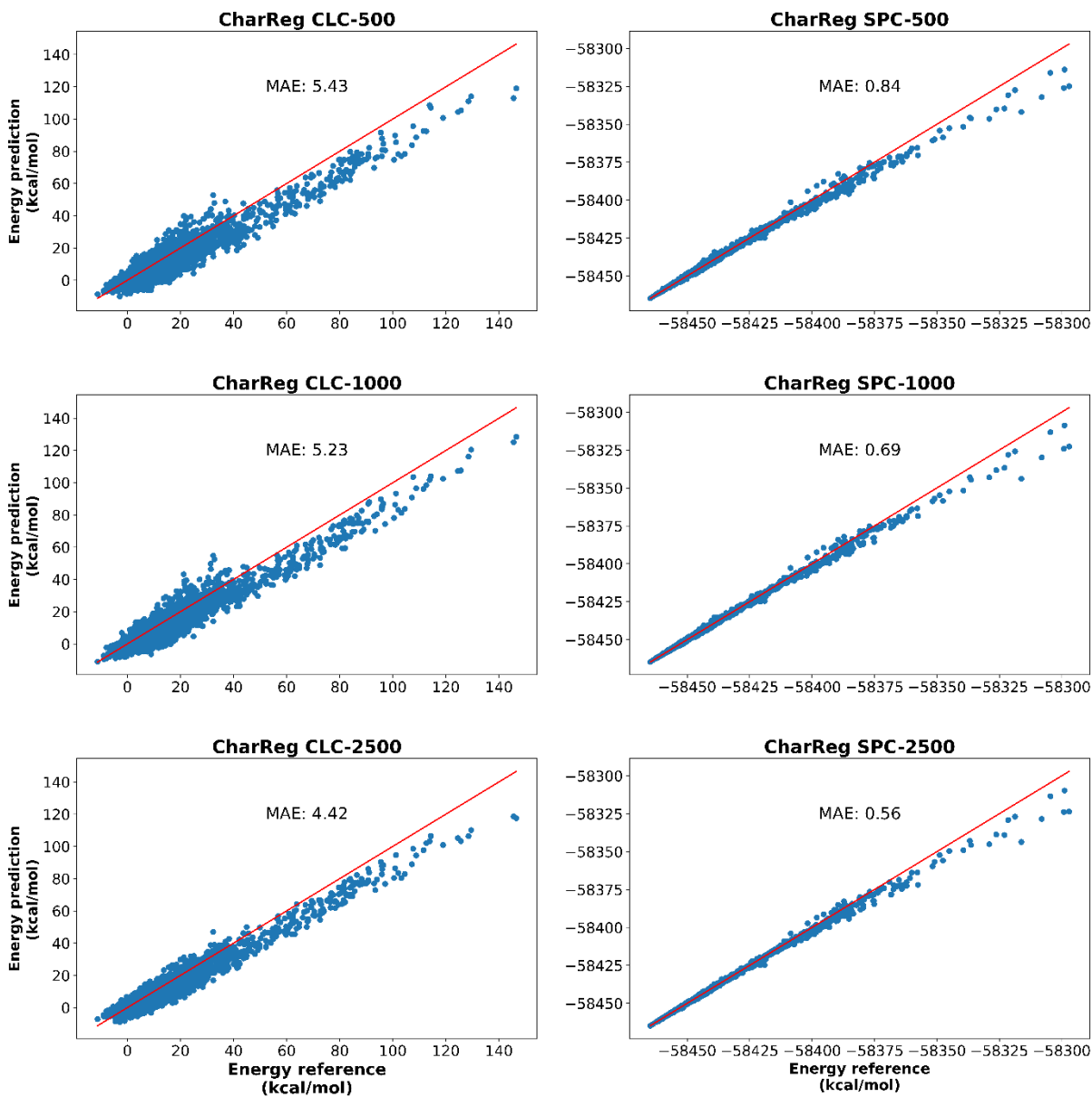
Supplementary Figure 33. ADP atomic force predictions made by trained MLPs with the unbiased distributions vs reference test values at the classical and *ab initio* level of theory.



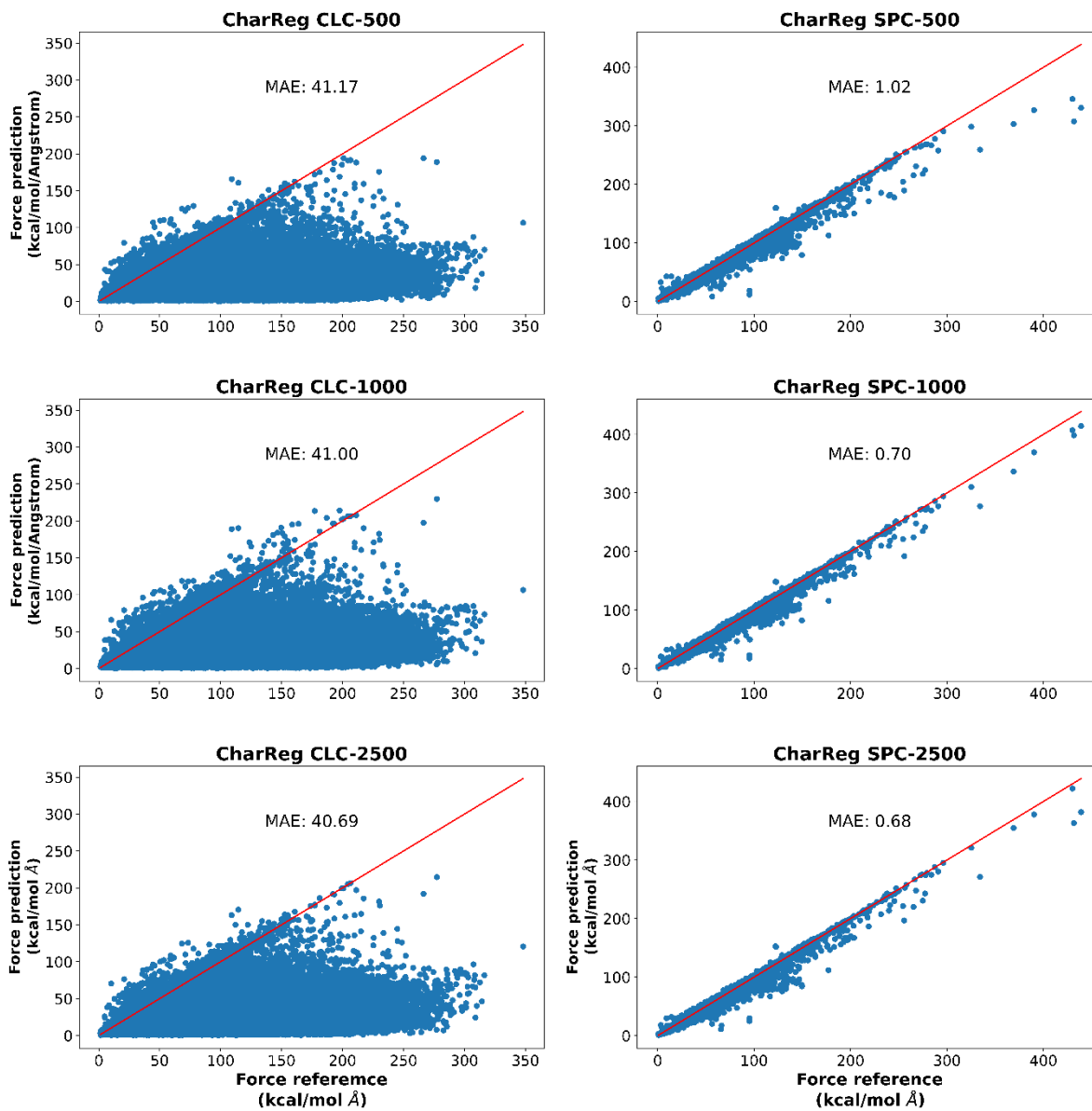
Supplementary Figure 34. ADP potential energy predictions made by trained MLPs with the only minima distributions vs reference test values at the classical and *ab initio* level of theory.



Supplementary Figure 35. ADP atomic force predictions made by trained MLPs with the only minima distributions vs reference test values at the classical and *ab initio* level of theory.

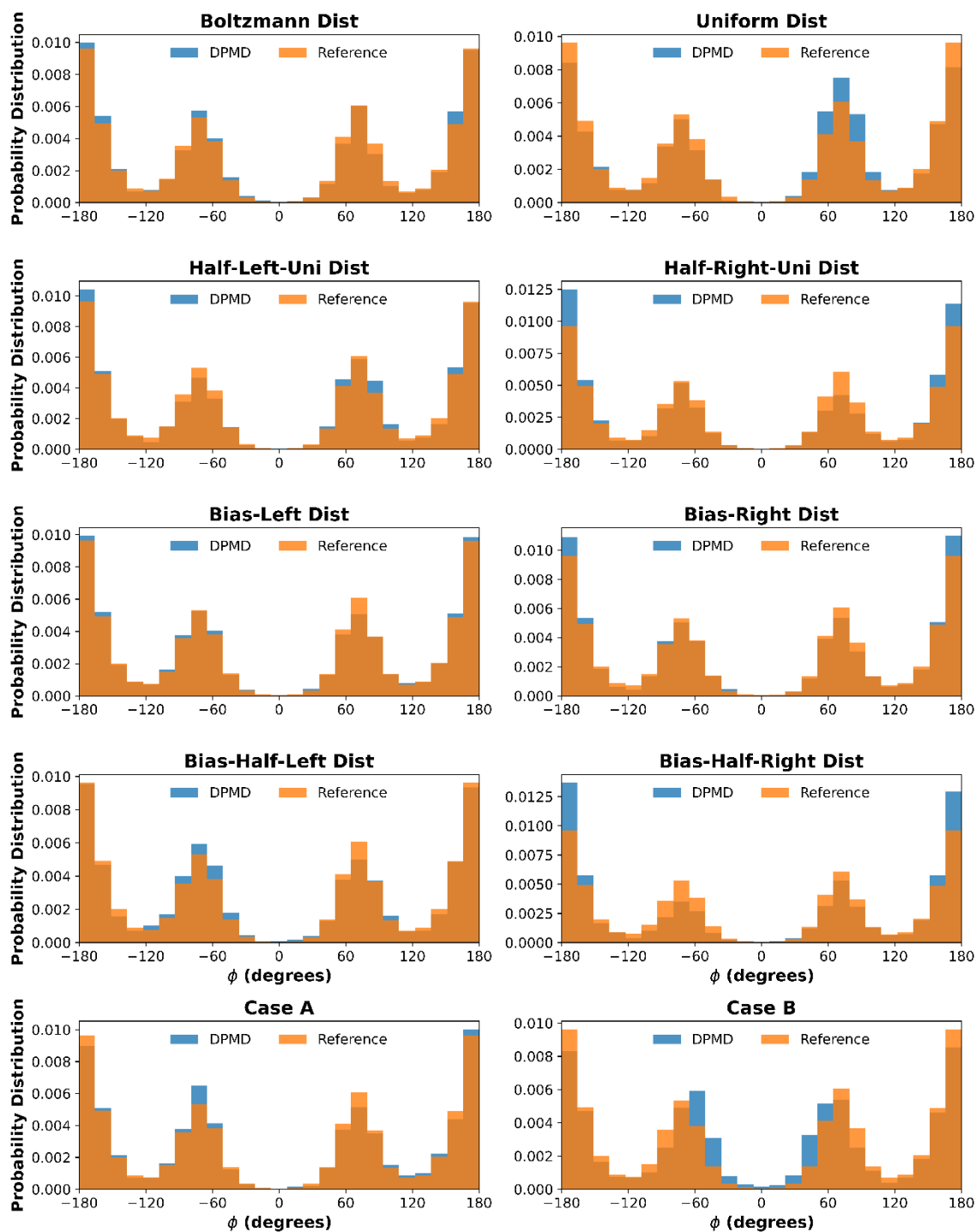


Supplementary Figure 36. ADP potential energy predictions made by trained MLPs with the characteristic regions distributions vs reference test values at the classical and *ab initio* level of theory.

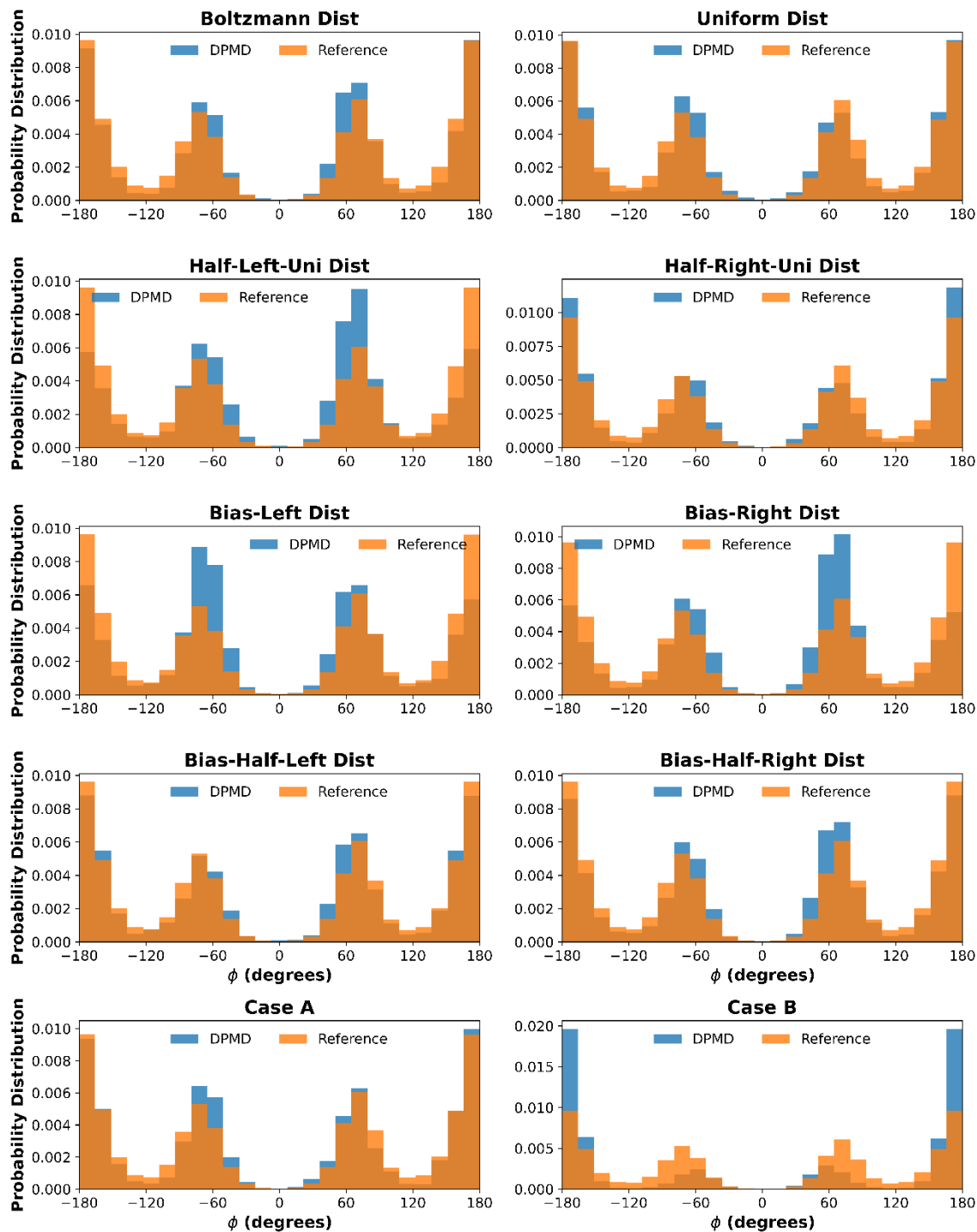


Supplementary Figure 37. ADP atomic force predictions made by trained MLPs with the characteristic regions distributions vs reference test values at the classical and *ab initio* level of theory.

Section VI: Butane dihedral sampled in deep potential simulations.

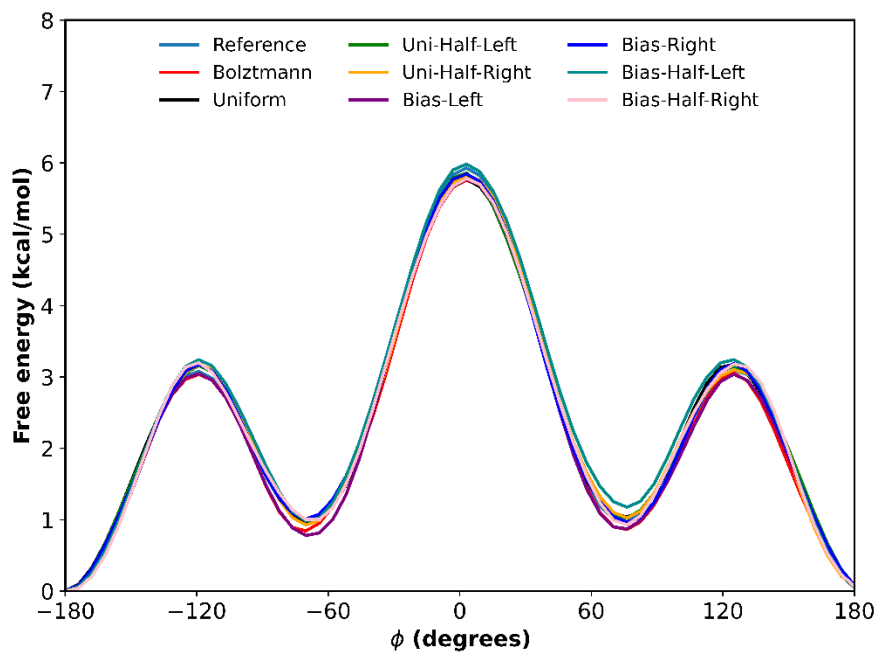


Supplementary Figure 38. Butane dihedral sampled in unbiased Deep potential molecular dynamics with models trained at the classical level of theory.



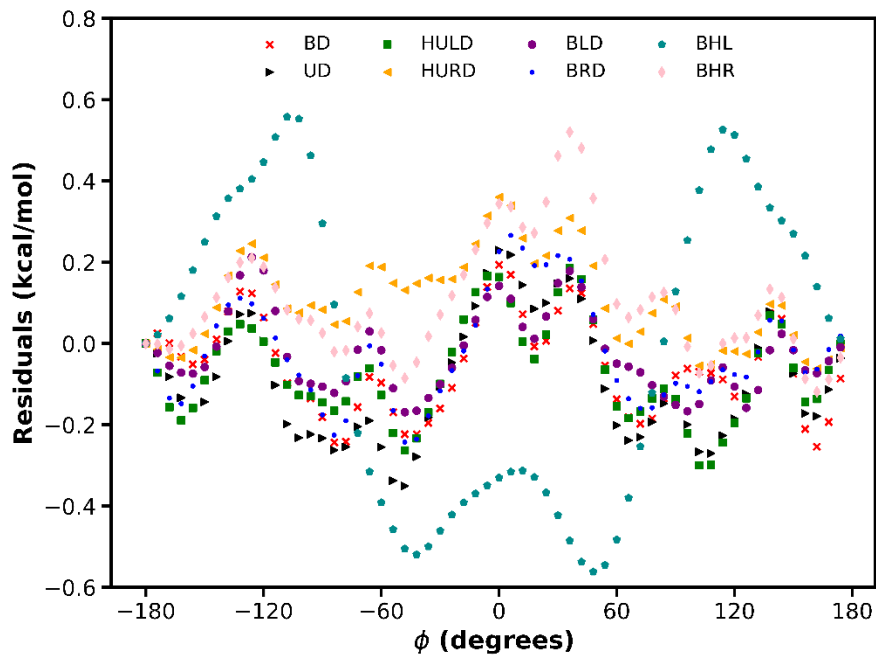
Supplementary Figure 39. Butane dihedral sampled in unbiased Deep potential molecular dynamics with models trained at the *ab initio* of theory.

Section VII. Butane FES predicted by Allegro models trained with Classical level of theory.



Supplementary Figure 40. Free energy surface of butane as a function of the rotation of the dihedral angle predictions with models trained with the eight distributions presented in Figure 1 at the classical level of theory.

Section VIII. Residuals of FES predicted by Allegro model trained with *ab initio* level of theory.



Supplementary Figure 41. Residuals of free energy predictions with butane training data distribution at the *ab initio* level of theory.

References

- (1) Biewald, L. Experiment Tracking with Weights and Biases. *Softw. available from wandb.com* **2020**, 2, 233.